

ERDC/ITL TR-00-1

Information Technology Laboratory



**US Army Corps
of Engineers®**
Engineer Research and
Development Center

Coastal Inlets Research Program

DMS Application: Ft. George Inlet

Report X

**Evaluation of Regional Sediment Management Demonstration Project: St.
Johns River Bypass/Backpass Operations**

Mark S. Gosselin, Michael B. Kabling,
and Elizabeth A. Cranston

September 2000

The contents of this report are not to be used for advertising, publication, or promotional purposes. Citation of trade names does not constitute an official endorsement or approval of the use of such commercial products.

The findings of this report are not to be construed as an official Department of the Army position, unless so designated by other authorized documents.

DMS Application: Ft. George Inlet

Report X

Evaluation of Regional Sediment Management Demonstration Project: St. Johns River Bypass/Backpass Operations

by Mark S. Gosselin, Michael B. Kabling, and Elizabeth A. Cranston

Information Technology Laboratory
U.S. Army Engineer Research and Development Center
3909 Halls Ferry Road
Vicksburg, MS 39180-6199

Final report

Approved for public release; distribution is unlimited

Engineer Research and Development Center Cataloging-in-Publication Data

Destroy this report when no longer needed. Do not return it to the originator.

Contents

Contents.....	iii
List of Figures	iv
List of Tables.....	ix
Preface.....	xi
Conversion Factors, Non-SI to SI Units of Measurement	xii
1—Introduction.....	1
Regional Sediment Management	2
Study Approach: Application of the Diagnostic Modeling System.....	3
Report Organization.....	4
2—Ft. George Inlet and Proposed Borrow Sites	5
Ft. George Inlet.....	5
Historical Inlet Migration	7
Tidal Datums.....	14
Wave Climate.....	15
Bathymetric Description.....	20
Proposed Borrow Sites.....	24
3—Circulation Modeling	29
Model Setup.....	29
Mesh Development.....	30
Calibration	34
Model Simulations.....	37
Simulation Results	40
Existing Conditions	41
Alternative 1: Flood Shoal Mining.....	44
Alternative 2: Ward’s Bank Mining	49
Alternative 3: North Jetty Shoal Mining.....	52
Impacts to Bridge Scour	55
Sediment Transport.....	56
Sediment Transport Theory	56

Existing Conditions.....	59
Alternative 1: Flood Shoal Mining.....	62
Alternative 2: Ward’s Bank Mining.....	65
Alternative 3: North Jetty Shoal Mining	68
4—Nearshore Wave Modeling and Littoral Transport Analyses	72
Wave Modeling	72
Wave Climate.....	72
Wave Model Setup.....	74
Refraction and Shoaling Computations.....	75
Alongshore Transport Computation	76
Wave Model Results.....	76
Existing Conditions.....	77
Alternative 2: Ward’s Bank Mining.....	81
5—Conclusions.....	89
Alternative 1: Flood Shoal Mining.....	89
Alternative 2: Ward’s Bank Mining.....	90
Alternative 3: North Jetty Shoal Mining	91
Littoral Drift Transport Node	91
Summary	92
References.....	93
Appendix.....	96

List of Figures

Figure 1. Ft. George Inlet location map.....	6
Figure 2. Historical shorelines at Ft. George Inlet (1853–1958)	8
Figure 3. Historic shorelines at Ft. George Inlet (1958–1980)	9
Figure 4. Transect locations	12
Figure 5. Shoreline change rate along Little Talbot Island.....	13
Figure 6. Shoreline change rate along Ward’s Bank	14
Figure 7. Wave rose at WIS Station 2026 (1976 – 1995).....	17
Figure 8. Bathymetry contours near Ft. George Inlet (2001).....	21
Figure 9. Bathymetry contours near Ft. George Inlet (1998 - from Olsen Associates, Inc.)	22
Figure 10. Bathymetric change between 1998 and 2001	23

Figure 11. Locations of proposed borrow sites.....	24
Figure 12. Location of CRBA area PO2.....	25
Figure 13. Dredging and backpassing associated with Alternative 1.....	26
Figure 14. Dredging and backpassing associated with Alternative 2.....	27
Figure 15. Dredging associated with Alternative 3.....	28
Figure 16. Model domain	31
Figure 17. Model mesh in vicinity of Ft. George Inlet	32
Figure 18. Water level gage locations	36
Figure 19. Calibration at ocean gage	36
Figure 20. Calibration at bay gage.....	37
Figure 21. Existing conditions bathymetry.....	39
Figure 22. Flood shoal mining bathymetry (Alternative 1).....	39
Figure 23. Ward’s Bank mining bathymetry (Alternative 2)	40
Figure 24. North jetty shoal mining bathymetry (Alternative 3).....	40
Figure 25. Velocity vectors and velocity magnitude contours (m/s) of existing conditions in the Ft. George Inlet vicinity during peak flood velocity	41
Figure 26. Velocity vectors and velocity magnitude contours (m/s) of existing conditions in the Ft. George Inlet vicinity during peak ebb velocity	42
Figure 27. Velocity vectors and velocity magnitude contours (m/s) of existing conditions in the north jetty shoal vicinity during peak flood velocity	43
Figure 28. Velocity vectors and velocity magnitude contours (m/s) of existing conditions in the north jetty shoal vicinity during peak ebb velocity	44
Figure 29. Velocity vectors and velocity magnitude contours (m/s) of Alternative 1 in the Ft. George Inlet vicinity during peak flood velocity	45
Figure 30. Calculated flow rates through Ft. George Inlet during spring tides (existing conditions and Alternatives 1 and 2)	46
Figure 31. Velocity difference contours (m/s) between Alternative 1 and existing conditions during peak flood velocity	47

Figure 32. Velocity vectors and velocity magnitude contours (m/s) of Alternative 1 in the Ft. George Inlet vicinity during peak flood velocity	48
Figure 33. Velocity difference contours (m/s) between Alternative 1 and existing conditions during peak ebb velocity	48
Figure 34. Velocity vectors and velocity magnitude contours (m/s) of Alternative 2 in the Ft. George Inlet vicinity during peak flood velocity	49
Figure 35. Velocity difference contours (m/s) between Alternative 2 and existing conditions during peak flood velocity.....	50
Figure 36. Velocity vectors and velocity magnitude contours (m/s) of Alternative 2 in the Ft. George Inlet vicinity during peak ebb velocity	51
Figure 37. Velocity difference contours (m/s) between Alternative 2 and existing conditions during peak ebb velocity	52
Figure 38. Velocity vectors and velocity magnitude contours (m/s) of Alternative 3 during peak flood velocity	53
Figure 39. Calculated flow rate through the St. Johns River Entrance during spring tides (existing conditions and Alternative 3)	53
Figure 40. Velocity difference contours (m/s) between Alternative 3 and existing conditions during peak flood velocity.....	54
Figure 41. Velocity vectors and velocity magnitude contours (m/s) of Alternative 3 during peak ebb velocity.....	55
Figure 42. Velocity difference contours (m/s) between Alternative 3 and existing conditions during peak ebb velocity	55
Figure 43. Contours of sediment transport rate (m ³ /s/m) during peak flood velocity for existing conditions at Ft. George Inlet	60
Figure 44. Contours of sediment transport rate (m ³ /s/m) during peak ebb velocity for existing conditions at Ft. George Inlet	61
Figure 45. Contours of sediment transport rate (m ³ /s/m) during peak flood velocity for existing conditions in the St. Johns River	61
Figure 46. Contours of sediment transport rate (m ³ /s/m) during peak ebb velocity for existing conditions in the St. Johns River	62
Figure 47. Contours of sediment transport rate (m ³ /s/m) during peak flood velocity for Alternative 1.....	63
Figure 48. Contours of sediment transport rate (m ³ /s/m) during peak ebb velocity for Alternative 1.....	63

Figure 49. Contours of differences in sediment transport rate ($\text{m}^3/\text{s}/\text{m}$) between Alternative 1 and existing conditions during peak flood velocity	64
Figure 50. Contours of differences in sediment transport rate ($\text{m}^3/\text{s}/\text{m}$) between Alternative 1 and existing conditions during peak ebb velocity	65
Figure 51. Contours of sediment transport rate ($\text{m}^3/\text{s}/\text{m}$) during peak flood velocity for Alternative 2.....	66
Figure 52. Contours of sediment transport rate ($\text{m}^3/\text{s}/\text{m}$) during peak ebb velocity for Alternative 2.....	66
Figure 53. Contours of differences in sediment transport rate ($\text{m}^3/\text{s}/\text{m}$) between Alternative 2 and existing conditions during peak flood velocity	67
Figure 54. Contours of differences in sediment transport rate ($\text{m}^3/\text{s}/\text{m}$) between Alternative 2 and existing conditions during peak ebb velocity	68
Figure 55. Contours of sediment transport rate ($\text{m}^3/\text{s}/\text{m}$) during peak flood velocity for Alternative 3.....	69
Figure 56. Contours of sediment transport rate ($\text{m}^3/\text{s}/\text{m}$) during peak ebb velocity for Alternative 3.....	69
Figure 57. Contours of differences in sediment transport rate ($\text{m}^3/\text{s}/\text{m}$) between Alternative 3 and existing conditions during peak flood velocity	70
Figure 58. Contours of differences in sediment transport rate ($\text{m}^3/\text{s}/\text{m}$) between Alternative 3 and existing conditions during peak ebb velocity	71
Figure 59. Model domain and existing depth contours.....	75
Figure 60. Computed wave heights and directions (Case 33: $H_{mo} = 1.3$ m, T_p = 12 sec).....	79
Figure 61. Computed wave heights and directions (Case 52: $H_{mo} = 0.9$ m, T_p = 8 sec)	80
Figure 62. Computed sediment transport potential (Existing Conditions)....	81
Figure 63. Alternative 2 (Ward's Bank mining) depth contours	82
Figure 64. Wave results for case 43 ($H_{mo} = 1.3$ m, $T_p = 13$ s, $\mathbf{q} = 69.4^\circ$).....	84
Figure 65. Wave results for case 52 ($H_{mo} = 0.9$ m, $T_p = 8$ s, $\mathbf{q} = 89.6^\circ$).....	85
Figure 66. Wave results for case 62 ($H_{mo} = 0.8$ m, $T_p = 8$ s, $\mathbf{q} = 106.6^\circ$).....	86

Figure 67. Computed sediment transport potential: Alternative 2.....	88
Figure 68. Net Sediment Transport Rate Potential (Alternative 2 and Existing Conditions).....	88
Figure A-1. Wave heights and directions (Case 21: $H_{mo} = 1.4$ m, $T_p = 5$ s, $\theta = 21.9^\circ$)	97
Figure A-2. Wave heights and directions (Case 23: $H_{mo} = 1.1$ m, $T_p = 13$ s, $\theta = 22.3^\circ$)	97
Figure A-3. Wave heights and directions (Case 31: $H_{mo} = 1.2$ m, $T_p = 5$ s, $\theta = 44.3^\circ$)	98
Figure A-4. Wave heights and directions (Case 32: $H_{mo} = 1.5$ m, $T_p = 8$ s, $\theta = 46.0^\circ$)	98
Figure A-5. Wave heights and directions (Case 33: $H_{mo} = 1.1$ m, $T_p = 5$ s, $\theta = 67.4^\circ$)	99
Figure A-6. Wave heights and directions (Case 41: $H_{mo} = 1.1$ m, $T_p = 5$ s, $\theta = 67.4^\circ$)	99
Figure A-7. Wave heights and directions (Case 42: $H_{mo} = 1.3$ m, $T_p = 8$ s, $\theta = 68.8^\circ$)	100
Figure A-8. Wave heights and directions (Case 43: $H_{mo} = 1.3$ m, $T_p = 13$ s, $\theta = 69.9^\circ$)	100
Figure A-9. Wave heights and directions (Case 51: $H_{mo} = 0.9$ m, $T_p = 6$ s, $\theta = 88.0^\circ$)	101
Figure A-10. Wave heights and directions (Case 52: $H_{mo} = 0.9$ m, $T_p = 8$ s, $\theta = 89.6^\circ$)	101
Figure A-11. Wave heights and directions (Case 53: $H_{mo} = 1.1$ m, $T_p = 12$ s, $\theta = 86.0^\circ$).....	102
Figure A-12. Wave heights and directions (Case 61: $H_{mo} = 1.0.9$ m, $T_p = 5$ s, $\theta = 108.8^\circ$).....	102
Figure A-13. Wave heights and directions (Case 62: $H_{mo} = 0.8$ m, $T_p = 8$ s, $\theta = 106.6^\circ$)	103
Figure A-14. Wave heights and directions (Case 63: $H_{mo} = 1.0$ m, $T_p = 12$ s, $\theta = 108.6^\circ$).....	103
Figure A-15. Wave heights and directions (Case 72: $H_{mo} = 0.9$ m, $T_p = 8$ s, $\theta = 132.2^\circ$)	104
Figure A-16. Wave Simulation Results for Case 21.....	105
Figure A-17. Wave Simulation Results for Case 23.....	106
Figure A-18. Wave Simulation Results for Case 31.....	107

Figure A-19. Wave Simulation Results for Case 32.....	108
Figure A-20. Wave Simulation Results for Case 33.....	109
Figure A-21. Wave Simulation Results for Case 41.....	110
Figure A-22. Wave Simulation Results for Case 42.....	111
Figure A-23. Wave Simulation Results for Case 43.....	112
Figure A-24. Wave Simulation Results for Case 51.....	113
Figure A-25. Wave Simulation Results for Case 52.....	114
Figure A-26. Wave Simulation Results for Case 53.....	115
Figure A-27. Wave Simulation Results for Case 61.....	116
Figure A-28. Wave Simulation Results for Case 62.....	117
Figure A-29. Wave Simulation Results for Case 63.....	118
Figure A-30. Wave Simulation Results for Case 72.....	119

List of Tables

Table 1. Summary of Events Effecting the Shoreline at Ft. George Inlet.....	10
Table 2. NOAA Tidal Datums at Ft. George River and Little Talbot Island	15
Table 3. Normalized Probability of Wave Occurrence for WIS Station 2026 (1976 – 1995).....	16
Table 4. Occurrences of Wave Height by Month for WIS Station 2026 (1976 – 1995).....	18
Table 5. Occurrences of Peak Wave Period by Month for WIS Station 2026 (1976 – 1995).....	19
Table 6. Occurrences of Peak Wave Direction by Month for WIS Station 2026 (1976 – 1995).....	20
Table 7. Survey information for mesh construction.....	32
Table 8. Flow Rates for Connecting Creeks to the St. Johns River.....	34
Table 9. Error Results for Water Level Calibration.....	37
Table 10. Calculated tidal prisms during spring tide.....	45
Table 11 Calculated tidal prisms during spring tide (St. Johns River).....	52

Table 12. Wave angle and band limits	73
Table 13. Wave angle and band limits (WIS 2026, 1976–1995)	73
Table 14. Representative Wave Conditions for Ft. George River	74

Preface

The study described in this report was performed under the Diagnostic Modeling System (DMS) Work Unit of the Coastal Sedimentation and Dredging Program administered by Headquarters, U.S. Army Corps of Engineers (HQUSACE). Research and Development activities of the DMS are being conducted at the U.S. Army Research and Development Center (ERDC) Coastal and Hydraulics Laboratory (CHL), Vicksburg, MS. HQUSACE Program Monitors are Messrs. Charles B. Chesnutt, Barry W. Holliday, and Mike Klosterman.

Work was performed by Dr. Mark S. Gosselin, Ms. Elizabeth A. Cranston, and Dr. Michael B. Kabiling of Taylor Engineering, Inc. of Jacksonville, FL. The contract monitor and principal investigator of the DMS work unit was Dr. Nicholas C. Kraus.

This work reflects joint funding through the Regional Sediment Management for Northeast Florida agreement between the U.S. Army Corps of Engineers (USACE), Jacksonville District (SAJ), and the Florida Department of Environmental Protection (FDEP), Bureau of Beaches and Coastal Systems (BBCS). Support through the FDEP was contracted through the Bureau of Natural and Cultural Resources (BNCR), Division of Recreation and Parks. Contract oversight by these agencies was provided by Mr. Thomas Smith (USACE), Mr. Russell Snyder (FDEP BBCS), and Mr. Mark Latch (FDEP BNCR).

This work benefited from work originally performed for the USACE SAJ to examine tidal circulation and shoaling in the Jacksonville Harbor Navigation Project, Jacksonville, Florida.

At the time of publication of this report, Dr. James R. Houston was Director of ERDC, and COL John W. Morris III, EN, was Commander and Executive Director.

Conversion Factors, Non-SI to SI Units of Measurement

Non-SI units of measurement used in this report can be converted to SI units as follows:

Multiply	By	To Obtain
cubic feet	0.028317	cubic meters
cubic yards	0.7645549	cubic meters
feet	0.3048	meters
miles (U.S. statute)	1.609347	kilometers

1 Introduction

This report documents a study to evaluate a Regional Sediment Management Demonstration Project concerning the operations around the St. Johns River Entrance. The Regional Sediment Management initiative comprises a jointly funded effort between the U.S. Army Corps of Engineers (USACE), Jacksonville District (SAJ) and the Florida Department of Environmental Protection (FDEP) to address beneficial use of dredged material and sediment related issues within a regional, rather than local, context. Specifically, the Demonstration Project examines bypassing beach quality material across the St. Johns River Entrance to the Duval County beaches south of the entrance and identifying the optimum location for placement of the bypass material. The FDEP Strategic Beach Management Plan has identified a 10-mile segment of critical erosion that extends from the St. Johns River Entrance to the Duval-St. Johns County line. The Plan also calls for continued beach nourishment in Duval County and further study of the St. Johns River Entrance.

The SAJ has identified several sources for beach renourishment including Buck Island and the Jacksonville Harbor deepening project. Alternative borrow sites identified in and around Ft. George Inlet include the extensive ebb shoal system, the flood shoal north of the A1A Bridge, and the shoal that forms just south of the north jetty at the southern tip of Ward's Bank. Another element of this Demonstration Project concerns the persistent erosion of the south end of Little Talbot Island. Concrete riprap shore protection provided by the Florida Department of Transportation (FDOT) effectively stabilizes a segment of the north bank of the inlet channel near the eastern end of the SR A1A Bridge. The channel, however, remains free to shift northward over its eastern segment. This process has led to continued erosion of the southeastern corner of Little Talbot Island and a northward growth of Ward's Bank. In turn, the inlet channel has changed its former east-west orientation toward NE-SW and has increased in length. The ensuing shoreline recession now compromises state park facilities on Little Talbot Island. Several of the potential borrow sites for the St. Johns River bypass operations could also serve as borrow sites for renourishment of the southern tip of Little Talbot Island.

To address these concerns, SAJ contracted Taylor Engineering to apply the Diagnostic Modeling System (DMS) to investigate three alternatives that

involve dredging sediments from the Ft. George Inlet vicinity and either bypassing the sediments south of the St. Johns River Entrance or backpassing them to the southern tip of Little Talbot Island. The specific task of this study is to determine the impacts to the coastal processes that would result from each of the dredging operations as well as to determine the location of the transport node south of the St. Johns River Entrance so that beach quality sands placed south of the inlet reenter the littoral system. This report details the results of this study.

Regional Sediment Management

On June 16, 1999, the USACE entered into an agreement with the FDEP. The FDEP identified the need to implement Regional Sediment Management (RSM) practices in the Sea Islands and St. Johns Beaches Sub-Regions of the Northeast Atlantic Coast Region as defined by the FDEP Bureau of Beaches and Coastal Systems. As defined, the limits of these sub-regions extend from the northern Nassau County line through Duval County to the southern St. Johns County line. RSM resources and opportunities extend well upland and well offshore of the immediate coastline and involve numerous State, Federal, and local agencies. Under the terms of the agreement, the USACE will provide technical assistance to the FDEP and coordinate RSM activities in the two sub-regions. The agreement also calls for establishing a forum to facilitate coordination with other Federal and local agencies. Additionally, the USACE will participate in a study with cost sharing and financing in accordance with the terms of the agreement. Section 22 of the Water Resources Development Act of 1974 (Public Law 93-251) provides justification for this agreement in that it authorizes the Secretary of the Army, acting through the Chief of Engineers, to help the states prepare comprehensive plans for the development, use, and conservation of water and related land resources. Additionally, Section 319 of the Water Resources Act of 1990 (Public Law 101-640) authorizes the Secretary to collect from nonfederal entities fees for recovering 50% of program costs. The scope of work included in this agreement calls for interested parties to meet several times to focus on the implementation of regional sediment management practices through identification and development of potential coordinated projects.

Throughout 1999 and 2000, workshops held in three affected counties — St. Johns, Duval, and Nassau — addressed RSM concerns in Northeast Florida. These workshops provided a venue to present Federal, State, and local perspectives and to identify opportunities for RSM. Participants identified several Potential Demonstration Projects (PDPs) as cost effective and innovative approaches to RSM.

One of the PDP's identified during these meetings concerned bypassing beach quality material across the St. Johns River Entrance to the Duval County beaches south of the river and identifying the optimum location for placement of the bypassed material. The FDEP Strategic Beach Management Plan has identified a 10-mile segment of critical erosion that extends from the

St. Johns River Entrance to the Duval-St. Johns County line. The Plan also calls for continued beach nourishment in Duval County and further study of the St. Johns River Entrance. As part of its mission to protect these beaches, the USACE has identified Buck Island as a borrow source for renourishment of the Duval County shore. The Jacksonville Harbor deepening project may also provide suitable material. In addition, achieving long-term project goals will require identifying and permitting alternative offshore borrow sites. Germane to this study, specifics associated with this PDP included identifying the location of the transport node south of the St. Johns River Entrance as well as determining the environmental impacts to several of the alternative sediment sources located in and around Ft. George Inlet and Ward's Bank.

Study Approach: Application of the Diagnostic Modeling System

One of the key methodologies employed during this study is the Diagnostic Modeling System (DMS). The DMS, under guidance of the Coastal Sedimentation and Dredging Program administered by Headquarters, USACE, provides the USACE with a rapid, inexpensive, and reliable capability to develop and evaluate navigation channel operations and maintenance (O&M) alternatives based on limited information on the hydrodynamic and sediment transport conditions at a site.

The DMS provides a quick and concise capability to identify, categorize, and evaluate navigation channel sediment deposition hot spots for correction. The tools included in the DMS help engineers identify problem areas of shoaling, characterize the causes of these problems, and develop practical, cost-effective solutions. The methodology relies heavily on the use of established public domain coastal hydrodynamic models such as ADCIRC in combination with a suite of engineering analyses and procedures founded upon fundamental principles of fluid dynamics and sediment transport. For this reason, the methodology is referred to as the Diagnostic Modeling System, or DMS. The DMS is not intended to provide the level of detailed information required for final design or in-depth study. Rather, it is intended to quickly diagnose the problem, categorize it according to its key characteristics, and identify typical corrective actions. The diagnostic procedure should conclude within a time span shorter than the project dredging cycle.

This application of the DMS builds upon previous SAJ work that examined shoaling within the Jacksonville Harbor Project. Part of this application included construction of a two-dimensional circulation model. The USACE model ADCIRC provided the circulation modeling and much of the extracted model mesh came from the community model the USACE Engineering Research and Development Center (ERDC) currently maintains.

The study approach comprises three facets: bathymetric comparisons and calculations, circulation modeling, and wave transformation modeling. Bathymetries covering Ft. George Inlet provided not only information about the evolution of the shoal system around the inlet but also estimates of the amount of material located in the shoals and the material volumes required to nourish the Little Talbot Island shoreline. These bathymetries served as input to construct the circulation models. Circulation models were then constructed for existing conditions as well as the three alternatives. The existing conditions model provided the baseline from which to compare how each of the three alternatives modify tidal circulation patterns. Results from this modeling provided the inputs to calculate the tidally induced sediment transport. Finally, wave models of existing conditions as well as the alternatives were constructed. Again, the existing conditions model established the baseline from which to compare the alternatives. Results from the wave model provided the inputs to calculate the associated sediment transport with the CERC formula.

Report Organization

Following this introduction, Chapter 2 provides a brief overview of Ft. George Inlet as well as the proposed borrow sites. Chapter 3 describes the circulation modeling and associated tidal driven sediment transport calculations performed in support of this study including setup, calibration, and reduction of the results. Chapter 4 presents the wave modeling and associated longshore sediment transport calculations. Finally, Chapter 5 presents the conclusions and recommendations of this study.

2 Ft. George Inlet and Proposed Borrow Sites

Examining the specific impacts of each of the proposed borrow sites requires prior knowledge of the inlet's physical characteristics, historical behavior, and existing coastal processes. This knowledge provides proper context to evaluate the impacts of each alternative. This chapter presents a description of the inlet, historic inlet behavior through an examination of shoreline change, and the coastal processes (offshore waves and tides) present at the inlet. This chapter concludes with a discussion of the proposed borrow sites for bypassing and backpassing operations.

Ft. George Inlet

Ft. George Inlet is located on the Atlantic Coast in Duval County, Florida. The natural inlet lies immediately north of the St. Johns River Entrance and approximately 8 km south of Nassau Sound (Figure 1). Ft. George River connects to Simpson Creek approximately 2.6 km upstream of its mouth, proceeds northwest, and connects with the Intracoastal Waterway (ICWW) about 5 km upstream of the inlet. Northern and southern boundaries include Little Talbot Island and Ward's Bank. Ft. George Inlet is currently unstabilized. The throat of the inlet measures approximately 200 m across (on average) at low tide. The main channel through the inlet reaches an average depth of approximately -4.0 m-NGVD with a maximum depth of about -6.1 m-NGVD. The channel through the inlet aligns 33° (measured from north). After it enters the inlet on flood tide, flow swings around and continues approximately due north up the Ft. George River.

The undeveloped Little Talbot Island borders the inlet to the north. The island currently measures 7.8 km long from Nassau Sound north to the A1A Bridge south. State Road A1A runs north to south through the island. The road enters the island at the southern tip via a two-lane bridge the Florida Department of Transportation (FDOT) recently designated for replacement. Ft. George River and Simpson's Creek border the island to the east. The State of Florida owns the majority of the island and manages it as Little Talbot Island State Park. The southern tip of the island has experienced significant erosion over the past 67 years. This erosion threatens several upland resources including SR-A1A, the A1A Bridge, parking lots, and park

facilities. In fact, in 1998, the erosion undermined the foundations of a pier located at the island's southern end. To protect SR-A1A and the bridge, FDOT constructed a rubble revetment that measures approximately 1,000 m long and wraps the southern tip of the island from beneath the A1A Bridge along the north bank of the channel throat. Although it requires frequent maintenance, the revetment has prevented loss of the roadway. However, it does not deter the continued erosion of the southern shoreline of the island.

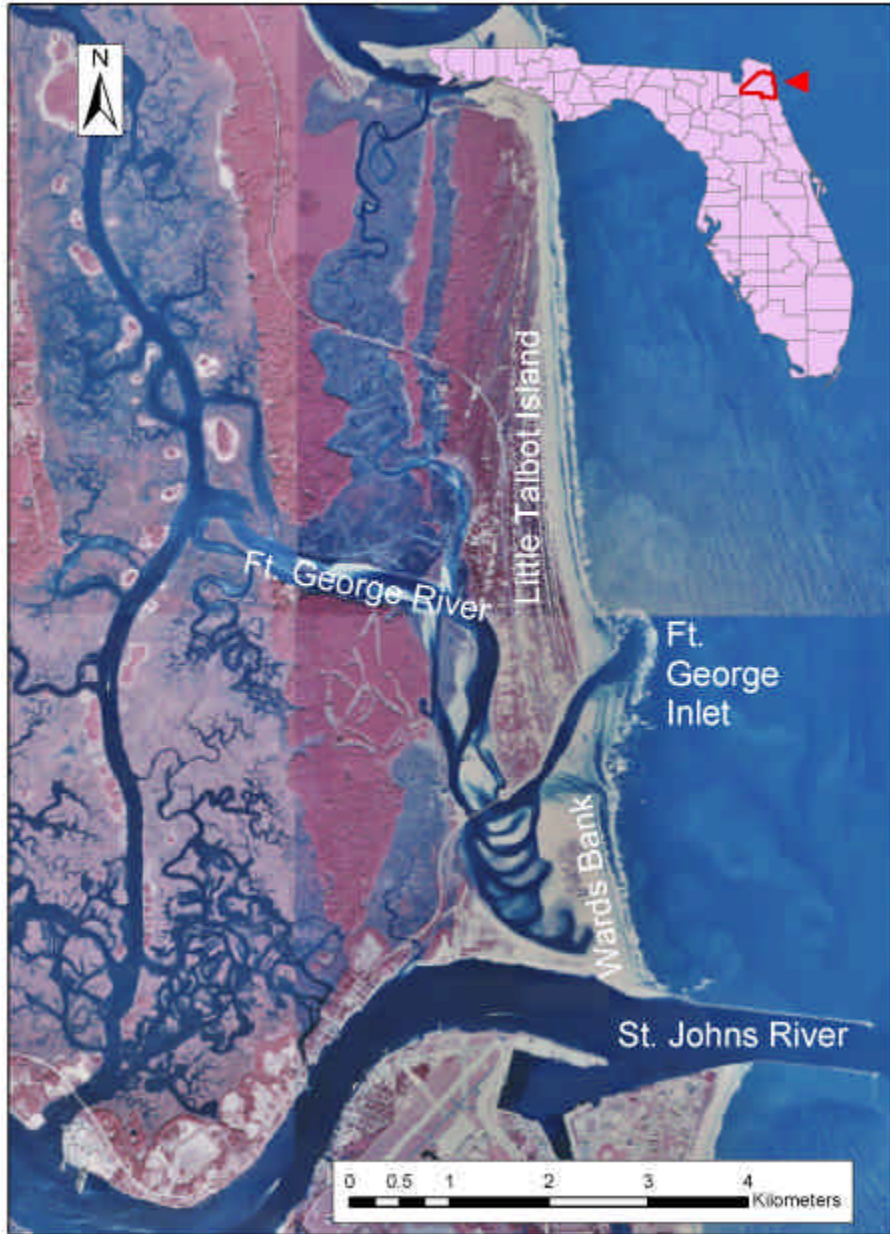


Figure 1. Ft. George Inlet location map

Ward's Bank borders the inlet to the south. This spit abuts the north jetty of the St. Johns River Entrance. The spit has been accreting and migrating

steadily northward since the mid-1930s. The feature originally appeared as a result of sand impoundment at the north jetty. In 1934, the north jetty was capped to reduce sediment transport through the structure. Since that time, the spit has grown to its current dimensions where it overlaps Little Talbot Island. Huguenot Memorial Park, a City of Jacksonville park, comprises the majority of the spit.

Historical Inlet Migration

Examination of the inlet's historic migration patterns leads to a better understanding of the coastal processes at the inlet. This analysis draws from previous studies, historical shoreline surveys, and field assessments. Findings in previous investigations present a detailed assessment of both the historical and present shoreline morphologies. Thus, this section combines previous research findings with historic shoreline data to evaluate inlet migration and coastal processes near the inlet.

Numerous studies of the historical inlet migration of Ft. George Inlet exist in the literature, including Kojima and Mehta (1979), Mehta and Marino (1987), Marino et al. (1990), and Olsen Associates Inc. (1999). In addition, the Florida Department of Natural Resources (DNR) has compiled historical Florida shoreline surveys from the U.S. Coast and Geodetic Survey, the U.S. Geological Survey, and the National Ocean Service of the National Oceanic and Atmospheric Administration. These surveys date back to the 1800s. Shorelines from these surveys, digitally overlaid with a common scale and datum, illustrate their historical shoreline behavior. In the study area, shoreline surveys are available for 1853, 1871 (Little Talbot Island shoreline only), 1924, 1933, 1958, 1963 – 1964, 1970 (Little Talbot Island south shoreline only), 1973 – 1975 (missing southwest shoreline of Little Talbot Island), 1977, and 1979 – 1980. Figures 2 and 3 present these shoreline overlays. Figure 2 shows the shorelines (1853, 1871, 1924, 1933, and 1958) before construction of the AIA Bridge. Figure 3 presents shoreline positions (1958, 1963 – 1964, 1970, 1973 – 1975, 1977, and 1979 – 1980) following construction of the present bridge. Both figures include the 1958 shoreline to provide a basis of comparison. The summary of previous investigations below discusses these figures.

The findings of Kojima and Mehta (1979) detailed area conditions from the beginning of the available records to 1978. The authors identified six phases of historical migration of the Ft. George River channel and inlet. The phases — summarized in Table 1 and illustrated in the historical MHW shorelines in Figures 2 and 3 — identify the processes that have influenced the channel's location in the past and continue to the present.

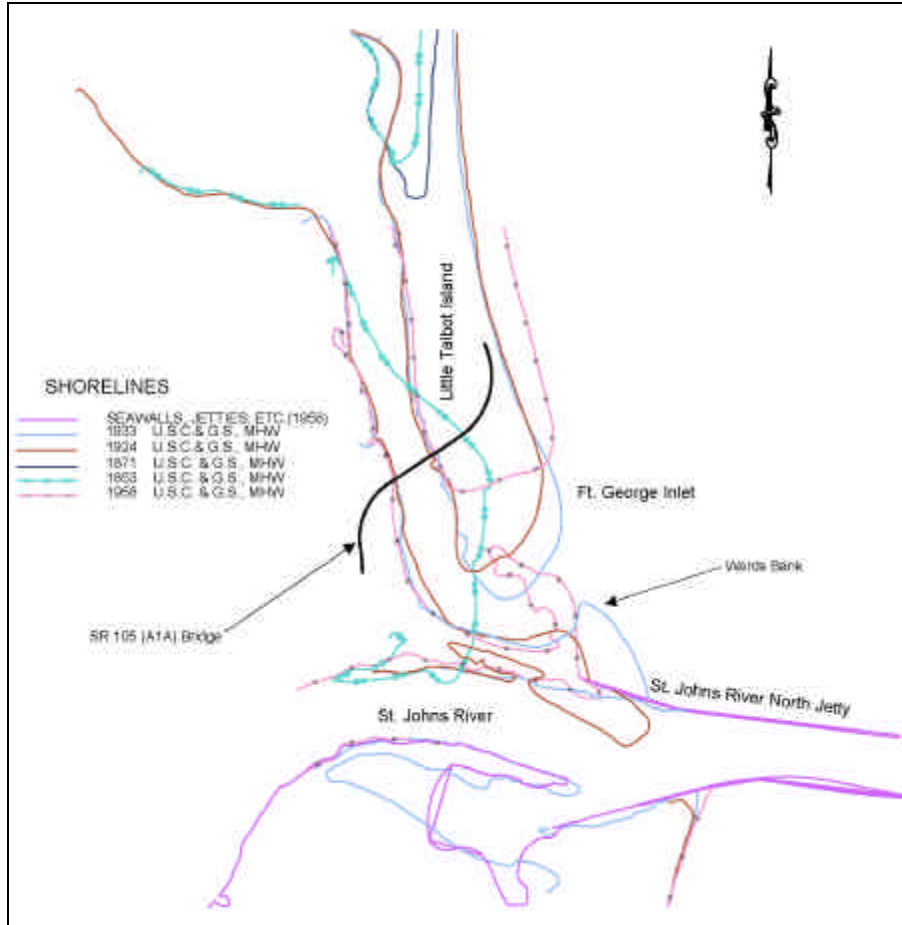


Figure 2. Historical shorelines at Ft. George Inlet (1853–1958)

During the initial period, pre-1885, no engineering activities were conducted near the inlet. Both the St. Johns River and Ft. George inlets existed as natural inlets. Following construction of the submerged permeable St. Johns River north jetty in 1885, entrapment of sand from the littoral zone caused the south shoreline of Little Talbot Island to advance south. This induced a southerly migration of Ft. George Inlet that subsequently caused severe erosion at the north jetty of the St. Johns River. Figure 2 illustrates these channel migrations as changes in shoreline location between 1871 and 1924. To protect the north jetty, groins were constructed along the south shore of Ft. George Inlet (Ward’s Bank) and backfilled with 2.5 million cy of dredge material. In addition, the north jetty was capped and made impermeable in 1934.

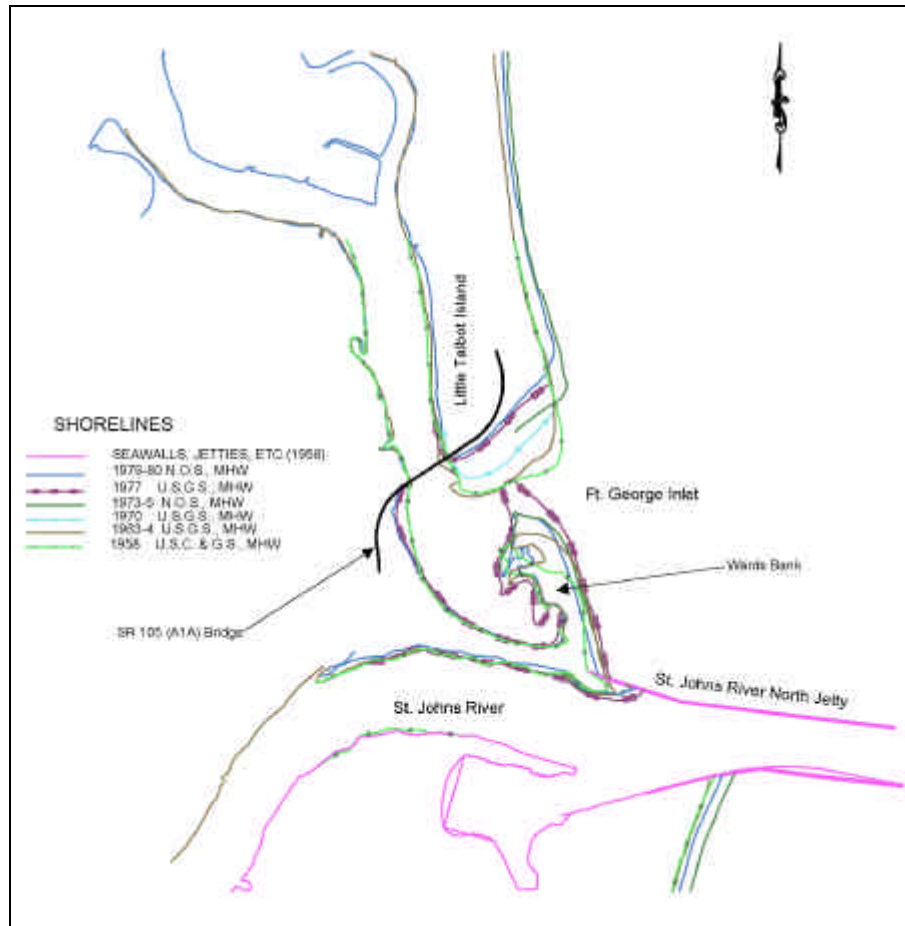


Figure 3. Historic shorelines at Ft. George Inlet (1958–1980)

Following modifications to the north jetty, the inlet began to reverse its migration along a northerly track. As a result, Ward’s Bank began to advance north along with Little Talbot Island’s south shoreline. Figure 2 illustrates this trend as changes in shoreline location from 1933 to 1958. Kojima and Mehta (1979) attributed this northerly migration to sediment bypassing the inlet and to the impermeable north jetty’s influence on the littoral system.

Given the change in shoreline location presented in Figure 3, migration of the inlet continued through the 1970s. The continuing northerly inlet migration formed a sharp bend in the river immediately upstream of the inlet. The altered flow dynamics formed secondary flows. These flows produced a western shoreline migration immediately south of the bridge beginning in 1958 as both Figures 2 and 3 illustrate.

Table 1. Summary of Events Effecting the Shoreline at Ft. George Inlet		
Period	Events	Shoreline Change
Pre-1885	No engineering activities.	The Ft. George River Inlet existed as a natural inlet.
1885 – 1934	Construction of permeable submerged jetties at the St. Johns River Entrance channel. Subsequently raised to high water in 1910.	The inlet migrated south, while the south shoreline of Little Talbot Island advanced southward.
1934 – 1943	North St. Johns River jetty capped, impermeable in 1934.	The inlet and the south shoreline of Little Talbot Island continued to advance south.
1943 – 1949	SR 105 (A1A) Ft. George Bridge over Ft. George River constructed in 1949.	The inlet and Ward's Bank shoreline began to advance northerly. Subsequently, the south shoreline of Little Talbot Island retreated.
1949 – 1978	Post SR 105 (A1A) Ft. George Bridge construction.	The inlet and Ward's Bank shoreline continued to advance north and the south shoreline of Little Talbot Island continued to retreat. The bridge channel experienced serious scour.
1978 – 1999	FDOT constructed revetments to protect the bridge and roadway	Countermeasures stabilized the protected shoreline, but elsewhere the shoreline continued to change

In 1949, the SR 105 (A1A) Ft. George Bridge was constructed. The 378-m long span crossed the Ft. George River approximately 6,000 m north of the inlet. With the presence of the bridge, the northerly inlet migration and subsequent upstream migration of the channel banks became a problem. In 1978, the FDOT constructed revetments at the east abutment along the south shoreline of Little Talbot Island and at the west abutment along the shoreline of Ward's Bay. Mehta and Marino (1987) and more recently Olsen Associates (1999) found that the FDOT efforts have successfully stabilized these shorelines. However, both investigators found the inlet continues its migration north, and the south shoreline of Ward's Bay continues to erode where the revetment has not stabilized the shoreline.

Much of the preceding discussion focused on the inlet and shoreline behavior south of the bridge. North of the bridge, the shorelines appear much more stable with localized exceptions. Since 1933, the west shoreline of Ft. George River north of the bridge has exhibited no perceptible migration. Much of the east shoreline, however, has undergone a steady eastward retreat. The largest recession rate, about 3 m/yr from 1933 to 1980 and 9 m/yr from 1980 to 1998, occurs along a 600-m reach approximately one mile north of the bridge where the river bends south. The bend has shown no signs of migrating south towards the bridge. The shoreline between the bend and the bridge steadily receded from 1924 to 1986 (with some accretion from 1970 to 1980). Since 1986, however, this reach of the shoreline has appeared stable except for a 60-m section at the end of the revetment. This shoreline, resembling a classic crenulated bay downdrift of a headland, eroded 3 m/yr

since 1986. The predominant cause of erosion appears to be strong ebb flow eddies. Wave diffraction appears to be only a minor, if any, influence. If unabated, the erosion will soon encroach the bridge abutment. West/inland from the river bend, the river has remained in its present location since bridge construction.

Plotting the mean high water (MHW) positions, referenced to Florida DEP monuments, allowed evaluation of shoreline accretion/erosion along Little Talbot Island and Ward's Bank. Two sources provided the data (plotted in Figure 4) for this analysis — a 1979 – 1980 N.O.S. MHW survey and a 2001 Taylor Engineering MHW survey. Figure 4 also shows the locations of the monuments. These data served as input to calculate the shoreline accretion or erosion rates shown in Figures 5 and 6. Shoreline change rates for Little Talbot Island indicate that the island has experienced significant accretion at the northern tip (T-001A and R-001). This accretion is directly attributable to the attachment to the north end of the island of transient shoals that cross Nassau Sound. Beyond this localized area, the northern half of the island (R-003 through R-009) exhibits erosion (-5.8 m/yr on average) consistent with a shoreline downdrift of an inlet (Nassau Sound). The southern half of the island (R-010 through R-020) exhibits accretion (+4.2 m/yr on average) consistent with the shoreline updrift of an inlet (Ft. George Inlet). The exception, of course, is the shoreline (R-021 through R-025) influenced by the migration of the inlet. In this area, the shoreline has receded -9.1 m/yr on average with a maximum of -15.4 m/yr at monument R-024.

Figure 6 shows the shoreline change rates for Ward's Bank. From the figure, the northern tip of the bank exhibited significant accretion over the last 21 years. The tip of the spit (R-026B) exhibited the most accretion, growing 16.0 m/yr. Interestingly, the ocean side of the spit has receded an average of 0.7 m/yr during this period. The net effect of these trends is an elongation of the spit as the inlet migrates northward.

In summary, the location and configuration of Ft. George Inlet has varied considerably over the period studied. Most inlet movement results from the numerous structural modifications to the St. Johns River Entrance. North of the SR 105 (A1A) Ft. George Bridge, the east river shoreline appears stable except for two locations. Similarly, the coastal shoreline of Little Talbot Island erodes north of the revetment. As stated in the previous chapter, backpassing sediment to the south tip of Little Talbot Island may mitigate this erosion to some extent.

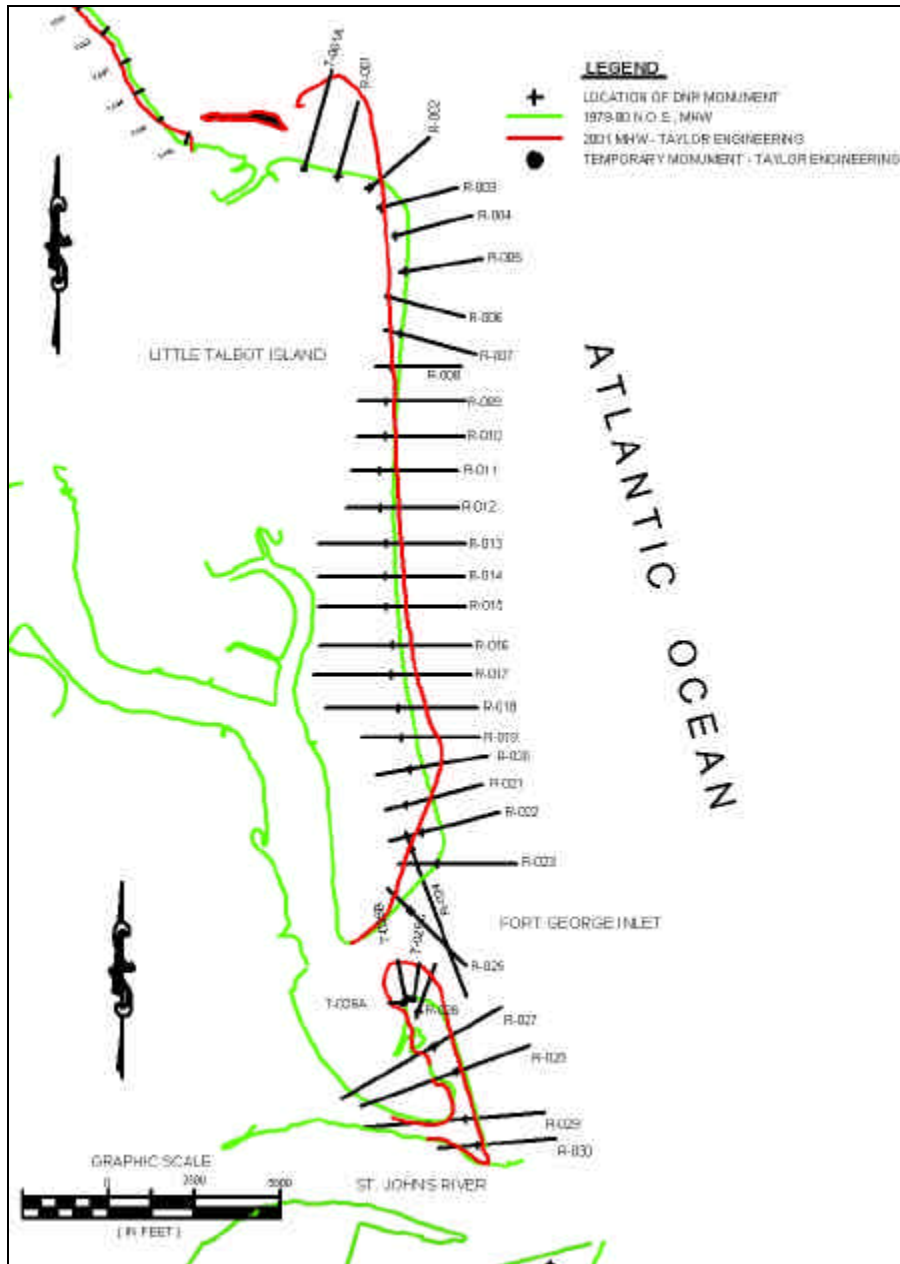


Figure 4. Transect locations

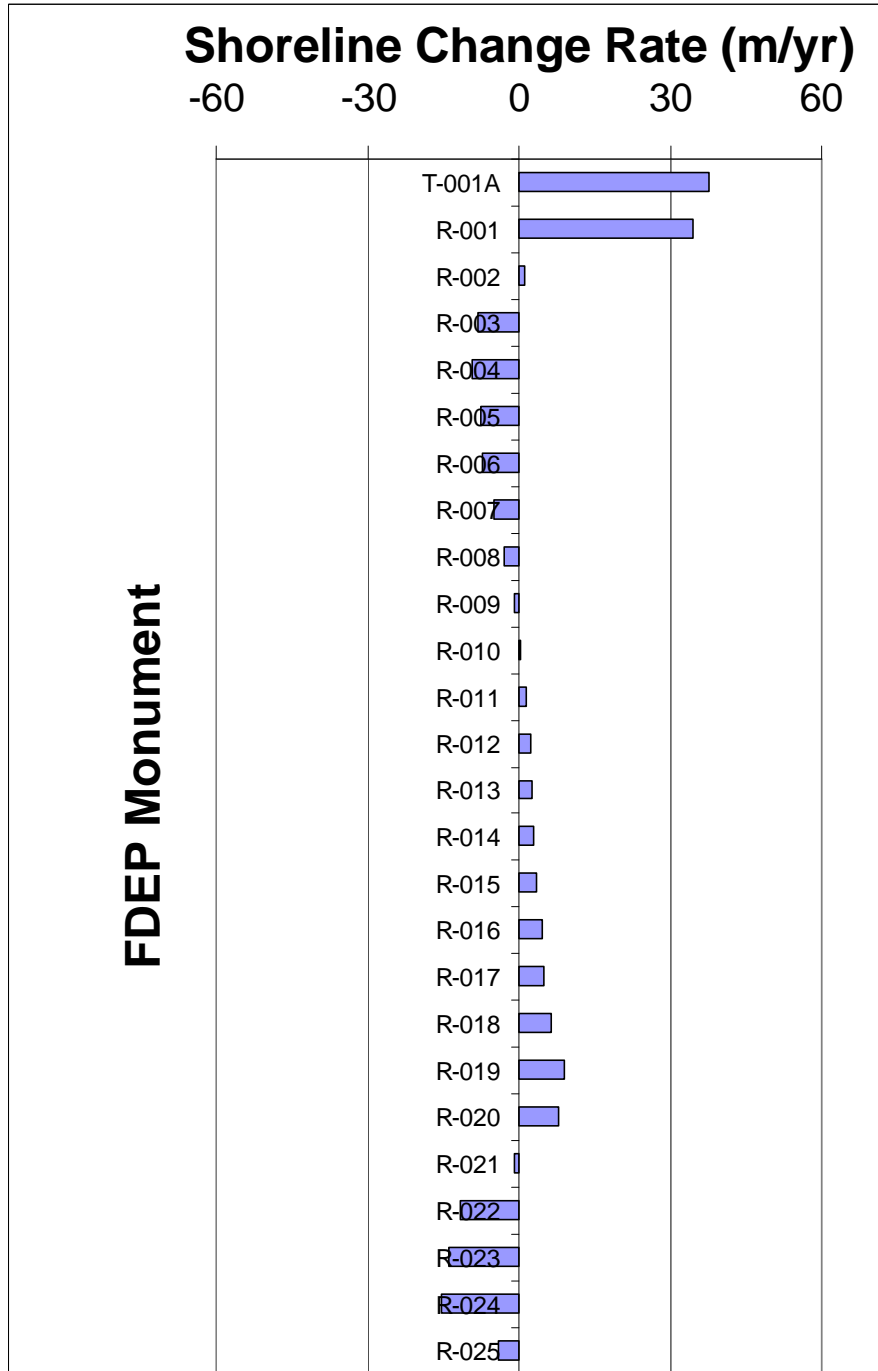


Figure 5. Shoreline change rate along Little Talbot Island

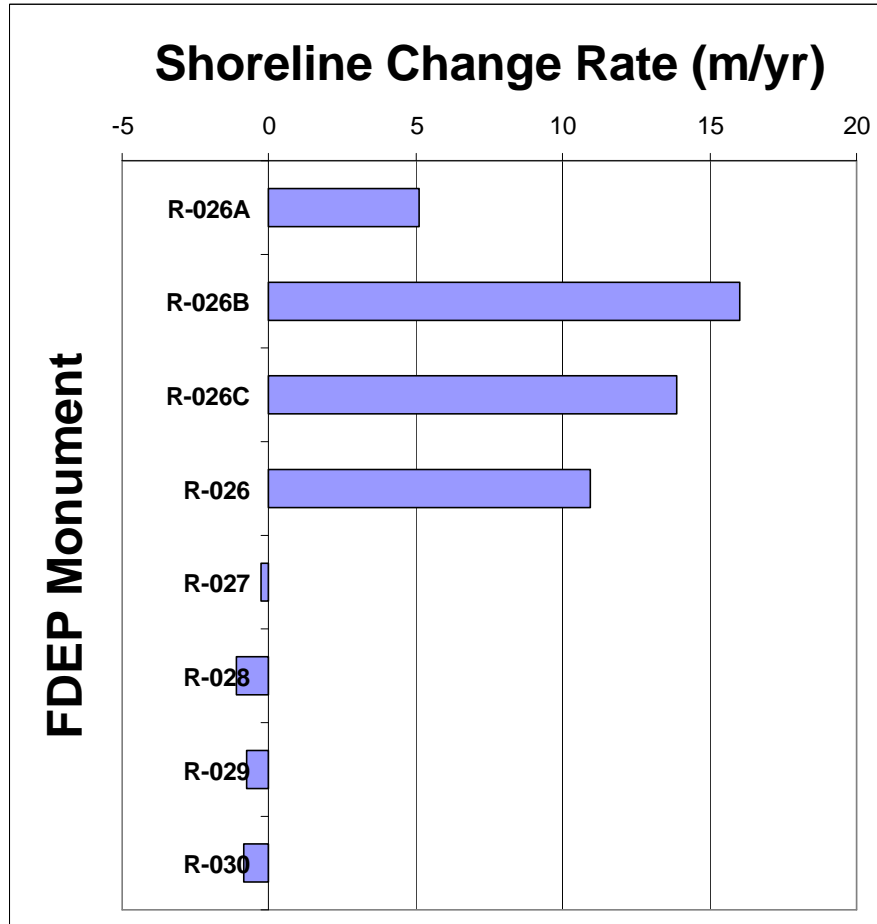


Figure 6. Shoreline change rate along Ward's Bank

Tidal Datums

Table 2 presents tidal datums near Ft. George Inlet. The values for Ft. George River are based on five months of observations, from April 1978 to September 1978 at Kingsley Plantation on the northern tip of Ft. George Island (Lat 30° 26.4' Long 81° 26.3'). Those observations were referenced to the NOAA's National Oceanic Service (NOS) Mayport (872 0220) control tide station for the 1960 – 1978 tidal epoch. The values for Little Talbot Island are based on four months of observations, from May 1974 to August 1978 at the end of the fishing pier on the southern end of Little Talbot Island on the Atlantic Ocean (Lat 30° 25.8' Long 81° 24.3'). Those observations were referenced to the NOAA's National Oceanic Service (NOS) Fernandina (872 0030) control tide station for the 1960 – 1978 tidal epoch. The tides at Ft. George Inlet are semidiurnal.

Tidal Datum Type	Elevation (m, NGVD)	
	Ft. George River	Little Talbot Island (Atlantic Ocean)
Highest Observed Water Level	+1.43	+1.77
Mean Higher High Water (MHHW)	+0.98	+1.13
Mean High Water (MHW)	+0.88	+1.01
Mean Tide Level	+0.15	+0.15
Mean Low Water (MLW)	-0.58	-0.67
Mean Lower Low Water (MLLW)	-0.64	-0.73
Lowest Observed Water Level	-1.04	-1.71

Wave Climate

WIS Station 26, located at 30.25°N latitude and 81.25°W longitude, provided the characterization of the offshore wave data. The data from this station spanned the 20-yr period 1976 to 1995. Except for a few extreme hurricanes, the data included most hurricanes that passed the area during these years. Calculated wave statistics, shown in Table 3 and in the wave rose shown in Figure 7, indicate waves enter the area predominantly from the east (41%). Approximately 79% of these waves measure from 0.5 to 1.5 m in height. The next most probable wave direction is the ENE quadrant (27%) followed by the ESE quadrant (10%). Average wave height for all direction bands measures 1.07 m.

Tables 4, 5, and 6 give the WIS-provided occurrences of wave height, peak wave period, and peak direction. Table 4 shows large waves mostly occur from September to December during hurricane season and from January to March due to northeastern winds. Northeastern waves occur every month with lower occurrences in July and August. Waves larger than 5 m tend to occur from September to January. Table 5 indicates incident waves have predominant periods between 8 to 10 s. Peak wave directions occur predominantly between 56° and 101° clockwise from true north.

Table 3. Normalized Probability of Wave Occurrence for WIS Station 2026 (1976 – 1995)

Wave Direction	Wave Height (m)						Total Prob./Dir
	0 - 0.5	0.5 - 1.0	1.0 - 1.5	1.5 - 2.0	2.0 - 4.0	> 4.0	
N	0.000257	0.006297	0.006999	0.004073	0.001352	0.000000	0.018977
NNE	0.000650	0.007769	0.008573	0.005835	0.003970	0.000034	0.026831
NE	0.002242	0.020671	0.019131	0.012115	0.010387	0.000445	0.064990
ENE	0.011858	0.083436	0.087902	0.045294	0.036413	0.001882	0.266786
E	0.031913	0.222964	0.101164	0.033984	0.019559	0.000992	0.410575
ESE	0.010421	0.058368	0.017454	0.006400	0.002909	0.000017	0.095568
SE	0.000530	0.018121	0.007016	0.003884	0.001249	0.000000	0.030801
SSE	0.000205	0.009309	0.004569	0.001437	0.000530	0.000000	0.016051
S	0.000325	0.006348	0.003354	0.000667	0.000103	0.000000	0.010797
SSW	0.000205	0.005305	0.003371	0.000308	0.000034	0.000000	0.009223
SW	0.000325	0.005031	0.002772	0.000205	0.000086	0.000000	0.008419
WSW	0.000068	0.003936	0.001831	0.000222	0.000034	0.000000	0.006092
W	0.000154	0.003474	0.001335	0.000205	0.000051	0.000000	0.005219
WNW	0.000154	0.003097	0.003097	0.000359	0.000120	0.000000	0.006828
NW	0.000034	0.003268	0.005938	0.000941	0.000154	0.000000	0.010335
NNW	0.000137	0.004535	0.005801	0.001711	0.000291	0.000000	0.012474
Total Prob./ Range	0.05948	0.461927	0.280305	0.117642	0.077242	0.003371	

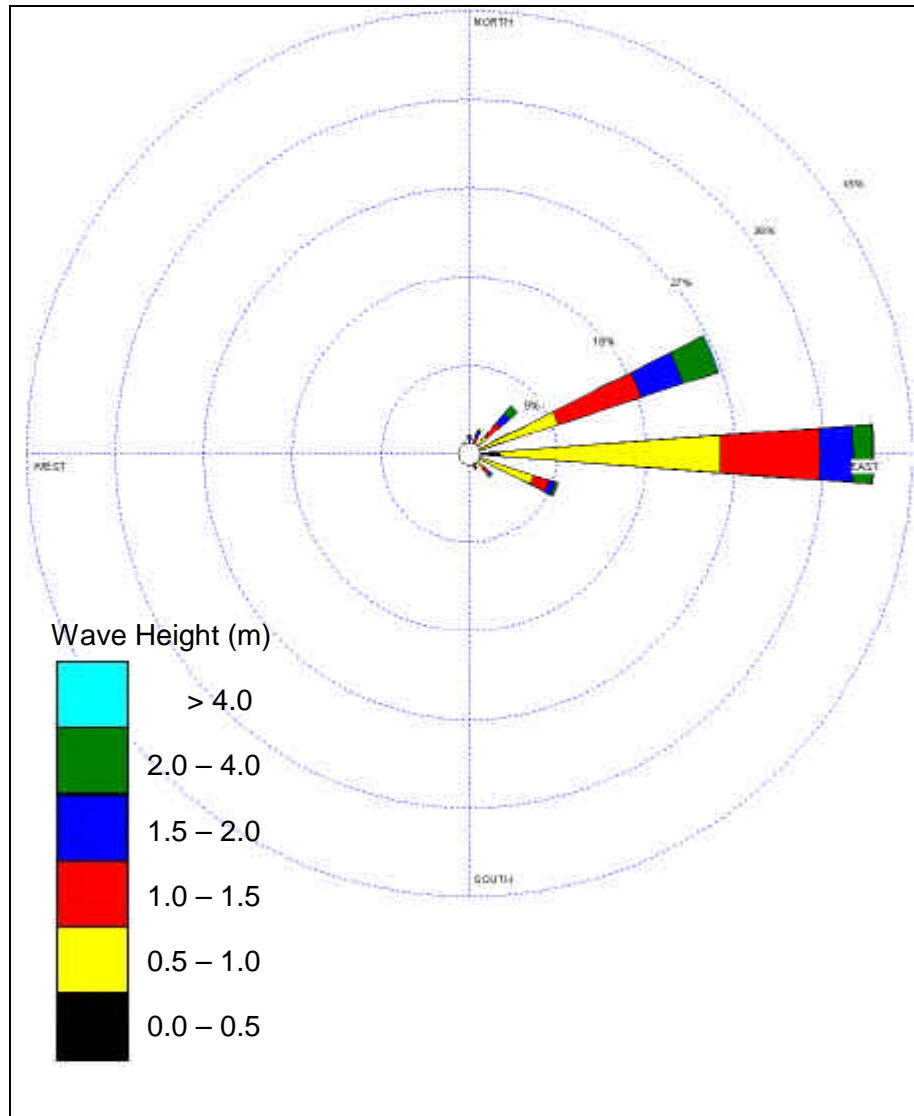


Figure 7. Wave rose at WIS Station 2026 (1976 – 1995)

Table 4. Occurrences of Wave Height by Month for WIS Station 2026 (1976 – 1995)													
H_{m0} (m)	JAN	FEB	MAR	APR	MAY	JUN	JUL	AUG	SEP	OCT	NOV	DEC	TOTAL
0.00 - 0.49	207	190	207	185	270	523	753	515	236	98	95	199	3478
0.50 - 0.99	1684	1625	1696	2059	2941	3400	3798	3361	2122	1330	1206	1773	26995
1.00 - 1.49	1586	1550	1816	1699	1387	728	353	784	1384	1817	1730	1547	16381
1.50 - 1.99	783	613	806	643	290	125	44	157	599	1067	1036	712	6875
2.00 - 2.49	382	316	273	178	65	23	9	79	253	400	466	437	2881
2.50 - 2.99	204	118	100	21	7	1	1	36	72	170	165	179	1074
3.00 - 3.49	69	43	38	10			2	18	30	55	49	60	374
3.50 - 3.99	24	22	21	5				8	40	16	26	23	185
4.00 - 4.49	15	26	3					2	19	4	12	14	95
4.50 - 4.99	4	17							14	1	5	10	51
5.00 - 5.49	2								4		3	3	12
5.50 - 5.99									27	2	7	3	39
> 6.00													0
TOTAL	4960	4520	4960	4800	4960	4800	4960	4960	4800	4960	4800	4960	58440

Tp (sec)	JAN	FEB	MAR	APR	MAY	JUN	JUL	AUG	SEP	OCT	NOV	DEC	TOTAL
3.0 - 3.9	47	43	23	25	40	97	141	80	35	10	26	42	609
4.0 - 4.9	310	343	296	265	190	198	159	139	93	99	160	367	2619
5.0 - 5.9	183	231	213	132	170	101	94	103	208	218	169	285	2107
6.0 - 6.9	177	220	186	144	217	353	320	349	391	341	252	236	3186
7.0 - 7.9	161	225	303	277	586	1004	1256	1196	883	595	342	236	7064
8.0 - 8.9	300	435	462	510	1073	1389	1626	1515	762	789	650	606	10117
9.0 - 9.9	727	742	705	664	949	740	795	612	631	896	866	706	9033
10.0 - 10.9	850	666	684	583	577	344	261	349	426	653	735	460	6588
11.0 - 11.9	549	432	466	478	373	221	190	201	332	421	421	438	4522
12.0 - 12.9	401	227	398	528	327	164	71	158	292	357	256	352	3531
13.0 - 13.9	322	181	446	481	216	97	42	101	239	246	284	358	3013
14.0 - 14.9	317	189	282	332	126	48	4	67	158	122	217	296	2158
15.0 - 15.9	194	157	178	184	72	33	1	32	121	70	147	257	1446
16.0 - 16.9	152	162	125	83	24	6		25	91	54	109	165	996
17.0 - 17.9	104	111	71	55	10	3		15	41	38	72	71	591
18.0 - 18.9	76	74	51	20	7	2		10	29	21	34	41	365
19.0 - 19.9	50	43	30	24	3			2	27	19	35	19	252
> 20.0	40	39	41	15				6	41	11	25	25	243
TOTAL	4960	4520	4960	4800	4960	4800	4960	4960	4800	4960	4800	4960	58440

Table 6. Occurrences of Peak Wave Direction by Month for WIS Station 2026 (1976 – 1995)

DIR. BAND & CENTER	JAN	FEB	MAR	APR	MAY	JUN	JUL	AUG	SEP	OCT	NOV	DEC	TOTAL
348.75 - 11.24 (0.0)	100	100	42	24	19	6			4	51	80	126	552
11.25 - 33.74 (22.5)	57	66	36	36	27	4	3	2	16	106	68	126	547
33.75 - 56.24 (45.0)	114	99	91	56	71	35	14	31	64	234	128	155	1092
56.25 - 78.74 (67.5)	1961	1788	2140	2327	1933	1268	642	906	2247	2531	2066	2325	22134
78.75 - 101.24 (90.0)	2280	1989	2140	1981	2609	3211	3965	3817	2328	1947	2237	1736	30240
101.25 - 123.74 (112.5)	36	45	92	78	92	35	54	55	57	17	28	34	623
123.75 - 146.24 (135.0)	27	16	58	41	58	11	21	26	9	13	11	18	309
146.25 - 168.74 (157.5)	18	12	38	26	20	16	13	15	9	2	6	17	192
168.75 - 191.24 (180.0)	24	11	42	27	19	23	22	22	9	6	14	35	254
191.25 - 213.74 (202.5)	23	38	49	28	18	35	47	32	30	6	21	28	355
213.75 - 236.24 (225.0)	29	45	44	24	23	76	55	26	7	13	13	40	395
236.25 - 258.74 (247.5)	27	37	30	17	24	57	67	22	2	3	5	43	334
258.75 - 281.24 (270.0)	44	54	27	18	13	17	49		2	4	7	38	273
281.25 - 303.74 (292.5)	70	76	35	46	17	4	8			14	25	58	353
303.75 - 326.24 (315.0)	104	58	54	40	13	2		3	6	4	41	88	413
326.25 - 348.74 (337.5)	46	86	42	31	4			3	10	9	50	93	374
TOTAL	4960	4520	4960	4800	4960	4800	4960	4960	4800	4960	4800	4960	58440

Bathymetric Description

The numerical simulation of waves and tidal currents in the Ft. George Inlet vicinity requires specific knowledge of the subaqueous region surrounding the inlet. Obtaining this information required two separate survey efforts. Taylor Engineering performed a berm break survey of Little Talbot Island, Ft. George Inlet, Ward's Bank, Nassau Sound, and South Amelia Island in June and July 2001. This information provided the inputs to calculate the shoreline changes presented in the Historical Inlet Migration subsection. The second survey effort involved obtaining a detailed description of the bathymetry offshore of the inlet, through the inlet, in Ward's Bay, and up the Ft. George River. Morgan & Eklund, Inc. performed the survey in July 2001. Figure 8 displays the results of this survey and the berm break survey.

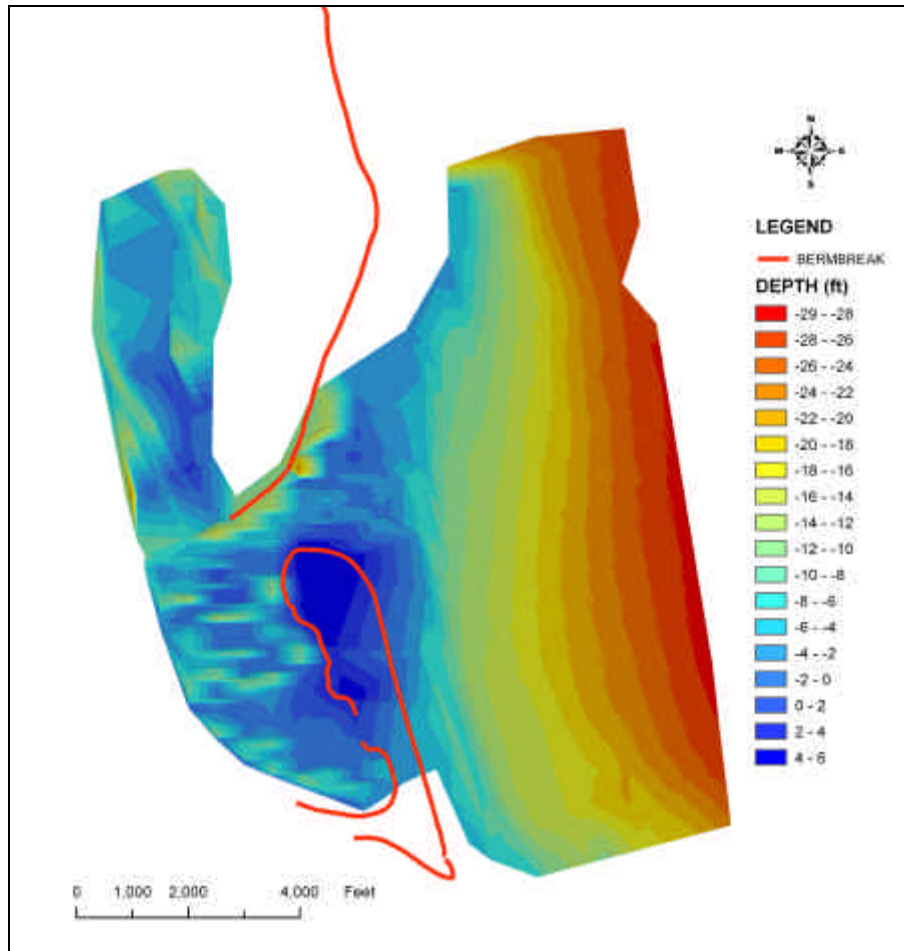


Figure 8. Bathymetry contours near Ft. George Inlet (2001)

The survey displayed in the figure captures several important bathymetric features. The survey indicates that a large coherent flood shoal lies just north of the A1A Bridge. South of this area, the survey shows several smaller bar-like shoals in Ward's Bay. A deep tidal channel runs just south of the southern tip of Little Talbot Island. The survey also shows tidal

flats that extend from the tip of Ward's Bank. Finally, the survey partially captures the ebb shoal at the northernmost, ocean edge of the survey boundary.

Discerning how the bathymetry evolves over time requires comparison to an earlier survey. The most complete bathymetric survey of this area occurred in 1998 in support of an Olsen Associates, Inc. shoreline erosion study in 1999. The survey, displayed in Figure 9, shows several of the same features pointed out in the 2001 survey. From the contours displayed in the figure, both the resolution and coverage of the 1998 survey were superior to the resolution and coverage of the 2001 survey.

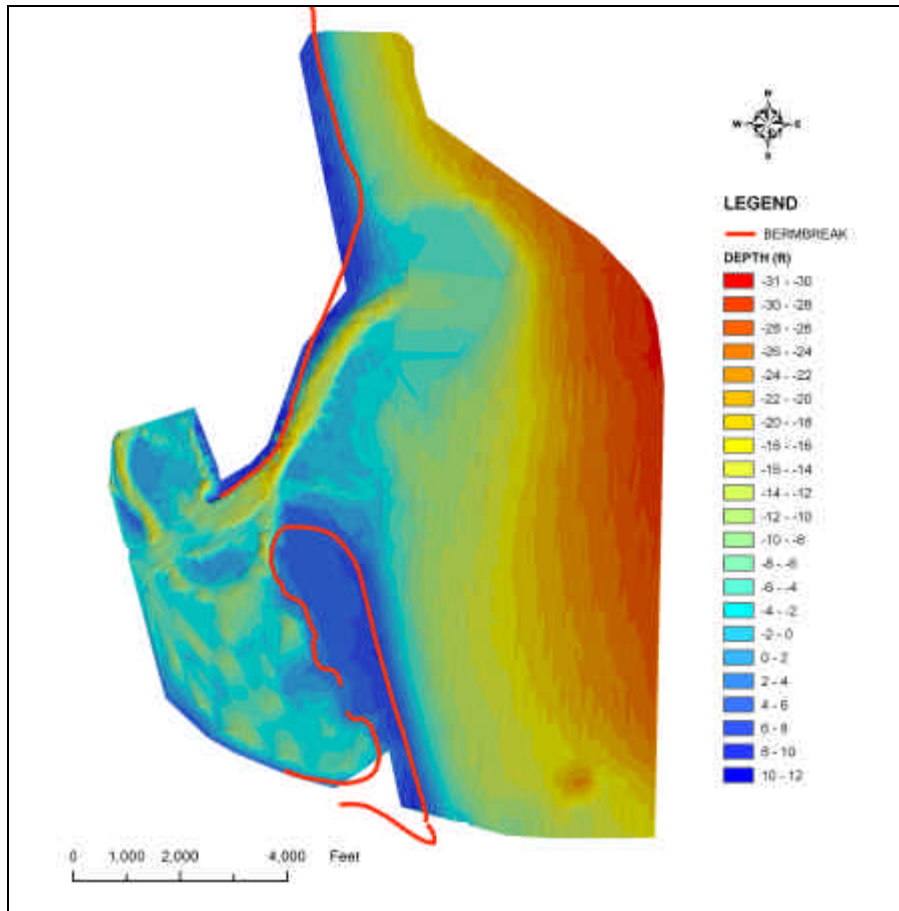


Figure 9. Bathymetry contours near Ft. George Inlet (1998 - from Olsen Associates, Inc.)

Both the 1998 and 2001 surveys were input into the DMS-Data Manager. The DMS-Data Manager is a GIS tool developed specifically to examine persistent shoaling in navigation channels. In this instance, the DMS-Data Manager created a surface indicating the difference between the two input bathymetries. Figure 10 shows the surface created by subtracting the 1998 bathymetry from the 2001 bathymetry over the area resulting from the spatial intersection of the two surveys. In the figure, positive contours

indicate areas where the bed has shoaled and negative contours indicate areas where the bed has eroded. The figure shows that this area experienced significant changes over this short, three-year period. The offshore region exhibited an overall accretional trend indicative of sediment impoundment north of the jetties that stabilize the St. Johns River Entrance. In the vicinity of the ebb shoal (area 1), a region of erosion (red contours) abuts a region of accretion immediately north (green contours). This pattern suggests northern migration of the ebb shoal following the migration of the tidal channel through the inlet. The area of accretion north of Ward's Bank (area 2) exhibited continued growth of the tidal flats north of the spit. The alternating strips of erosion and accretion near the tip of Little Talbot Island (area 3) illustrates the northward migration of the thalweg through the inlet. In the interior, a region of accretion north of the A1A Bridge (area 4) denotes the continued growth of the flood shoal. Within Ward's Bay (area 5), alternating patterns of erosion and accretion indicate that the bathymetry fluctuated greatly from 1998 to 2001. Finally, the center of Ward's Bank (area 6) exhibited erosion consistent with the findings of the shoreline behavior analysis presented earlier.

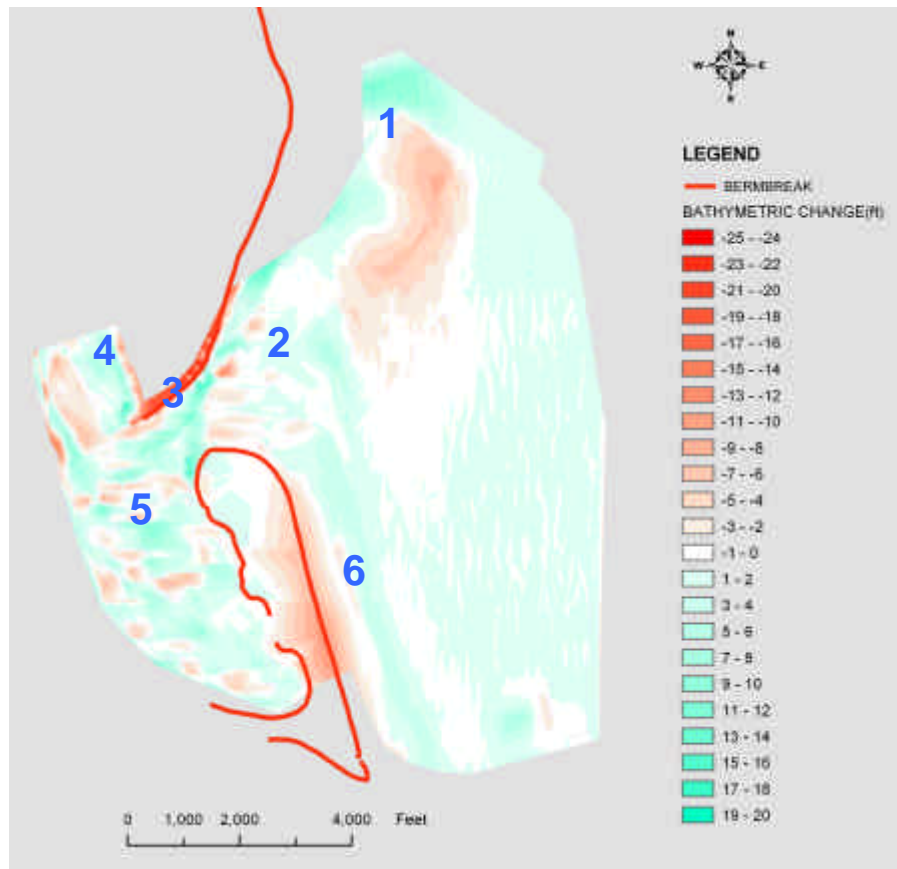


Figure 10. Bathymetric change between 1998 and 2001

Proposed Borrow Sites

The bathymetric comparison presented in the previous section indicated that the region surrounding Ft. George Inlet comprises several areas of significant shoaling. Recognizing this fact, the participants in the Regional Sediment Management program identified three possible sources of sediment for bypassing to the beaches south of the St. Johns River Entrance or backpassing to nourish the southern tip of Little Talbot Island. Figure 11 indicates the location of each area. Selection of these areas required complying with the boundaries delineated by the Coastal Barrier Resources Act (CBRA). This act, originally authorized in 1982, established a policy that coastal barriers and their adjacent inlets, waterways and wetlands resources be protected by restricting Federal expenditures that have the effect of encouraging development of coastal barriers. The act provided for a Coastal Barrier Resources System (CBRS) that identified undeveloped coastal barriers along the Atlantic and Gulf Coasts, including islands, spits, tombolos, and bay barriers subject to wind, waves, and tides such as estuaries and nearshore waters. Except for specific exempted projects (e.g. dredging, Federal navigation projects, some habitat management and enhancement efforts), no new Federal expenditures or financial assistance are allowed for areas within the system. The purpose was to minimize loss of human life, wasteful expenditure of Federal revenues, and damage to fish, wildlife, and other natural resources associated with the development of coastal barriers. Portions of Ward's Bank and Ward's Bay, as well as the north jetty, fall within CRBA area PO2 (Figure 12).



Figure 11. Locations of proposed borrow sites



Figure 12. Location of CRBA area PO2

The first borrow site, area 1 in Figure 11, involves dredging the flood shoal north of the A1A Bridge. This area avoids the delineated CBRA area PO2. The most cost-effective operation for this site is backpassing to the southern tip of Little Talbot Island. For this study, this alternative assumes dredging to an elevation of -20 ft-NGVD. Based on this elevation, a volume of 1.2 million cubic yards of sediment available for backpass operations resides within this area. Environmental modeling of the area required generating an approximate shape and elevation of the nourished section of Little Talbot Island. For this study, the nourishment consisted of building the shoreline to a location approximately equivalent to the 1980 shoreline. Notably, this alternative did not significantly change the offshore region because the tidal channel through the inlet still exits at approximately the same location (only slightly south of the current location). The volume required to construct this renourishment equals approximately 930,000 cubic yards (assumes a +6 ft-NGVD elevation). This would make 270,000 cubic yards available for bypassing to the beaches south of the St. Johns River Entrance. Figure 13 details the dredged and constructed areas associated with this alternative.

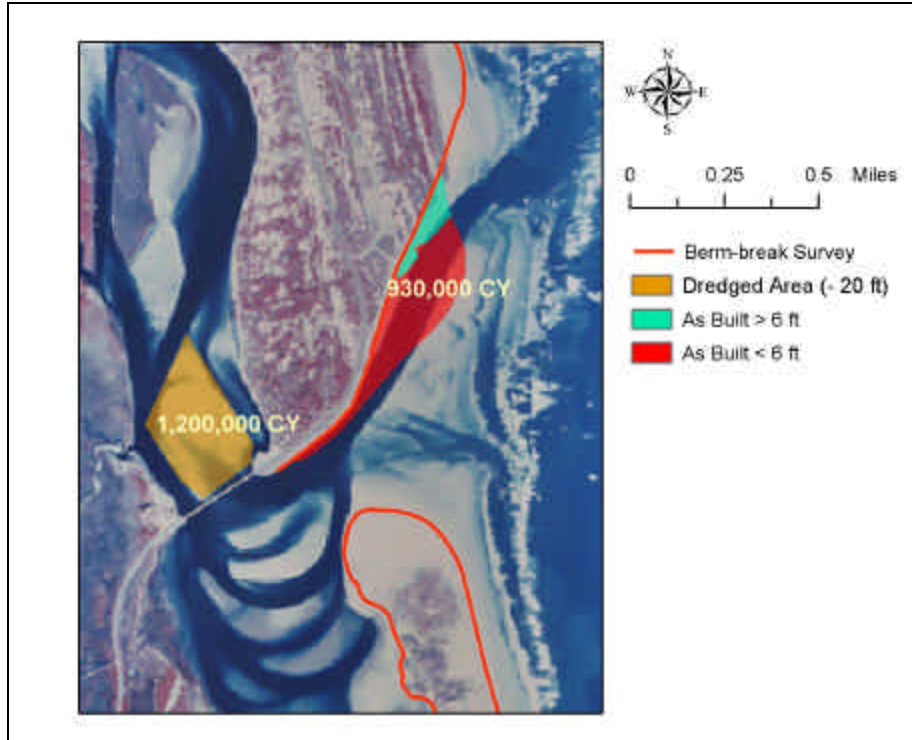


Figure 13. Dredging and backpassing associated with Alternative 1

The second borrow site, area 2 in Figure 11, lies within Ward’s Bay and across Ward’s Bank. The area also avoids CBRA area PO2. The most cost-effective operation for this site is backpassing to the southern tip of Little Talbot Island. The net effect of this alternative is reorientation of the inlet throat to an east-west alignment. For this study, this alternative assumes dredging to an elevation of -20 ft-NGVD. Based on this elevation, a volume of 3.5 million cubic yards of sediment available for backpass operations resides within this area. Environmental modeling of the area required generating an approximate shape and elevation of the nourished section of Little Talbot Island. For this study, the nourishment consisted of building the shoreline to a location approximately equivalent to the 1970 shoreline. The volume required to construct this nourishment equals approximately 2.2 million cubic yards (assumes a +6 ft-NGVD elevation). This would make 1.3 million cubic yards available for bypassing to the beaches south of the St. Johns River Entrance. Figure 14 details the dredged and constructed areas associated with this alternative.

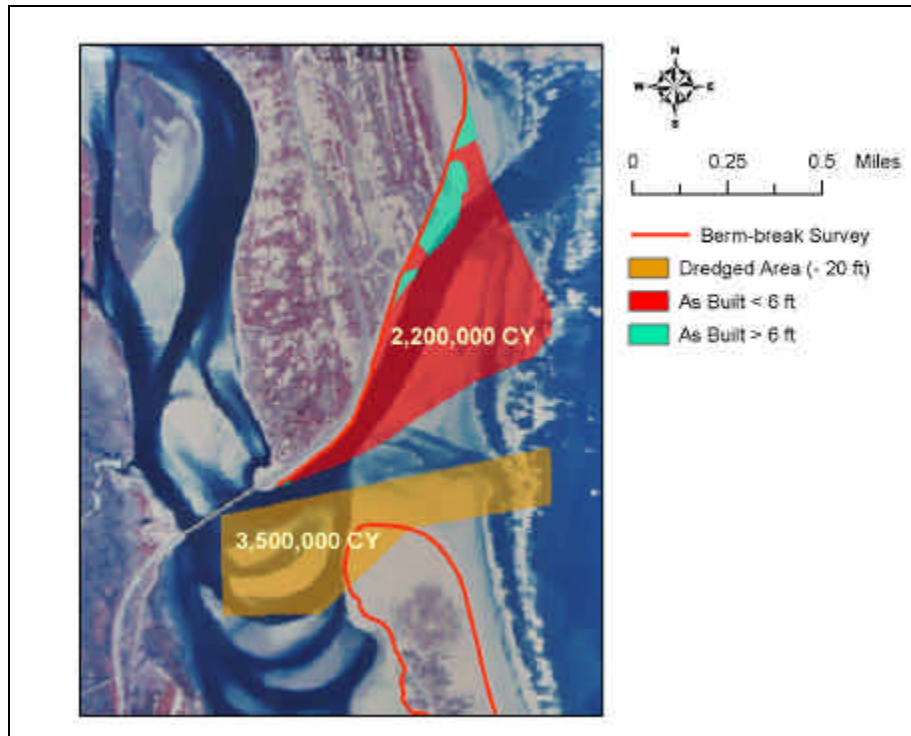


Figure 14. Dredging and backpassing associated with Alternative 2

The final alternative involves dredging the shoal that forms just south of the north jetty at the southern terminus of Ward's Bank. This shoal most likely forms as waves transport sediment through the west end of the north jetty. Although located within CBRA area PO2, mining this area may prove possible given the easements associated with the jetties. This alternative involves mining the shoal and bypassing the sediment south to the beaches south of the St. Johns River Entrance. The northern extent of this dredged area is offset 100 ft from the centerline of the jetty. This distance takes into account the width of the jetty foundation. According to the original construction documents from 1879, a typical cross section measures 174 ft in width (a half width of 87 ft from the centerline); timber planks beneath stone riprap compose the structure's foundation. Documents detailing the rehabilitation of the structure report that the jetty comprises a crest width of 10 ft, a maximum crest elevation of +14 ft-MLW, and side slopes of 1:1.5. If the structure in this area descended to a depth of -38 ft-MLW (equivalent to the depth of the current navigation channel), then the half width distance would equal 83 ft. Ward's Bank, however, has existed as a coherent structure since the time of the jetty's construction. As such, the depths in the area of interest were probably shallow at the time of construction. Construction of the jetty at its western terminus that includes dredging to a depth of almost 40 ft becomes highly unlikely. Therefore, the half width of the foundation probably measures less than the reported 87 ft or the calculated 83 ft. Regardless, a 100 ft offset accommodates both these distances. This study assumes that this alternative will involve dredging to a depth of -30 ft-

NGVD. The volume of sediment available for bypassing equals approximately 1.3 million cubic yards. This estimate assumes a subaerial shoal elevation equal to +3 ft-NGVD. Figure 15 details the dredging associated with this alternative.

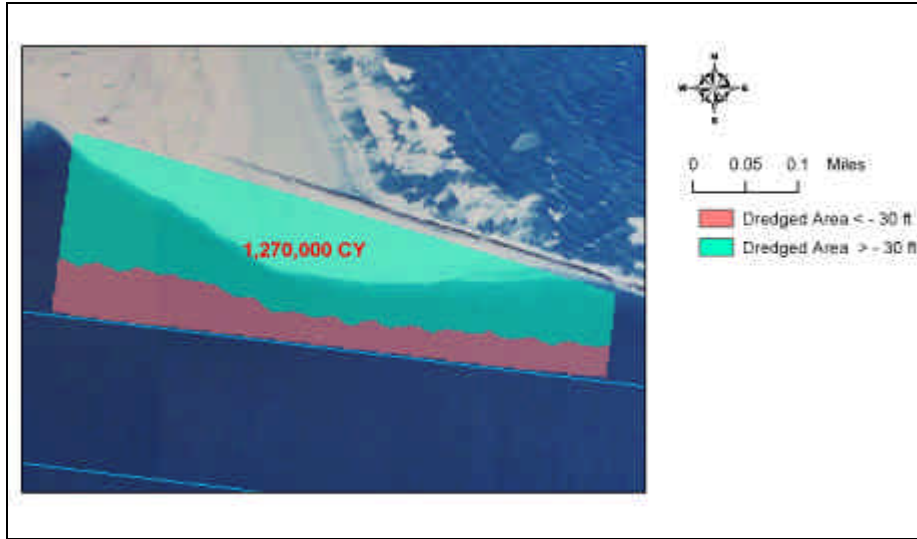


Figure 15. Dredging associated with Alternative 3

3 Circulation Modeling

As stated in Chapter 1, determining the impacts of the borrow sites and backpassing/bypassing operations includes an investigation into the specific changes to the tidal circulation patterns both within and around Ft. George Inlet and the St. Johns River. The circulation modeling detailed in this chapter builds upon work previously completed as a DMS application to shoaling within the Jacksonville Harbor Navigation Project, Jacksonville, Florida. This chapter discusses the circulation model setup, calibration, and simulations performed in support of this study. It also presents the procedure for examining the sediment transport within the channel associated with tidal circulation. The findings from this application are also discussed.

Model Setup

Ft. George Inlet, a natural inlet, lies just north of the St. Johns River near Jacksonville, Florida. Significant shoaling in multiple areas characterizes this migrating inlet. Northward migration of the channel through the inlet has caused severe erosion along the southern tip of Little Talbot Island and threatened A1A along this stretch of Little Talbot Island. The severity of the situation necessitated hardening the shoreline in 1978 by the FDOT to protect the infrastructure. An additional erosional shoreline lies on the north side of the A1A Bridge over the Ft. George River. Because tides dominate flow in the Ft. George River, the ADCIRC model (Advanced CIRCulation – Luetlich, et al. 1992) is the appropriate model to simulate flows in this area. Specifically designed to model hydrodynamic circulation of inlets and estuaries, the model implements tidal constituents obtained from the Le Provost et al. (1994) database to propagate the tide from offshore to the coastal or inland area of interest. ADCIRC — a two-dimensional, depth-integrated, finite-element hydrodynamic model — calculates water surface elevation and flow velocities over the defined mesh. The mesh is often extensive due to the large area required for tidal propagation. In the interest of efficiency, a design feature in ADCIRC allows its operation over a large range of element sizes. This allows the application of coarse resolution offshore and areas away from the point of interest, and the application of fine resolution in the desired area of study. ADCIRC can also simulate the effects of structures and specific channel features.

For this application, specifications for the simulation include tidal forcing applied to the open ocean boundary, constant flow boundary conditions applied to interior watersheds, quadratic bottom stresses, and wetting and drying. The wetting and drying option allows for simulation of areas such as tidal shoals exposed and inundated during the tidal cycle.

Mesh Development

Mesh development for this study takes advantage of the existing mesh developed for the Jacksonville Harbor Project. The Jacksonville Harbor mesh was extracted from the community model currently maintained by the USACE ERDC. Specifically, a large portion of the mesh was extracted from the community model for the entire southeast Atlantic coast. This portion includes the Florida and southeast Georgia region (St. Andrews Sound Entrance in Georgia to Ponce Inlet in Florida) and interior waters. Detail added to the community model at the specific project locations helped identify local flow parameters. Once completed, this detailed mesh will be reinserted into the community model to provide future benefits for other USACE projects within the model domain.

The detailed mesh, constructed to evaluate Ft. George Inlet, stretches approximately 175 km north and 230 km south of Ft. George Inlet and encompasses the Atlantic Ocean and the major water bodies from approximately Titusville, Florida to Savannah, Georgia (Figure 16). The mesh includes the St. Johns River (approximately 186 km) from its confluence with the Atlantic Ocean to Lake George; the inlets of Ft. George, Nassau Sound, St. Mary's Entrance, and St. Andrew's Sound; the interior waterways that connect these inlets to the St. Johns River; the Intracoastal Waterway from St. Augustine Inlet to Cumberland Sound; and the Atlantic Ocean to approximately 227 km offshore. The offshore boundary encompasses 562 km of the Atlantic Ocean. The model contains increased resolution within Ft. George Inlet (Figure 17). The mesh consists of 32,938 triangular elements and 19,781 nodes and covers a total area of 67,000 km². The largest element measures 59 km², and the smallest element measures 50 m². This translates to a largest to smallest area ratio of approximately 1,200,000:1.

Several data sources contributed to mesh construction. USGS Quadrangles, NOAA Navigation Charts and Digital Orthogonal Quadrangles (DOQQ) served as shoreline guides and provided additional bathymetry data where survey data was unavailable. A July/August 2001 survey of Ft. George Inlet provided the primary bathymetric description of the area of interest. A survey of Nassau Sound, conducted over the same period, gave a recent bathymetry for that area. Survey data from the USACE provided the primary source of bathymetric data for the St. Johns River area. These surveys covered the Jacksonville Harbor – Cuts 3-41, A, F, G, and the Terminal Cut, Chicopit Bay and Mt. Pleasant Creek, Mill Cove, and a triple sweep survey of the Intracoastal Waterway from 6.5 km south of the St. Mary's Entrance to approximately 29 km south of the St. Augustine Inlet. All of these surveys occurred during calendar year 2000 except the Chicopit Bay/Mt. Pleasant

Creek survey (dated March 1997). The St. Johns Water Management District (SJWMD) provided additional survey information from 1993 for the St. John's River from Palatka to the jetties at the river entrance and the maintained channel including Chicopit Bay. Table 7 summarizes the survey dates and coverages. The mesh horizontal control referenced Geographic NAD83, and the vertical control referenced the Mean Tide Level (MTL).

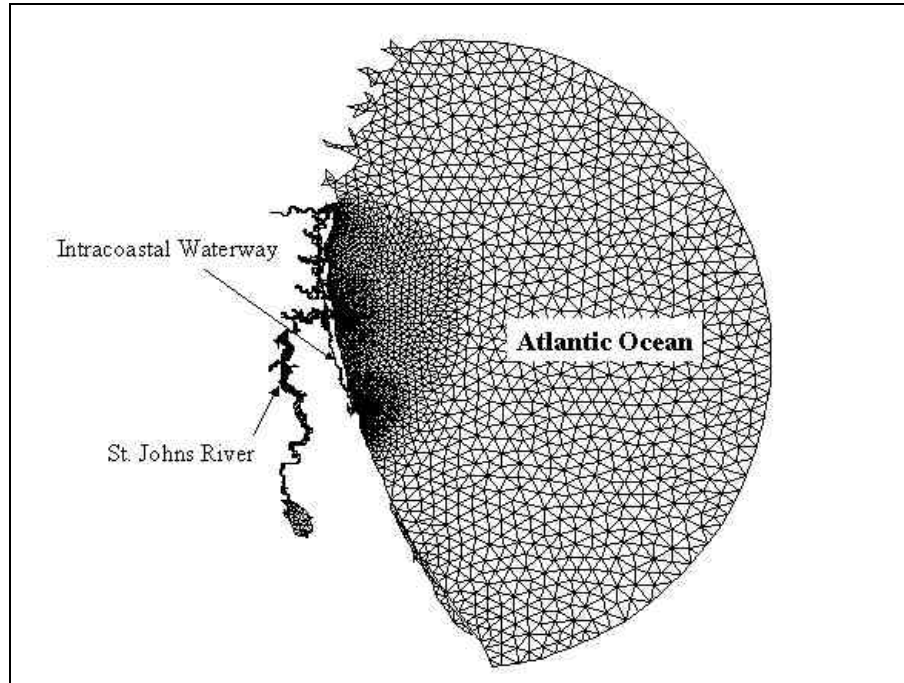


Figure 16. Model domain

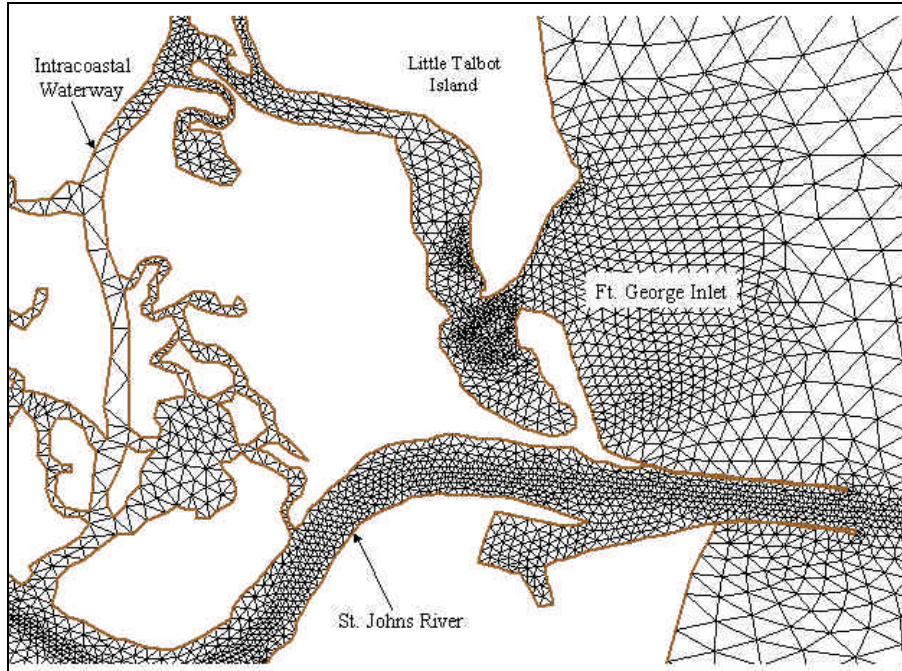


Figure 17. Model mesh in vicinity of Ft. George Inlet

Table 7. Survey information for mesh construction		
Agency	Date	Extent of Coverage
USACE	9/00-12/00	Jacksonville Harbor Project (Bar Cut 3 – Cut 41, Cuts A, F, and G, Terminal Channel Cut)
USACE	1/00	Intracoastal Waterway
USACE	3/97	Chicopit Bay / Mt. Pleasant
USACE	6/00	Mill Cove
SJWMD	1993	Jacksonville Harbor Project (Matthews Bridge to Jetties including Mill Cove)
SJWMD	1993	St. Johns River (Palatka to Jetties)
Morgan & Eklund	7/01	Ft. George Inlet
Morgan & Eklund	8/01	Nassau Sound

Boundary conditions

The boundary conditions consisted of both specified tidal forcing and constant flow boundary conditions. Along the ocean boundary, the K1, K2, M2, N2, O1, P1, Q1, and S2 tidal constituents generated the tides ADCIRC propagated through the mesh. By specifying the desired start day and duration of the simulation, the ADCIRC model applies the appropriate amplitude time sequence for each of the tidal constituents based on the Le Provost et al. (1994) database. The tide, therefore, accurately propagates from the ocean boundary toward the area of interest.

The simulation meshes contained several interior, constant flow boundary conditions. Table 8 presents the flow rates applied to the connecting creeks of the St. Johns River. The USGS delineated water management district GIS database provided the drainage areas for each tributary basin. Given the absence of flow rate data in some areas, the model simulations required estimates of mean flow rates from published historical data. Several daily flow rates (<http://waterdata.usgs.gov/nwis-w/FL>) for streams in the St. Johns River with similar land usage, slopes, and lake areas were plotted against their drainage areas to establish a trend (regression curve). Solutions from the corresponding regression equation estimated flow rates in all of the smaller contributing streams. This procedure generated estimated average flows for the month of March for the velocity calibration runs. These flows were deemed representative of the yearly averages and as such were applied for the remainder of the simulations as well. The exceptions to this were the St Johns and Nassau Rivers. Unlike the smaller streams, where rainfall provides the predominant flow, these rivers receive a substantial flow source from underground aquifers. The St Johns River (at the Main Street Bridge) experiences an average flow rate of 5,700 cfs (Spechler, 1996) based on 22 years of flow recorded from the U.S. Geological Survey (USGS). The Nassau River flow rate (4,137 cfs) was extrapolated from a published USGS gage at Hedges to include the entire river.

Table 8. Flow Rates for Connecting Creeks to the St. Johns River			
Stream Name	Contributing Creeks	Drainage Area (mi²)	Average flow rate (ft³/s)
Arlington River		21.1	32.5
	Pottsburg Creek	10.7	17.6
	Little Pottsburg Creek	3.6	6.6
	Silversmith	2.3	4.3
	Strawberry	4.6	8.3
Julington Creek		58.8	82.0
	Julington Creek	23.6	36.0
	Flora Branch	2.2	4.2
	Durbin Creek	26.2	39.6
	Oldfield Creek	4.5	8.1
	Cormorant Creek	2.3	4.5
Broward River		14.4	23.0
Dunn Creek		13.1	21.1
Browns Creek		4.9	8.7
Clapboard Creek		15.7	24.9
Greenfield Creek		2.9	5.5
Mt Pleasant Creek		3.3	6.1
Ortega River		40.7	58.8
	Ortega River	35.0	51.3
	Fishing Creek	5.7	10.0
Cedar River		18.7	29.1
	Cedar River	12.7	20.6
	Butcher Pen Creek	1.3	2.7
	Williamson Creek	1.5	2.9
	Unnamed Run	3.2	6.0
Lanceford Creek	Amelia River	27.3	41.1
Trout River		27.5	41.4
Ribault River		9.7	16.2
Moncrief Creek		5.9	10.4

Calibration

A calibrated model ensures an accurate depiction of the hydraulic characteristics in the area of interest. Calibration resulted from iterative adjustments to the model parameters and mesh extent until differences between measured water levels and calculated values generated from the ADCIRC model were acceptable. Error calculations quantify these results. For this study, error estimation included mean error, root-mean square (rms) error, and percent error.

The following equation provides an estimate of the mean error, E , the average of the deviation of the calculated from the measured values (water surface elevation):

$$E = \frac{\sum_{i=1}^N (\mathbf{c}_c - \mathbf{c}_m)_i}{N} \quad (1)$$

where \mathbf{c}_c is the calculated value, \mathbf{c}_m is the measured value, and N is the total number of data points. A positive value for the mean error would indicate that the model overestimates the event, while a negative value would indicate an underestimation.

The root-mean square error, E_{rms} , given by the following equation, indicates the absolute error of the comparison. The variables are the same as indicated above.

$$E_{rms} = \sqrt{\frac{\sum_{i=1}^N (\mathbf{c}_c - \mathbf{c}_m)_i^2}{N}} \quad (2)$$

The final error estimator, E_{pct} , is the percent error. This variable gives an indication of the degree to which the calculated values misrepresent the measured values. Percent error, defined in terms of rms error, is given as

$$E_{pct} = 100 \frac{E_{rms}}{R} \quad (3)$$

where R is a representative range of the variable \mathbf{c} . The R -value for the percent error water level calculations is the average of the measured tidal ranges, the difference between high and low values, over the period of the simulation.

The measured data for water level calibration came from an Olsen & Associates study on Ft. George Inlet (Olsen Associates, 1999). Water level comparisons were made at two locations: the ocean gage, located offshore of Nassau Sound near the U.S. Coast Guard's Nassau Sound navigation aid, and the bay gage, located approximately 3 km north of A1A Bridge over Ft. George River (Figure 18). Data from the ocean gage accounts for approximately a nine-day period from October 1, 1998 to October 10, 1998. The bay gage data accounts for an eight-day span from October 2 to October 9, 1998.

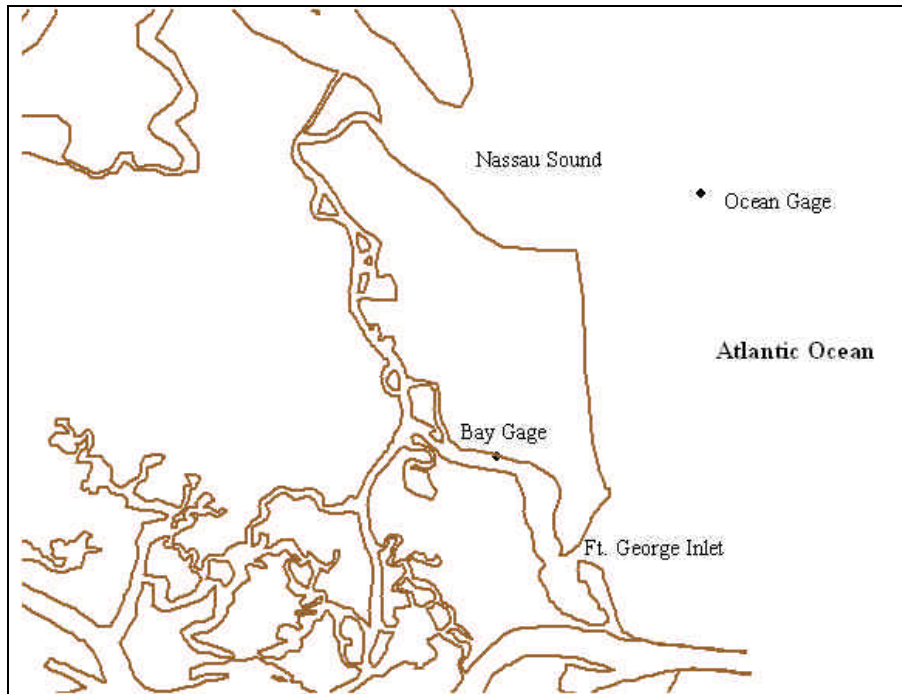


Figure 18. Water level gage locations

A friction factor of 0.0035 produced an average percent error of 9.7% for the water level calibration. Figures 19 and 20 compare the predicted model water level to the measured water level at the different gage locations. These figures indicate the model tended to overestimate the water level at both the bay and ocean gage.

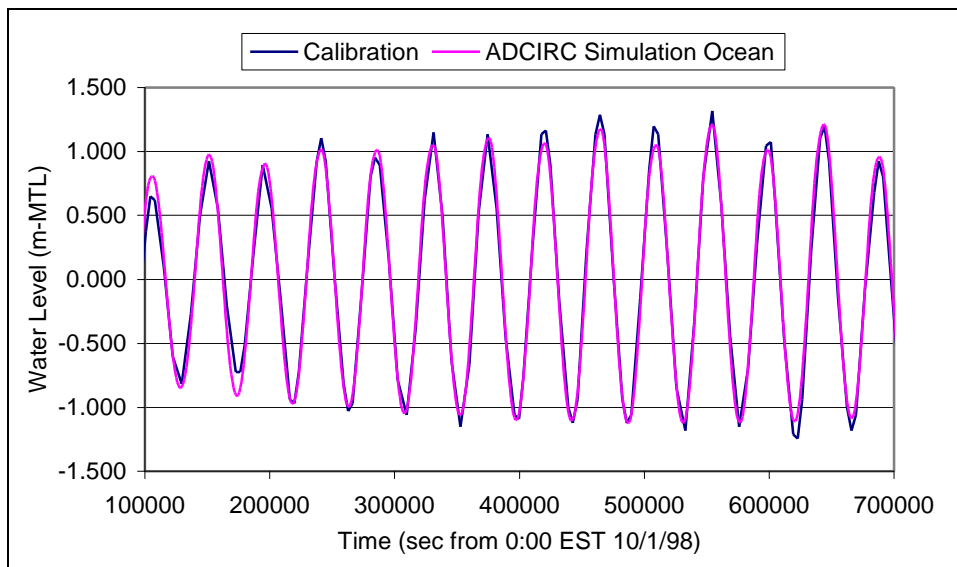


Figure 19. Calibration at ocean gage

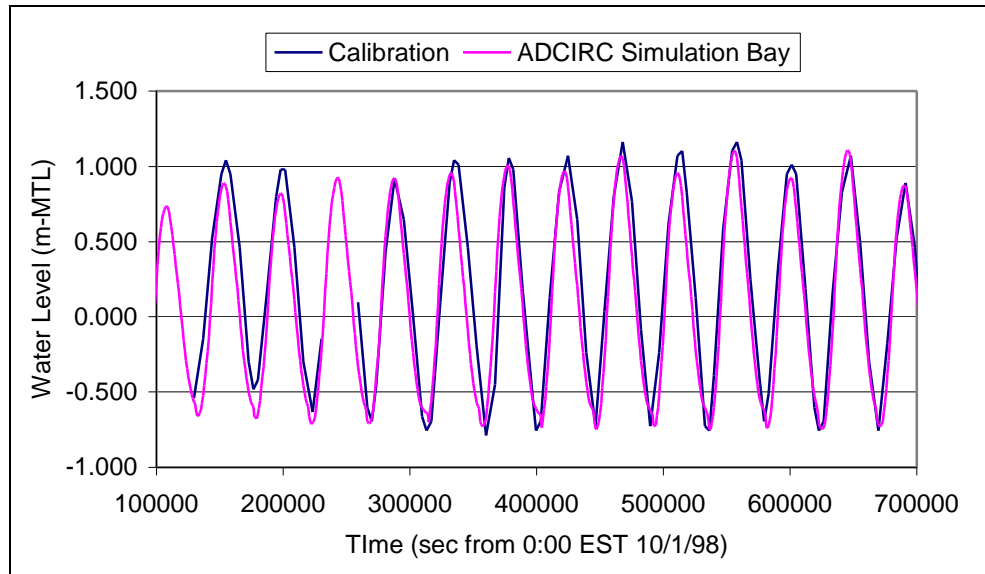


Figure 20. Calibration at bay gage

Table 9 presents the error calculations for the water level calibration. The simulated ocean gage data fell within 7.2% of the collected data, and the simulated bay gage data fell within 12.1% of the collected data. Results of the error estimation indicated a model well calibrated to water surface elevation.

Table 9. Error Results for Water Level Calibration			
Water Level Station	Mean Error, m	RMS Error, m	Percent Error
Ocean Gage	-0.01	0.16	7.2%
Bay Gage	-0.12	0.21	12.1%

Model Simulations

Model simulations indicate the expected impacts of each of the borrow sites and backpassing/bypassing operations to tidal circulations. Determining the exact changes in tidal circulation facilitates estimating the effectiveness of the alternative in terms of shore protection and ascertaining the change modifications have on the sediment transport climate and identifying the impacts that result from these changes. This investigation includes four simulations — existing conditions and each of the three alternatives presented in Chapter 2. The first simulation, an existing conditions simulation, provided a prediction of the tidal circulation that currently exists within Ft. George Inlet and the St. Johns River. It provided a baseline from which to compare simulations containing proposed shoal removal and backpassing operations. The three remaining simulations provided a means to examine the effects of shoal removal and bypassing/backpassing on flow within the affected areas. These simulations included:

- 1) Sediment removal from the shoal located immediately north of the A1A Bridge over Ft. George River and the corresponding backpassing to the southern tip of Little Talbot Island;
- 2) Sediment removal within Ward's Bay and across Ward's Bank and the corresponding backpassing to the southern tip of Little Talbot Island; and
- 3) Sediment removal from the area inside the Mayport jetties adjacent to Huguenot Park and subsequent bypassing to the beaches south of the jetties.

Given the detailed resolution of the mesh within Ft. George Inlet and the St. Johns River and time constraints, simulations only ran half of a lunar cycle. A two-week period that encompassed both spring and neap tide conditions, September 10 to September 24, 2001, provided the tidal boundary conditions for the simulations. As mentioned, the average yearly flows served as interior boundary conditions for the St. Johns River and contributing tributaries. Again, the tidal boundary conditions consisted of the K1, K2, M2, N2, O1, P1, Q1, and S2 tidal constituents. These constituents provided the tidal amplitudes appropriate to the date of the simulation based on the Le Provost et al. (1994) database. The model generated water surface elevation and velocity values at each node of the mesh.

The existing conditions mesh consisted of bathymetry values from the most recent surveys supplemented by navigation charts and USGS quadrangles as described in the Mesh Development section. For the two alternatives that involved mining shoals within Ft. George Inlet (Alternative 1: flood shoal mining and Alternative 2: Ward's Bank mining), elevations within the designated areas were deepened to approximately 6.1 m (-20 ft NGVD). The removed volume of sediment was added to the shoreline of Little Talbot Island to simulate backpassing of the sediment from Ft. George Inlet. The extended shoreline of Little Talbot Island was increased to an elevation of +1.8 m (+6.0 ft NGVD). Because the amount of sediment available for backpassing varies between these alternatives, the size and shape of the nourished area varied (for modeling purposes) as well. Also, because Alternative 1 calls for nourishment across the thalweg of the entrance channel without any additional dredging, the features of the model reflect the assumption that a channel, with the same cross-sectional area as the existing channel, would reestablish and hug the Little Talbot Island shoreline. For Alternative 3, north jetty shoal mining, the bathymetry within the designated area was deepened to approximately 9.1 m (-30 ft NGVD) to correspond to the bathymetry of the surrounding area. This alternative includes sediment bypassing to the beaches south of the St. Johns River Entrance. As the sediment placement on the shoreline south of the jetty would have negligible impact on flows within the St. Johns River or Ft. George Inlet, the mesh did not reflect beach nourishment from bypassing. Figures 21 through 24 display the existing and post-shoal removal bathymetries for each alternative.

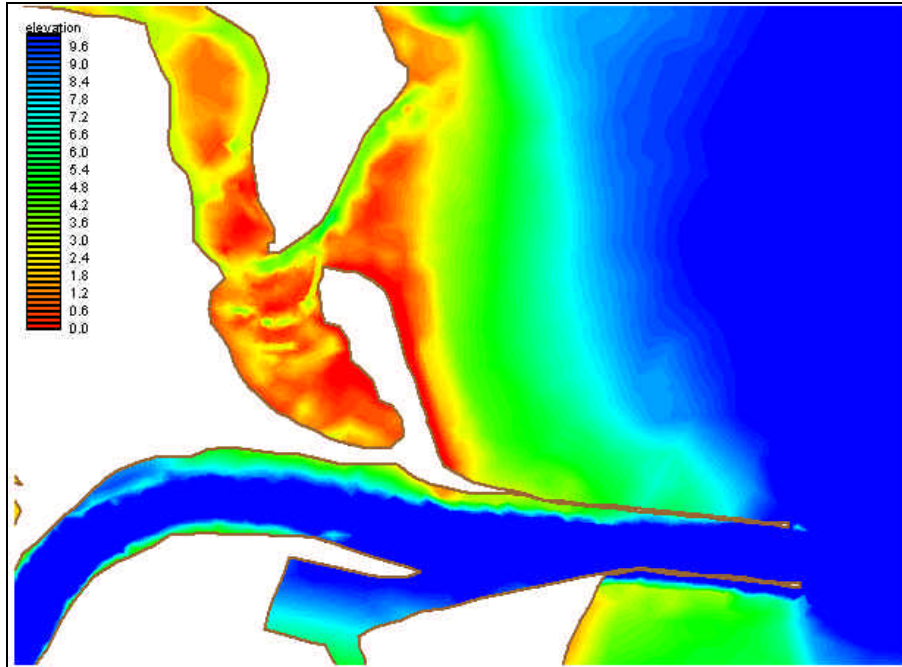


Figure 21. Existing conditions bathymetry

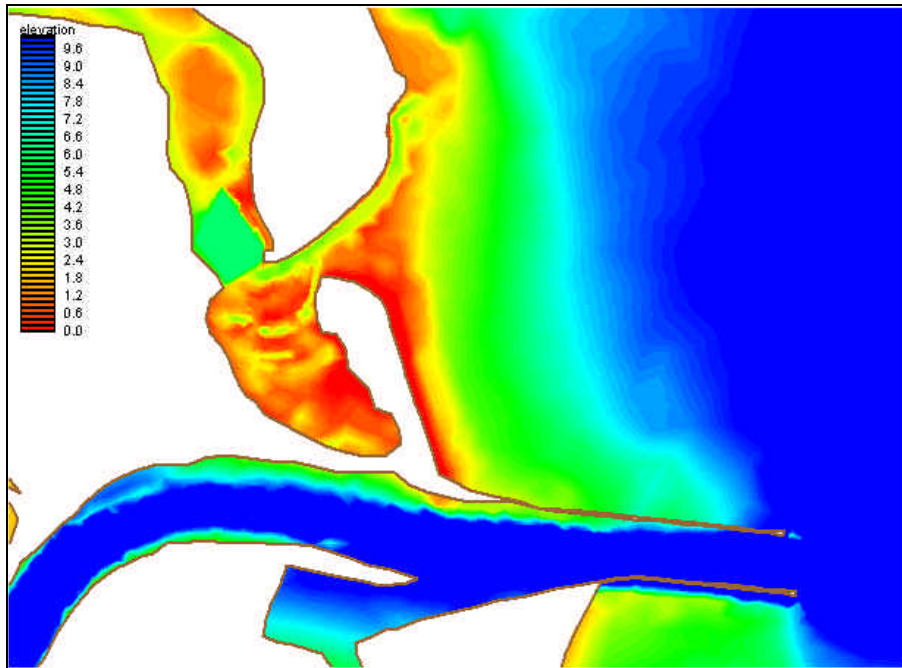


Figure 22. Flood shoal mining bathymetry (Alternative 1)

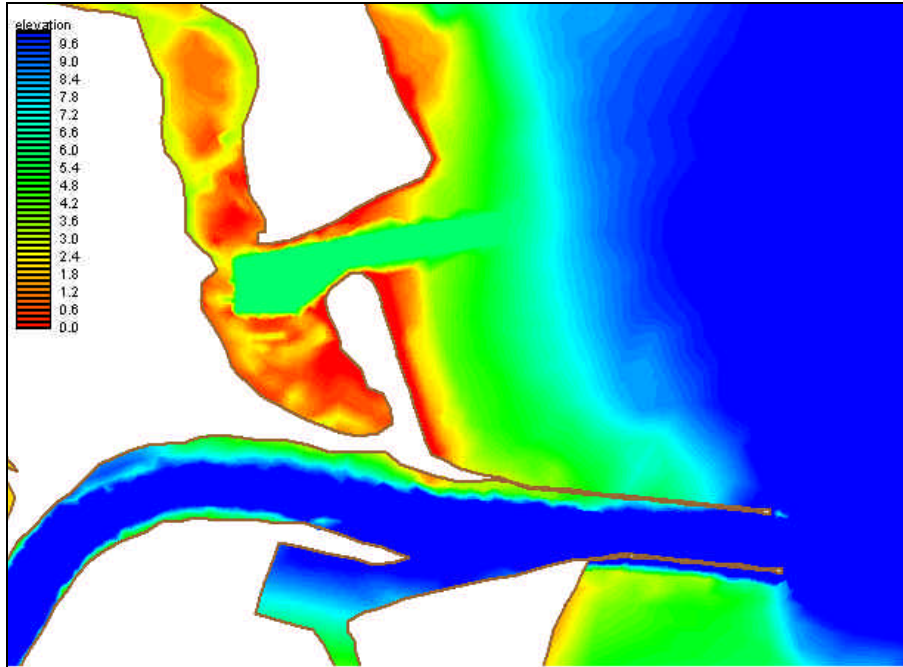


Figure 23. Ward's Bank mining bathymetry (Alternative 2)

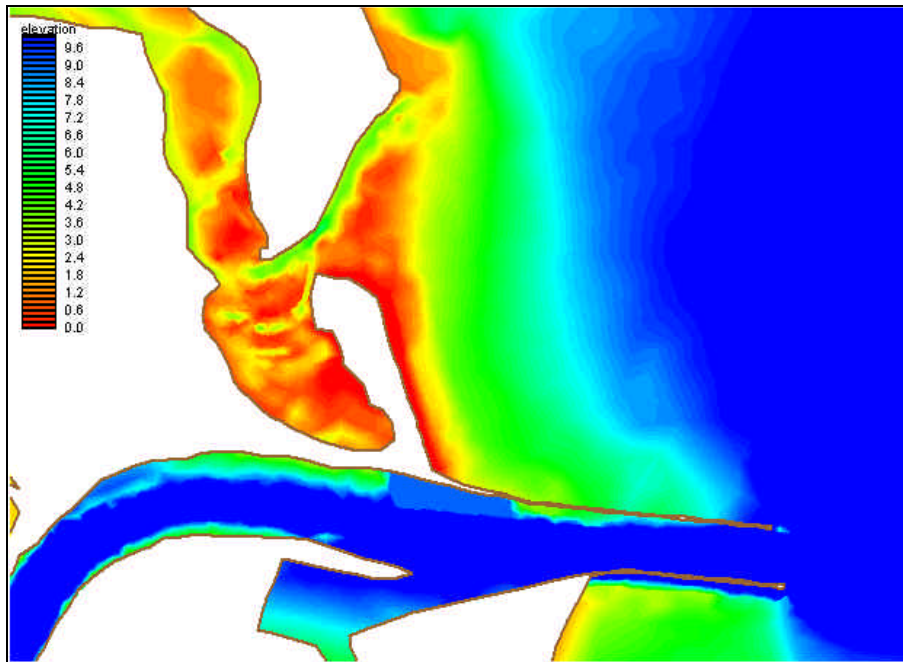


Figure 24. North jetty shoal mining bathymetry (Alternative 3)

Simulation Results

The modeling of the three shoal mining alternatives provided a means to assess the effects of the change in bathymetry on flow patterns and sediment

transport in these areas. Establishing the change in flow patterns due to these alternatives first requires a discussion of existing flow patterns.

Although the simulations lasted 14 days and included both spring and neap tides, a complete presentation of flows and elevations over the entire tidal cycle proved impractical. As such this chapter only presents the flows and sediment transport associated with spring ebb and flood tides at the times of maximum velocities through Ft. George Inlet and the St. Johns River. The flows associated with these times during the tidal cycle produce the highest sediment transport rates and, as such, should display the highest contrast in solutions between the existing and alternative simulations.

Existing Conditions

For the Ft. George Inlet alternatives, peak flood and ebb occur at 7.75 days (669,600 sec) and 8 days (690,300 sec) into the simulation. Figures 25 and 26 show the velocity contours overlaid with velocity vectors indicating magnitude and direction during peak flood and ebb of Ft. George Inlet. During peak flood, Figure 25 indicates slightly higher velocities, on the order of 1.25 m/s, along the southern tip of Little Talbot Island as the flow enters the narrow throat of the inlet. The majority of the flow then focuses on the western bank of the Ft. George River immediately north of the A1A Bridge. Here, the model estimates velocities on the order of 1.3 m/s. The broad, shallow flood shoal, located just north of the bridge, diverts the flow east and west around either side of the shoal.

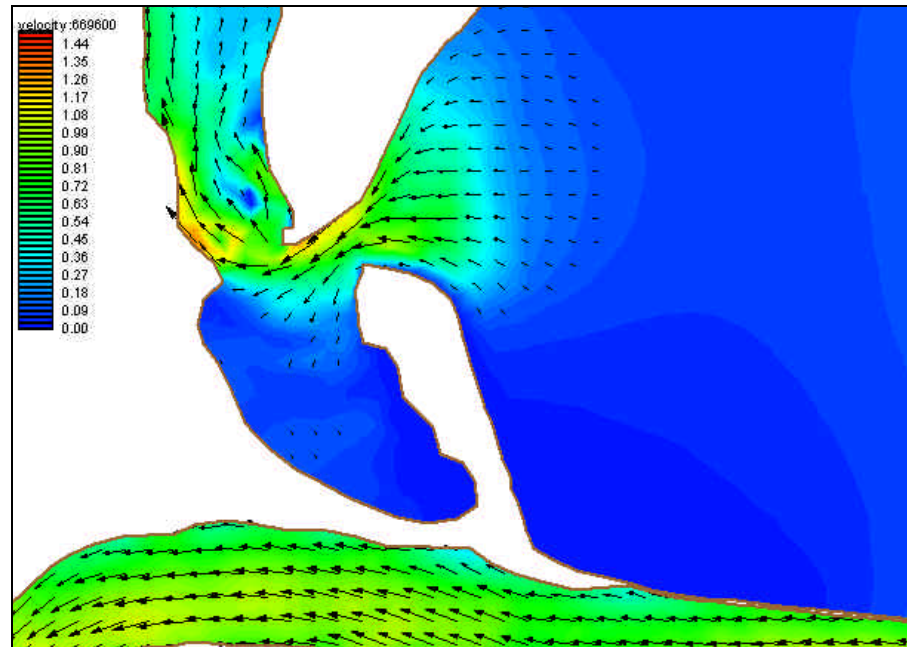


Figure 25. Velocity vectors and velocity magnitude contours (m/s) of existing conditions in the Ft. George Inlet vicinity during peak flood velocity

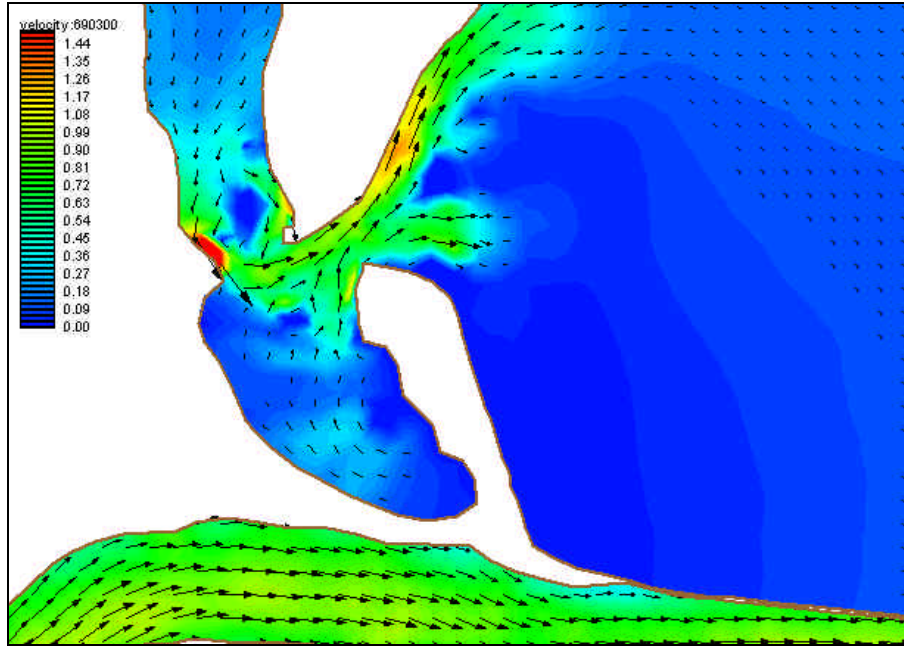


Figure 26. Velocity vectors and velocity magnitude contours (m/s) of existing conditions in the Ft. George Inlet vicinity during peak ebb velocity

Figure 26 shows the flow patterns during peak ebb flow. The figure shows similar patterns to the flood flow. Again, the flow diverts east and west around the flood shoal; the flow focuses along the west bank of the Ft. George River immediately north of the A1A Bridge where velocities reach 1.85 m/s; and the southern shore of Little Talbot Island also experiences increased velocities. The high velocities (approximately 1.3 m/s) through the inlet throat occur farther north along the shoreline of Little Talbot Island than during peak flood.

The peak flood and ebb velocities for the St. Johns River near the north jetty shoal occurred 7.8 days (673,200 sec) and 7.55 days (652,500 sec) into the simulation. Figures 27 and 28 depict velocity contours and velocities vectors indicating velocity magnitude and direction for the existing conditions simulation near the north jetty shoal.

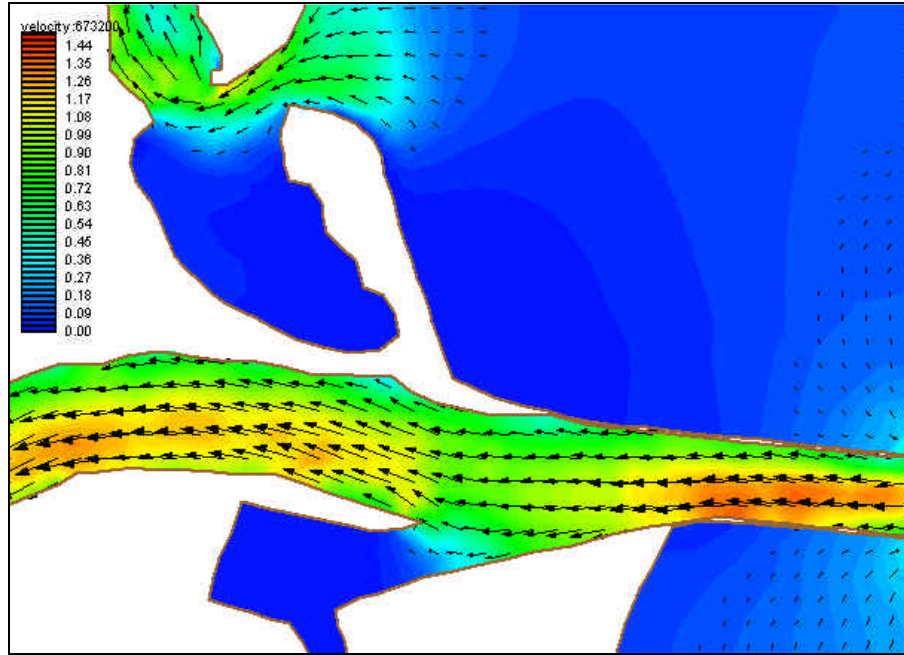


Figure 27. Velocity vectors and velocity magnitude contours (m/s) of existing conditions in the north jetty shoal vicinity during peak flood velocity

From Figure 27, the velocity vectors show a diversion of flow around the shoal attached to the north jetty during flood flow. The contours indicate a decrease in velocity in this area attributed to the widening of the channel near the entrance to the Mayport Basin. Velocities upstream of the shoal reach as high as 1.35 m/s, and velocities downstream of the shoal reach 1.25 m/s.

From Figure 28, the velocity contours during ebb flow, indicate faster velocities upstream and downstream of the north jetty shoal than during flood flow. Again, the model predicts flow diversion around the shoal and a region of low velocity adjacent to the shoal.

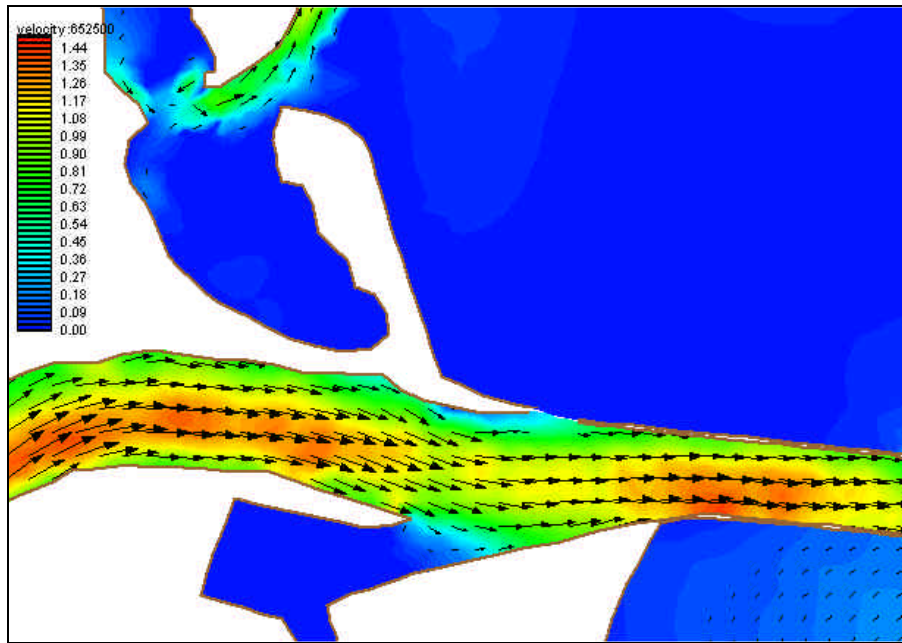


Figure 28. Velocity vectors and velocity magnitude contours (m/s) of existing conditions in the north jetty shoal vicinity during peak ebb velocity

Alternative 1: Flood Shoal Mining

The first alternative, flood shoal mining and subsequent backpassing, induces significant changes to the tidal circulation patterns. Figure 29 displays the simulation results during peak flood flow as contours of velocity magnitude overlaid with velocity vectors indicating direction. During peak flood flow, this alternative produces relatively high velocities (approximately 1.8 m/s) through the throat of the inlet. After flow enters the inlet, it follows the deep water created by the shoal removal and closely hugs the west bank of the Ft. George River immediately north of the A1A Bridge. This flow creates a circulation cell along the east bank of the river near the currently eroding shoreline.

Two features of the new bathymetry increase velocity magnitude through the inlet throat. First, the backpassing at the south end of Little Talbot Island has reduced the effective entrance width of the inlet. This constriction induces the higher velocities. Also, the removal of the flood shoal and reorientation of the inlet make flood flow more efficient. This results in a greater tidal prism and thus higher velocities. Table 10 shows the calculated tidal prism associated with spring flood tide. From the table, dredging the flood shoal would increase the flood tidal prism 18.2% during spring tides — a significant increase. Figure 30 shows the flow rate through the inlet during spring tides and flood flow. From the figure, the flow rates associated with Alternative 1 exhibit the same behavior as those from the existing conditions simulations but achieve slightly higher peak flow rates.

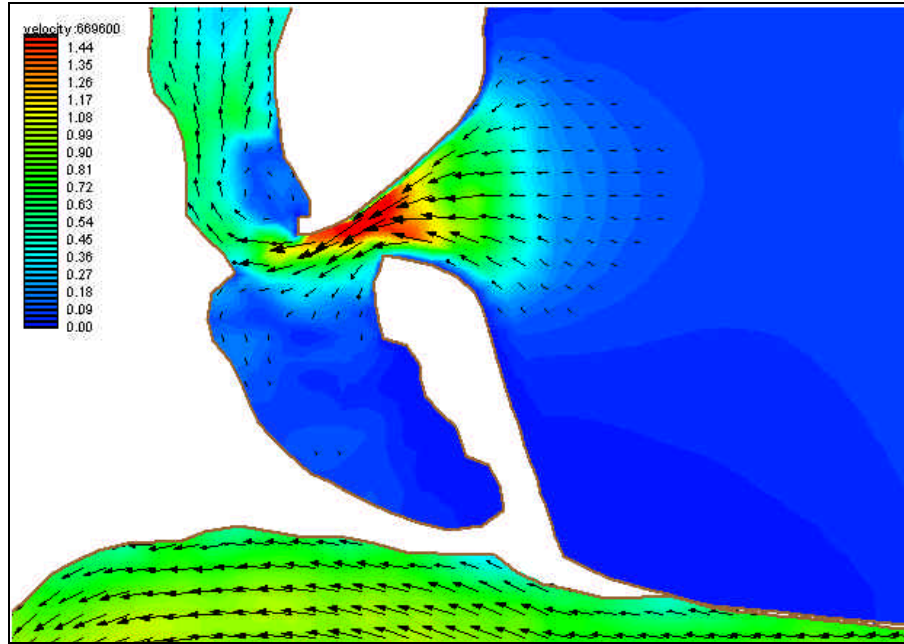


Figure 29. Velocity vectors and velocity magnitude contours (m/s) of Alternative 1 in the Ft. George Inlet vicinity during peak flood velocity

Table 10. Calculated tidal prisms during spring tide					
Simulation	Flood Tidal Prism (cf in millions)	Ebb Tidal Prism (cf in millions)	Flood/Ebb Ratio	% increase from existing - flood	% increase from existing - ebb
Existing Conditions	11.0	9.4	1.17	----	----
Alternative 1: Flood Shoal	13.0	9.8	1.32	18.2	4.3
Alternative 2: Ward's Bank	16.4	15.7	1.05	25.9	59.3

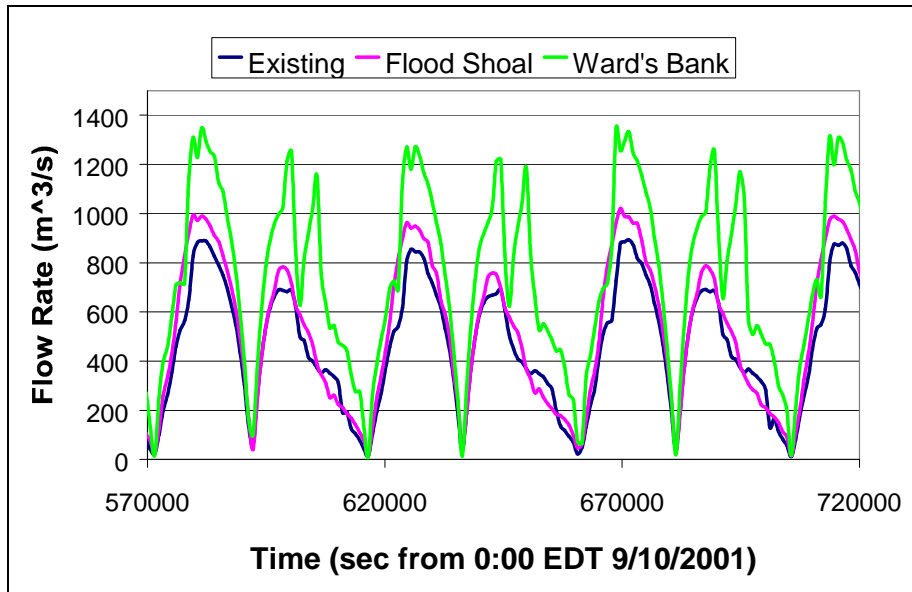


Figure 30. Calculated flow rates through Ft. George Inlet during spring tides (existing conditions and Alternatives 1 and 2)

Difference plots created for each alternative provide clearer pictures of the effects of changes in bathymetry on velocity. These plots display the existing conditions solution subtracted from the given alternative solution. The plots also display a contrasting color scale such that red areas indicate velocity decreases (compared with existing conditions) and green areas indicate velocity increases. Finally, the figures indicate the existing conditions shoreline for comparison purposes. Figure 31 shows the changes in velocity due to bathymetric changes from the flood shoal mining and backpassing of sediment to Little Talbot Island. The figure indicates a substantial velocity decrease of approximately 0.75 m/s across the Ft. George River in the area of the dredging and a substantial velocity increase, up to 0.78 m/s, in the throat of Ft. George Inlet along the southern tip of Little Talbot Island. The decrease in velocity corresponds to the dramatic increase in cross-sectional area north of the bridge. If the flow rate were to remain the same, a larger cross-sectional area would produce slower velocities. Applying this same logic to the inlet throat is inappropriate, however. At this location, the green areas indicate two features of the new bathymetry. First, the channel has relocated and second the tidal prism has increased. Later, this chapter presents the effects these changes in bathymetry and flow have on sediment transport.

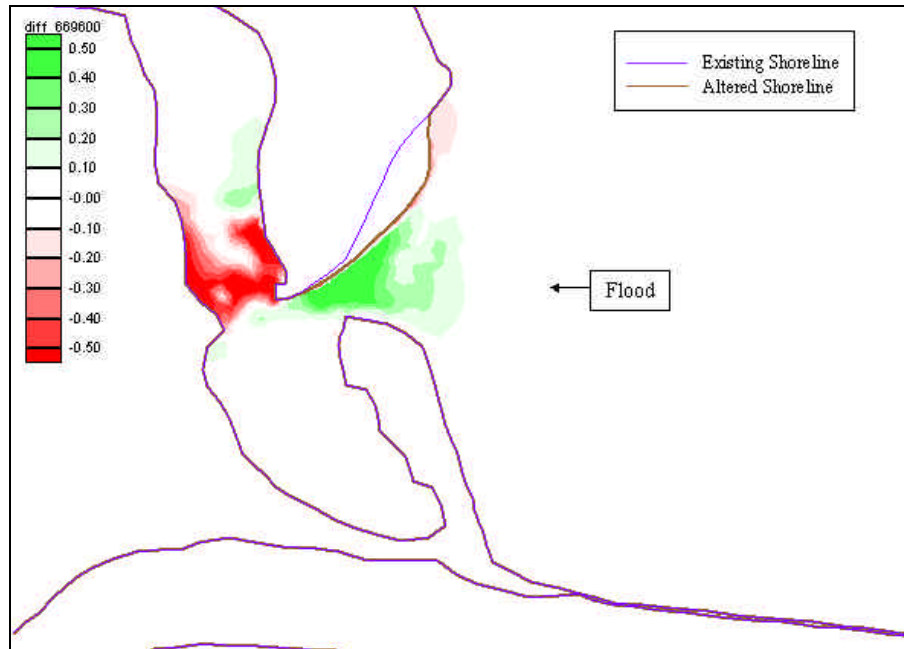


Figure 31. Velocity difference contours (m/s) between Alternative 1 and existing conditions during peak flood velocity

Figure 32 displays the simulation results for Alternative 1 during spring ebb tide as contours of velocity magnitude overlaid with velocity vectors. From the figure, the velocity vectors indicate the flow follows the deeper waters along the western bank of the Ft. George River south before turning northeast through the inlet. This results in low velocities along the eastern bank of the Ft. George River just north of the bridge. The figure also shows high velocities (on the order of 1.8 m/s) in the same area (along the southern shoreline of Little Talbot Island) as the results for the existing conditions simulation. Interestingly, the ebb tidal prism associated with spring tides for this alternative does not exhibit an equivalent increase as the increase observed during spring flood (Table 10). This produces a more pronounced disparity between flood and ebb tidal prisms that would further accentuate the tidal pumping through the Ft. George River and out through the St. Johns River and Nassau Sound.

Figure 33 displays the calculated changes in velocity associated with this alternative during peak ebb velocity. Shoal removal appears to reduce hydraulic pressure along the east and west banks immediately north of the bridge by centering the flow through the channel. No substantial decrease in velocity occurs in the center of the channel at the shoal's former location. Because the cross-sectional area in this location increases greatly from shoal removal, the flow through this area must significantly increase to maintain the same velocity magnitude. Substantial decreases in velocity occur along the banks — a decrease of up to 1.5 m/s along the west side of the channel and up to 1.35 m/s along the east side of the channel.

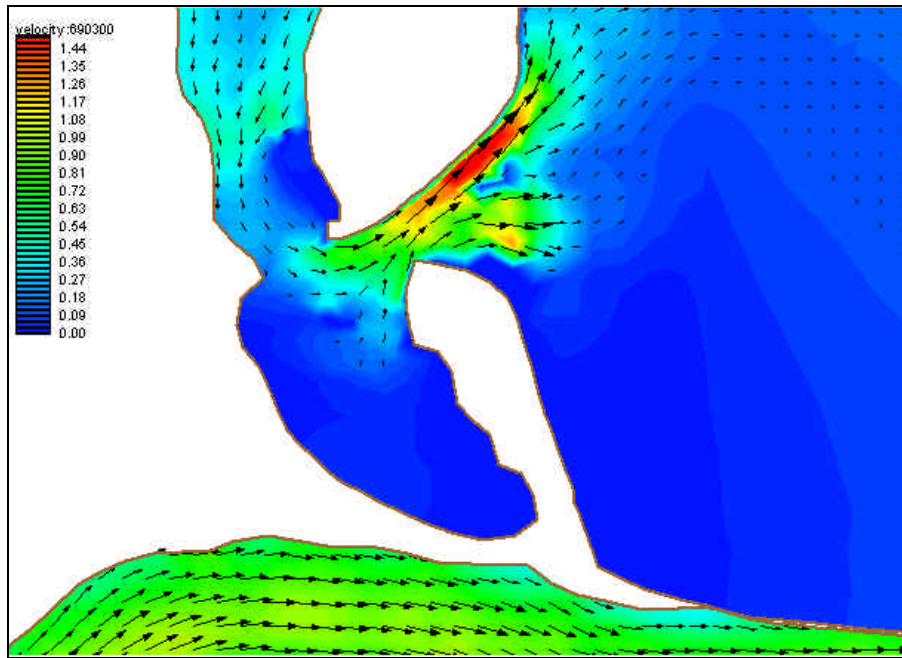


Figure 32. Velocity vectors and velocity magnitude contours (m/s) of Alternative 1 in the Ft. George Inlet vicinity during peak flood velocity

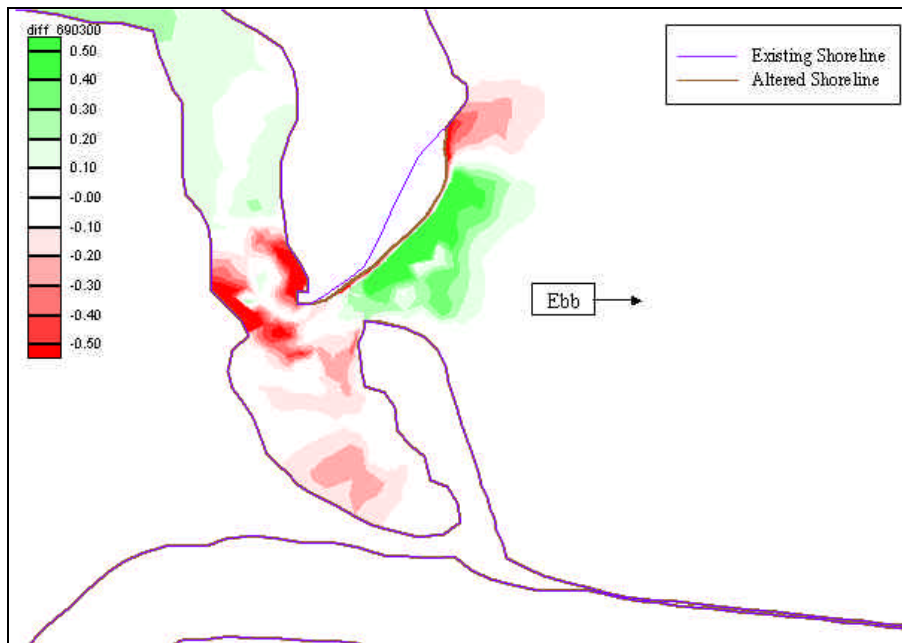


Figure 33. Velocity difference contours (m/s) between Alternative 1 and existing conditions during peak ebb velocity

Upstream of the flood shoal removal area across almost the entire river, an increase in velocity exists. This trend continues along the Ft. George River to its confluence with the ICCW and incorporates part of the ICCW. Decreases in velocity along the ICCW draining into Nassau Sound and the

St. Johns River correspond to the increase in velocities of the water bodies draining through Ft. George Inlet. Changes in velocity magnitude result from the increase in ebb tidal prism.

Figure 33 also shows increases in the velocity magnitude through the inlet. This increase (green area in the figure) results from the relocation of the channel to the south as well as a shift in the area of peak velocity to the west. Finally, the model predicts lower velocities in Ward's Bay. This feature results from inlet reorientation that provides a more direct path for the flow to exit on ebb.

Alternative 2: Ward's Bank Mining

The second alternative involves dredging through Ward's Bank and backpassing the sediment to Little Talbot Island. Figure 34 shows velocity magnitude contours and velocity vectors during peak flood for this alternative. From the figure, the flow patterns north of the A1A Bridge are similar to those of the existing conditions. However, the model predicts velocity increases along the west bank north of the bridge. Here, velocities reach approximately 1.4 m/s. The significant alterations to the bathymetry associated with this alternative involve moving the inlet slightly south and significantly increasing the cross-sectional area. The result is a drastic decrease in velocity magnitude (~0.53 m/s) through the inlet throat. Despite this decrease in velocity magnitude, the flood tidal prism through the inlet increases (25.9%, Table 10) significantly given the more efficient entrance.

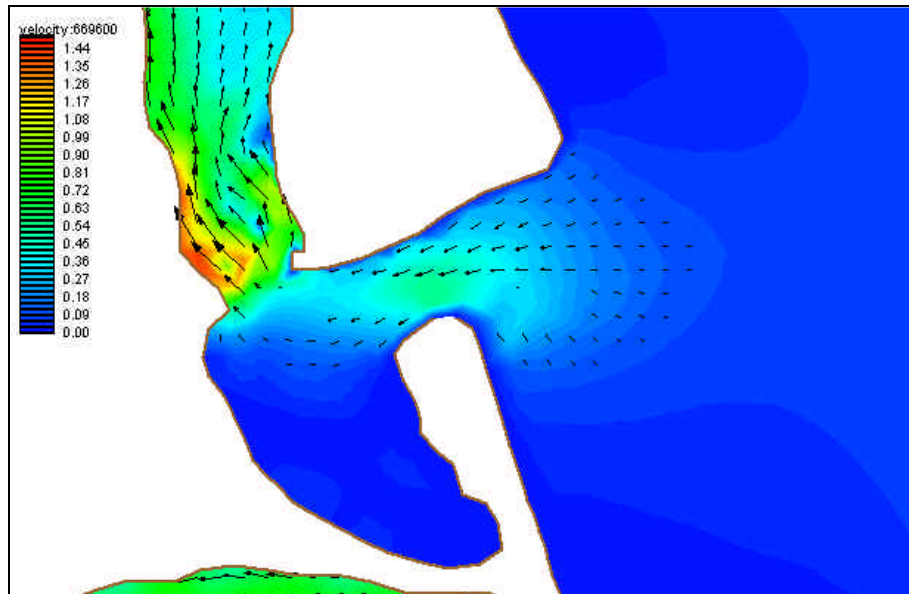


Figure 34. Velocity vectors and velocity magnitude contours (m/s) of Alternative 2 in the Ft. George Inlet vicinity during peak flood velocity

Figure 35 indicates the differences in velocity magnitude that result from Ward's Bank mining and backpassing operations. As described in the previous alternative, red denotes velocity decreases as compared with

existing conditions and green denotes velocity increases. The velocity decrease through the widened inlet throat described above becomes immediately apparent in Figure 35. The maximum decrease measures approximately 1 m/s. This velocity decrease results from the larger cross-sectional area through the inlet throat. The velocity increase (green area) at the tip of Ward's Bank results from the channel relocation. If the flow rate (flow rate is proportional to velocity times area) through the inlet had remained the same, a decrease in velocity would have accompanied the increase in cross-sectional area. For this case, the flood prism increased; however, the increase was insufficient to offset the significant increase in cross-sectional area. Lower velocities result. The increased velocity upstream of the bridge (denoted by the green contours) results from the larger flood tidal prism through the inlet. As the bathymetry in this area did not change, the higher flow rate produces increases in velocity.

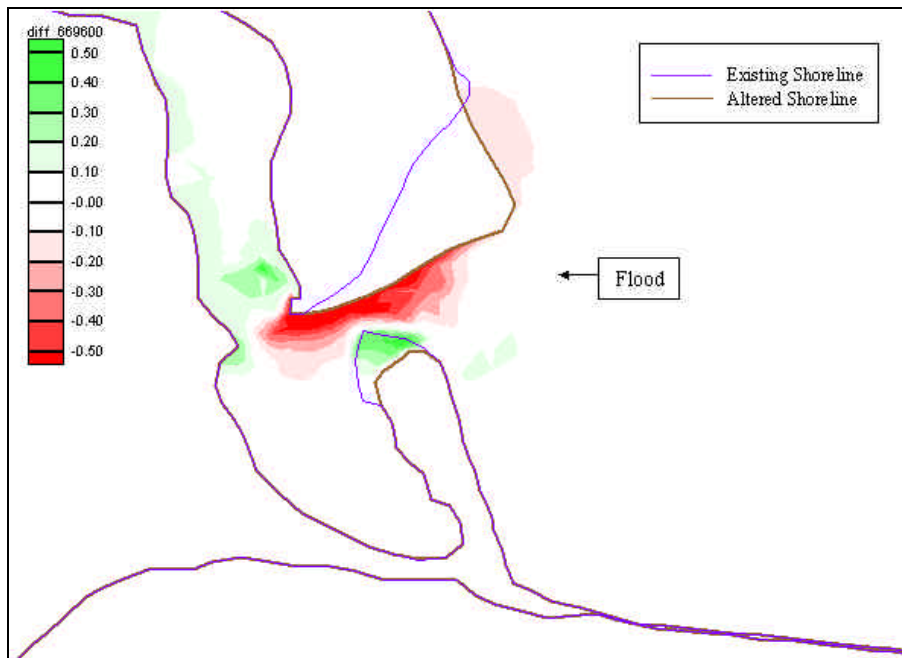


Figure 35. Velocity difference contours (m/s) between Alternative 2 and existing conditions during peak flood velocity

Figure 36 displays the velocity vectors and contours of velocity magnitude during peak ebb for this alternative. Similar to existing conditions, flow that branches around the flood shoal puts increased hydraulic pressure on the east and west banks of the Ft. George River immediately north of the A1A Bridge. Along the west bank, velocities reach as high as 2.5 m/s. Along the east bank, a maximum velocity of 1.5 m/s occurs. The flow pattern then deviates from existing conditions as the flow encounters the altered bathymetry. The main channel through the inlet for this alternative lies farther south, away from the Little Talbot Island shoreline. This permits a circulation cell to develop at the southern tip of Little Talbot Island. The spring ebb tidal prism associated with this alternative increases by almost

60% over existing conditions. The significant increase results from a much more efficient flow path on ebb tides. Also, the flow rate through the inlet changes significantly over the existing flow rate (Figure 30). From the figure, the peak flow rates on ebb almost equal those experienced on flood. This produces flood and ebb tidal prisms almost equal in magnitude. This result is a significant departure from the well documented tidal pumping associated with this inlet.

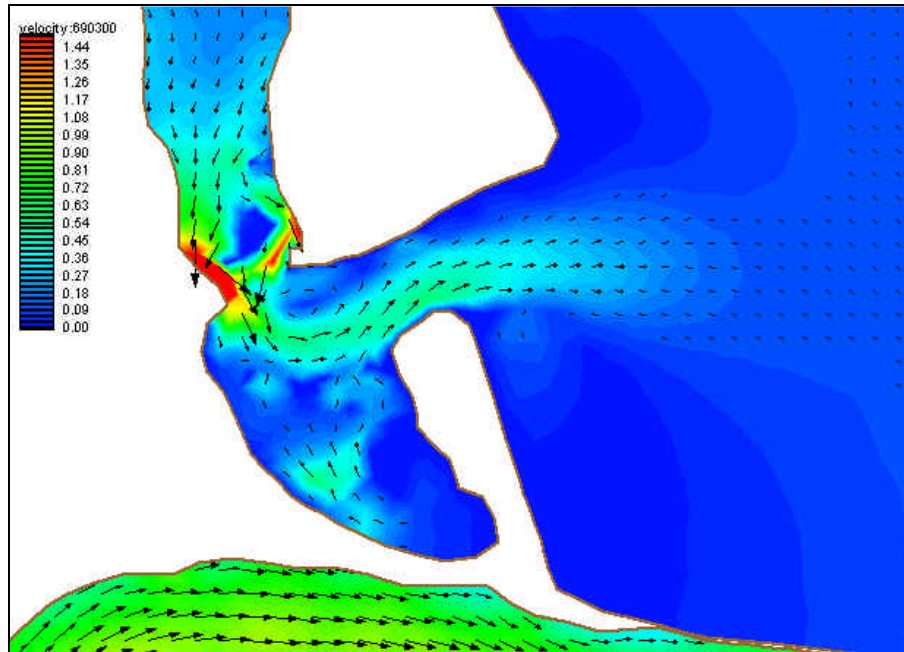


Figure 36. Velocity vectors and velocity magnitude contours (m/s) of Alternative 2 in the Ft. George Inlet vicinity during peak ebb velocity

Figure 37 indicates the velocity differences between this alternative and the existing conditions simulations during peak ebb flow. Decreases in velocity occur in the area of sediment removal and along the eastern bank of the altered throat section. In the dredged area, decreases as great as 0.92 m/s occur. The region of velocity decrease located on the ocean side at the southern tip of Little Talbot Island results from the relocation of the inlet south. Increases in velocity occur around the bridge especially along the west bank of the Ft. George River and near the mouth of the altered inlet. The increase (maximum increase – approximately 0.83 m/s) around the bridge and the west bank result from the significant increase in ebb tidal prism discussed previously. The increase in velocity located at the mouth of the inlet results from the change in location and orientation of the inlet.

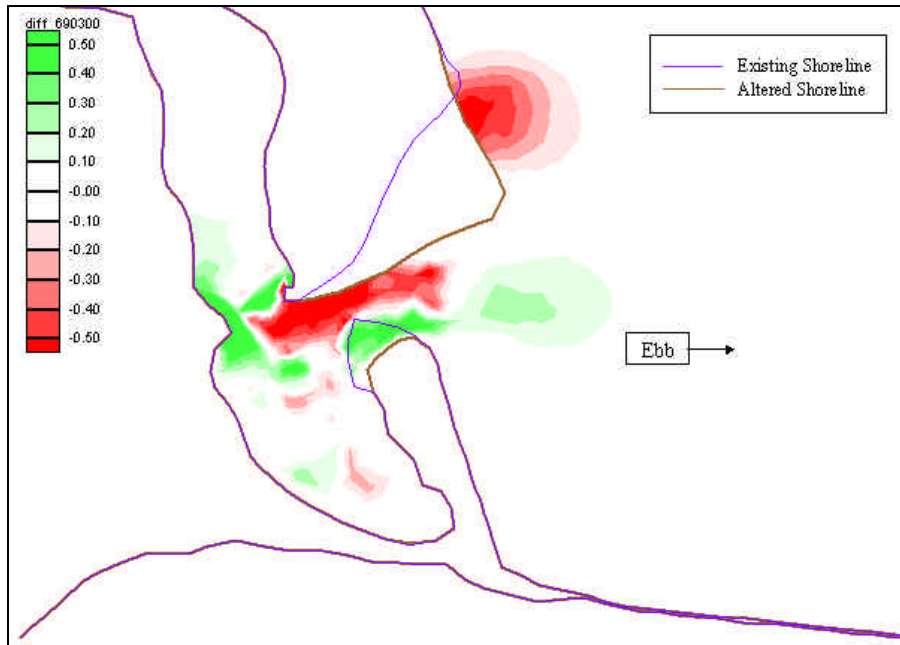


Figure 37. Velocity difference contours (m/s) between Alternative 2 and existing conditions during peak ebb velocity

Alternative 3: North Jetty Shoal Mining

The third alternative involves mining the shoal that forms along the north jetty within the St. Johns River. Figure 38 represents velocity vectors and contours of velocity magnitude associated with this alternative during peak flood flow. The velocity contours indicate a decrease in velocity near the Mayport Basin entrance and the north jetty shoal. Also observed in the existing conditions simulation results, this decrease in velocity results from channel widening associated with the entrance to the Mayport Basin. This alternative produces only negligible change in the flood tidal prism (Table 11) and flow rate through the St. Johns River Entrance (Figure 39).

Simulation	Flood Tidal Prism (cf in millions)	Ebb Tidal Prism (cf in millions)	Flood/Ebb Ratio	% increase from existing - flood	% increase from existing - ebb
Existing Conditions	113.62	127.71	0.89	----	----
Alternative 3: North Jetty Shoal	113.64	128.28	0.89	0.02	0.45

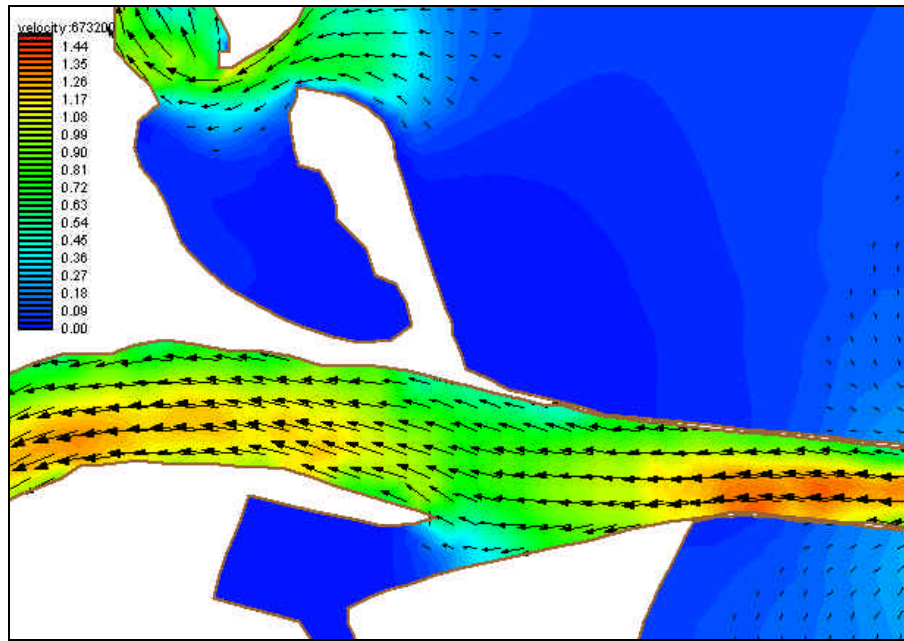


Figure 38. Velocity vectors and velocity magnitude contours (m/s) of Alternative 3 during peak flood velocity

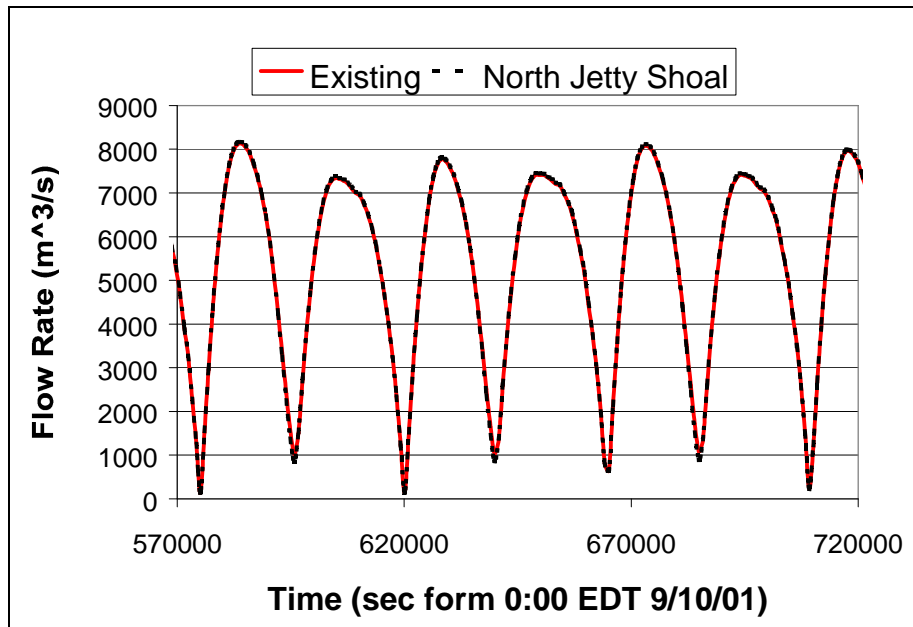


Figure 39. Calculated flow rate through the St. Johns River Entrance during spring tides (existing conditions and Alternative 3)

A difference plot (Figure 40) of velocities during peak flood helps show the exact changes in velocity as compared with the existing condition simulation. From the figure, velocities decrease just west of the Mayport Basin Entrance. This corresponds to the approximate location of the north

jetty shoal. Therefore, the decrease in velocity most likely results from a larger cross-sectional area due to shoal removal. An increase in velocity occurs immediately west of the sediment removal area. With the shoal removed, the flow no longer diverts around the shoal and thus the region of low velocity behind the shoal disappears.

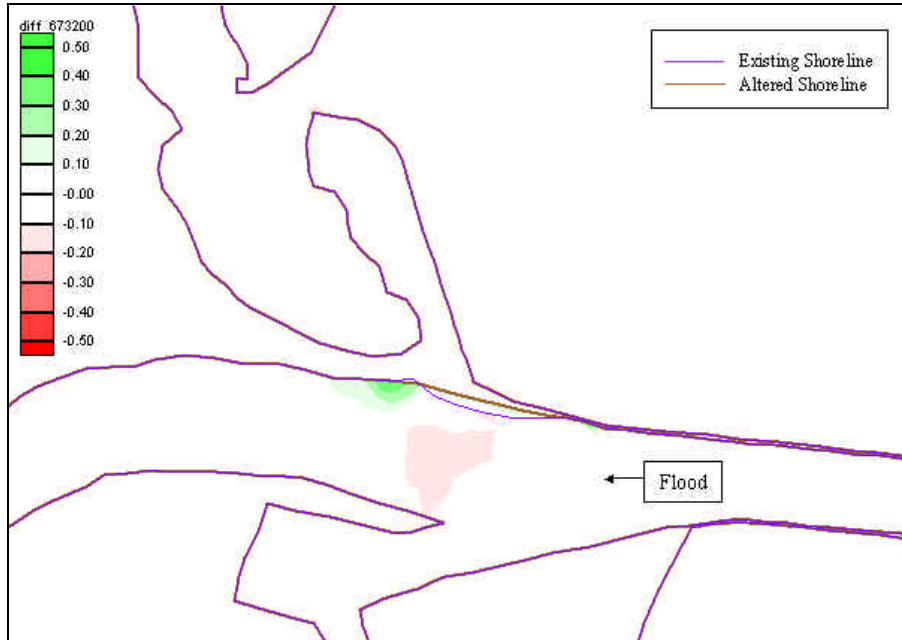


Figure 40. Velocity difference contours (m/s) between Alternative 3 and existing conditions during peak flood velocity

Figure 41 illustrates the velocity magnitude contours and velocity vectors during peak ebb flow for this alternative. Similar flow characteristics observed during flood also occur during ebb. The velocity vectors parallel the new shoreline through the area of the removed shoal. Again, a decrease in velocity near the Mayport Basin Entrance and the north jetty shoal occurs. This velocity decrease results from the widening of the channel in this area. As with the flood tidal prism, the change in the spring ebb tidal prism is negligible (Table 11).

The difference plot illustrated in Figure 42 indicates areas where velocity increases (green) or decreases (red) due to the north jetty shoal removal during peak ebb velocities. Similar to peak flood velocity conditions, a decrease in velocity occurs near the Mayport Basin Entrance given the increased cross-sectional area. Due to the flow direction during ebb, the area of reduced velocity shifts slightly east. The region of velocity increase immediately east of the shoal results from the removal of the wake region produced by the shoal in the existing conditions simulation.

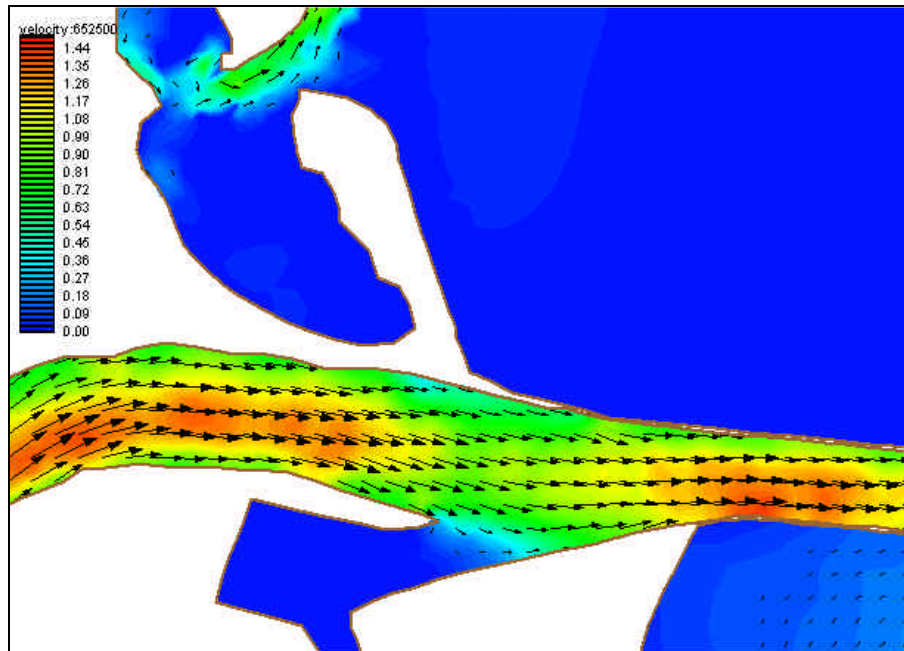


Figure 41. Velocity vectors and velocity magnitude contours (m/s) of Alternative 3 during peak ebb velocity

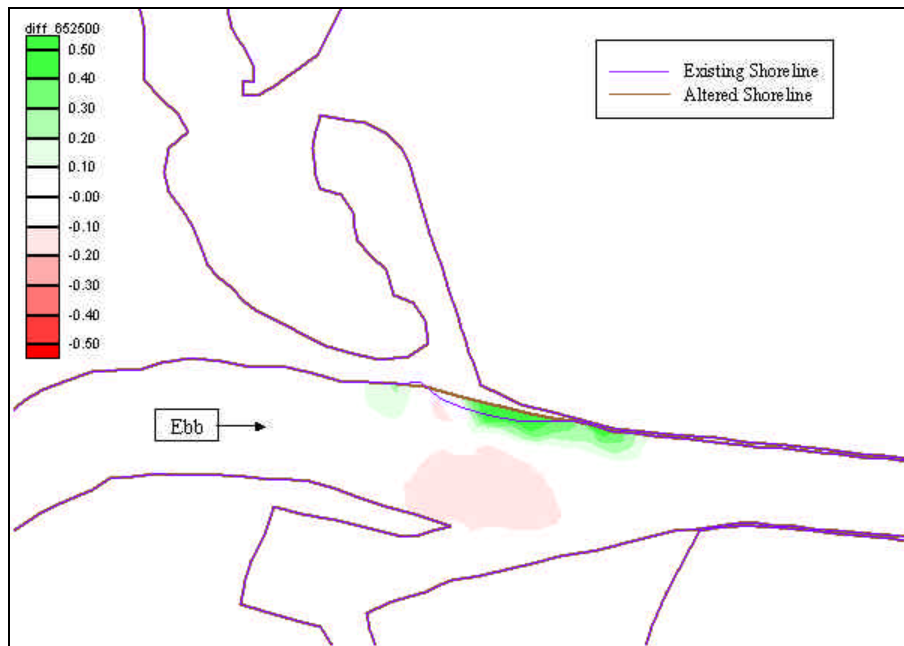


Figure 42. Velocity difference contours (m/s) between Alternative 3 and existing conditions during peak ebb velocity

Impacts to Bridge Scour

One of the concerns associated with implementation of any of the alternatives is possible scour around the foundations of the A1A Bridge that spans the Ft. George River. The two flow parameters that dominate calculation of pier scour are velocity magnitude and angle of attack. To begin, Alternative 1, removal of the flood shoal, offers no threat of increased erosion at the bridge. The velocity difference plots indicate a reduction in velocity along the east and west sides of the channel. The reduction in velocity falls as low as 0.77 m/s on ebb and 0.63 m/s on flood with little change in velocity occurring in the center of the channel. The angle of attack, however, increases slightly during flood. However, because velocity magnitude is the more dominant parameter, the significant decrease in velocity should more than compensate for the increased angle of attack. During ebb tide, the angle of attack is very similar to the existing conditions along the west bank. The removal of the flood shoal and, consequently, the change in flow paths, produce a smaller angle of attack in the center of the bridge and an approximate 90° change in direction from the existing bathymetry simulation during the same flow conditions.

Bridge scour is a very real concern for the second alternative (Ward's Bank mining). A substantial increase in velocity occurs along the west bank during ebb flow, and a slight increase in velocity occurs during flood flow. With an increase in ebb velocities as much as 0.8 m/s along the west side of the channel, scour at these bridge piles may result. Little velocity change occurs in the center of the channel during both ebb and flood flow, and the east side of the channel experiences a decrease in velocity. The angle of attack appears more favorable with the change in flow path due to sediment removal from Ward's Bank. During ebb flow, the east side and center of the channel experience a more head-on flow, decreasing the angle of attack on the piles. The flow direction on the west side of the channel mimics that during existing conditions (i.e., no change in angle of attack is apparent). During flood flow, the angle of attack appears to decrease along the entire length of the bridge. The flow direction does not appear to increase the likelihood of erosion; however, the increased velocity in the west side of the channel suggests the need for further investigation of possible erosion.

The third alternative, north jetty shoal mining, produces no change in flow patterns near the A1A Bridge. As such, this alternative will produce no changes in scour patterns around the bridge pilings.

Sediment Transport

Sediment Transport Theory

Post-processing the results from the tidal circulation simulations provided the means to examine the associated sediment transport within Ft. George Inlet and the St. Johns River. The sediment transport analysis consisted of examining sediment transport at single instances in time associated with maximum flow conditions at the area of interest. The simulation results (dynamic water depth and flow velocity) during each

examined time step provided the input into a sediment transport equation. This equation produced an estimate of the sediment transport rate at each node within the domain. Van Rijn (1984a, 1984b, and 1984c) provided the sediment transport formulae employed in this study. The total sediment transport rate equals the sum of the bed load and the suspended load. Van Rijn computed bed load sediment transport as the product of the saltation height, the particle velocity, and the bed load concentration. He determined the saltation height and particle velocity for a variety of sediments and flow parameters by numerically solving the equations of motion and calibrated his model through comparison with experiments. Measurements of bed load transport provided empirical determination of the sediment concentrations in the boundary layer.

Before calculating the bed load transport, one must define the dimensionless particle size parameter and the transport stage parameter. The particle size parameter, D_* , is found with the following equation:

$$D_* = D_{50} \sqrt[3]{\frac{(s-1)g}{\nu^2}} \quad (4)$$

In the equation, D_{50} is the median diameter of the bed material, s is the specific density of the sediment, g is gravity, and ν is the kinematic viscosity of the fluid. For this study, Gosselin et al. (2001) and Taylor Engineering, Inc. (2000) provided values of D_{50} . The nondimensional transport stage parameter, T , is calculated via the following equation:

$$T = \frac{(u'_*)^2 - (u_{*,cr})^2}{(u_{*,cr})^2} \quad (5)$$

where u'_* is the bed shear velocity related to grains (on the bed) and $u_{*,cr}$ is the critical shear velocity according to Shields' Curve. The parameter u'_* is an estimate for the average shear velocity at the up sloping part of the bed forms.

Given D_* and T , calculation of the bed load transport, q_b , is now possible via the equation:

$$q_b = D_{50}^{3/2} \left[0.053 \frac{T^{2.1}}{D_*^{0.3}} \right] \sqrt{(s-1)g} \quad (6)$$

Bed load transport is given in units of volume of transported material per unit time per unit width.

Van Rijn computed suspended load sediment transport rate as the depth integration of the product of local concentration and flow velocity. His method employs a reference concentration derived from the equations for bed load transport. Measured concentration provided the calibration for the derived equations.

The suspended load is calculated as the product of the sediment concentration and the flow velocity integrated over the water column. The following equations result from the integration of the differential equation describing the vertical distribution of sediment concentration in a steady uniform current:

$$q_s = \frac{u_* c_a}{\kappa} \left[\frac{a}{h-a} \right]^{Z'} \left[\int_a^{0.5h} \left[\frac{h-z}{z} \right]^{Z'} \ln \left(\frac{z}{z_0} \right) dz + \int_{0.5h}^h e^{-4Z'(z/h-0.5)} \ln \left(\frac{z}{z_0} \right) dz \right] \quad (7)$$

where u_* is the friction velocity, c_a is the reference concentration, κ is von Karman's constant, a is the reference concentration level, h is the local water depth, Z' is a suspension parameter, z_0 is the zero velocity level above the bed, and z is the vertical coordinate (positive upwards from the bed). This equation is represented by the simpler expression

$$q = F u h c_a$$

$$F = \frac{\left[\frac{a}{h} \right]^{Z'} - \left[\frac{a}{h} \right]^{1.2}}{\left[1 - \frac{a}{h} \right]^{Z'} [1.2 - Z']} \quad (8)$$

for the range $0.03 < Z' < 3$ and $0.01 < a/h < 0.1$ with a maximum error of approximately 25%. In the equations, the reference concentration is defined as

$$c_a = \frac{0.035 D_{50}}{2.3} \frac{T^{1.5}}{a D_*^{0.3}} \quad (9)$$

where the dimensionless parameters T and D_* are as defined previously, and D_{50} is the median grain size. In the above equation, c_a is the reference concentration at an elevation a above the bed. To avoid errors associated with setting the reference level, a , too low, van Rijn assumes a reference level equal to one half the bed form height or the equivalent roughness height given a bed form with unknown dimensions. The minimum reference level should equal 1/100th the local water depth.

Finally, the suspension parameter in the suspended load equation, Z' , is defined by

$$Z' = Z + j \quad (10)$$

where

$$Z = \frac{w_s}{bku_*}, \quad (11)$$

$$j = 2.5 \left(\frac{w_s}{u_*} \right)^{0.8} \left(\frac{c_a}{c_0} \right)^{0.4} ; \quad 0.01 \leq \frac{w_s}{u_*} \leq 1, \text{ and} \quad (12)$$

$$b = 1 + 2 \left(\frac{w_s}{u_*} \right)^2 ; \quad 0.1 < \frac{w_s}{u_*} < 1. \quad (13)$$

In the above equations, w_s is the sediment fall velocity and c_0 is the maximum volumetric bed concentration (~ 0.65). These equations provide the estimates of sediment transport rate discussed below.

Existing Conditions

The following sections discuss the sediment transport rates experienced within Ft. George Inlet and the St. Johns River during both spring ebb and flood flows for the existing conditions and three alternatives. Sediment transport rate calculations followed the procedure outlined above. These sections present sets of figures for each alternative that include plots of sediment transport rates and contours of differences in sediment transport rates between the existing conditions and that of the given alternative. These difference plots are similar to those constructed to examine the changes in velocity in the previous section. Remember, discerning shoaling activity from examination of sediment transport rates requires caution. The gradients of sediment transport rather than the rate magnitudes contain the important information. Increases in sediment transport rate in the direction of flow indicate regions of erosion and decreases indicate regions of deposition. Examining the differences in sediment transport rate also requires the same caution.

The following set of figures shows the sediment transport rates for the existing conditions at the times of maximum flood and ebb velocity. These figures provide visual points of comparison for the alternative cases. From Figures 43 and 44, the mechanisms of flood and ebb shoal formation are

apparent for the Ft. George Inlet area. During flood flow, the negative gradient in sediment transport potential occurs in the same location as the existing flood shoal north of the A1A Bridge. During ebb flow, the high rates occurring at the south end of Little Talbot Island explain the shoreline erosion in this area. Also, the negative gradient in sediment transport potential as flow exits the throat contributes to the formation of the ebb tidal shoal.

Figures 45 and 46 give the contours of sediment transport rate of the St. Johns River during peak flood and ebb flow for comparison with the third alternative — north jetty shoal removal and bypassing. As the figures show, a distinct region of low sediment transport occurs at the entrance of the Mayport Basin Entrance on both flood and ebb tides. Not coincidentally, this area also experiences significant shoaling within the navigation channel that requires frequent dredging.

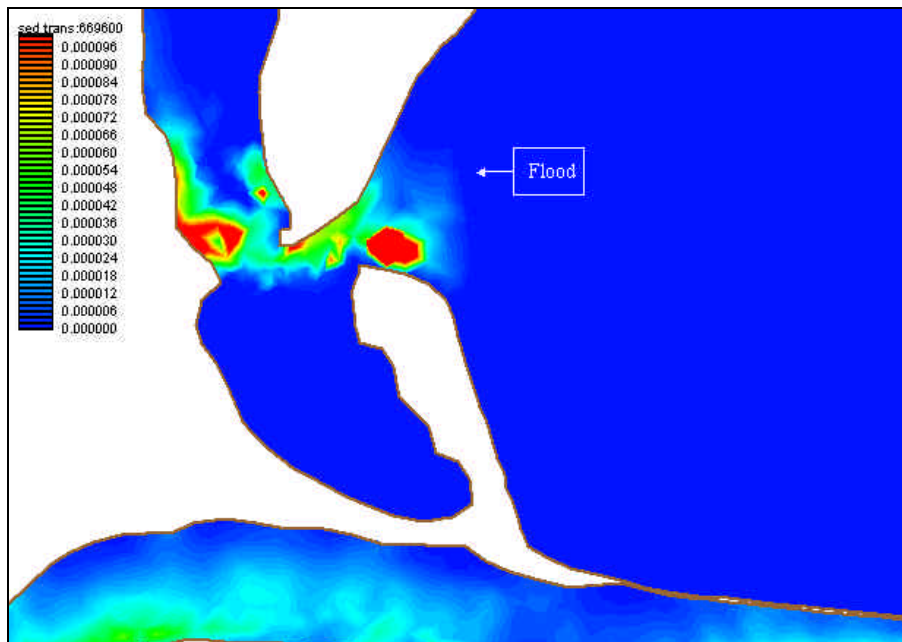


Figure 43. Contours of sediment transport rate ($m^3/s/m$) during peak flood velocity for existing conditions at Ft. George Inlet

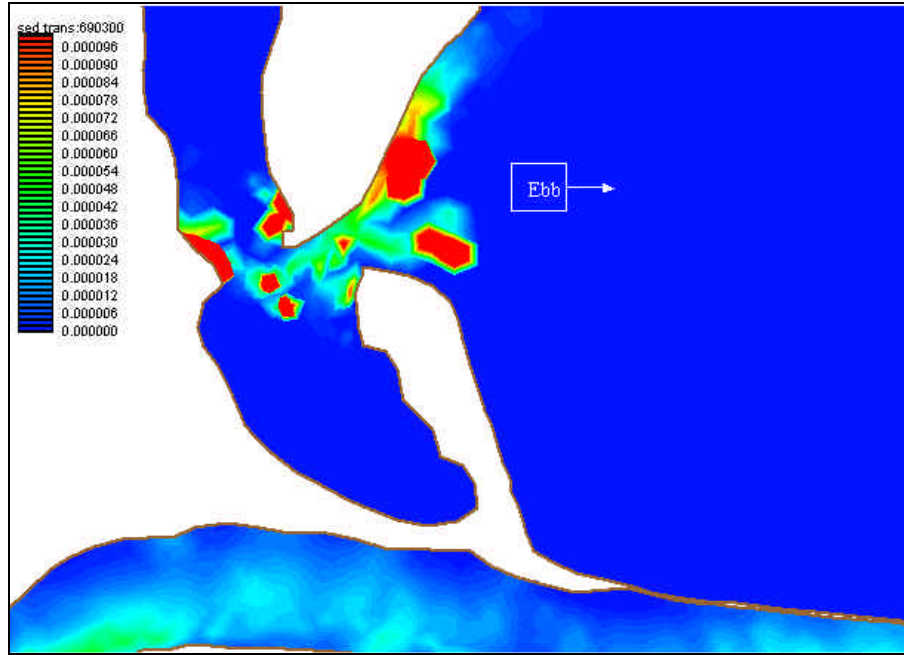


Figure 44. Contours of sediment transport rate ($\text{m}^3/\text{s}/\text{m}$) during peak ebb velocity for existing conditions at Ft. George Inlet

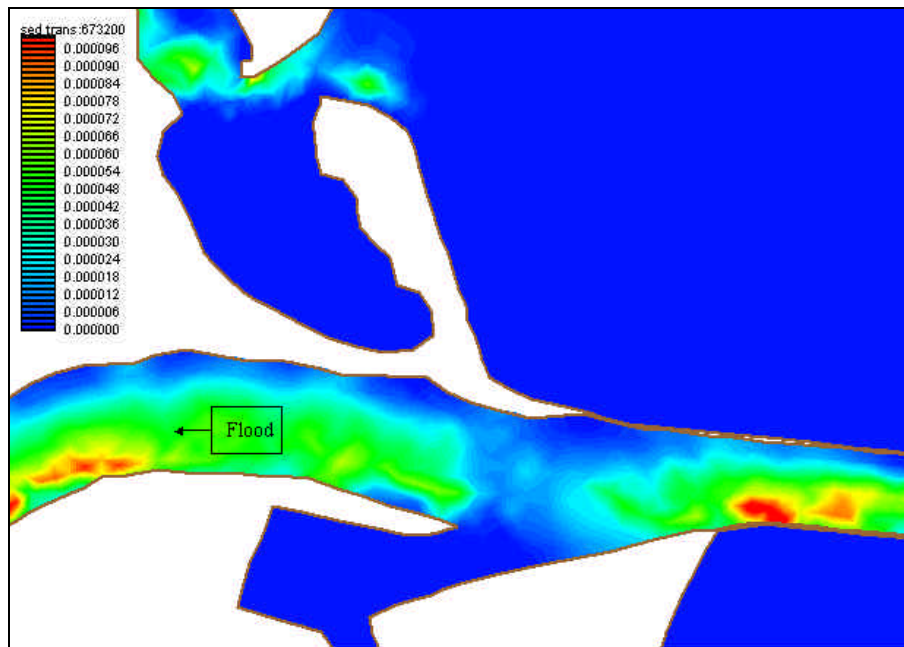


Figure 45. Contours of sediment transport rate ($\text{m}^3/\text{s}/\text{m}$) during peak flood velocity for existing conditions in the St. Johns River

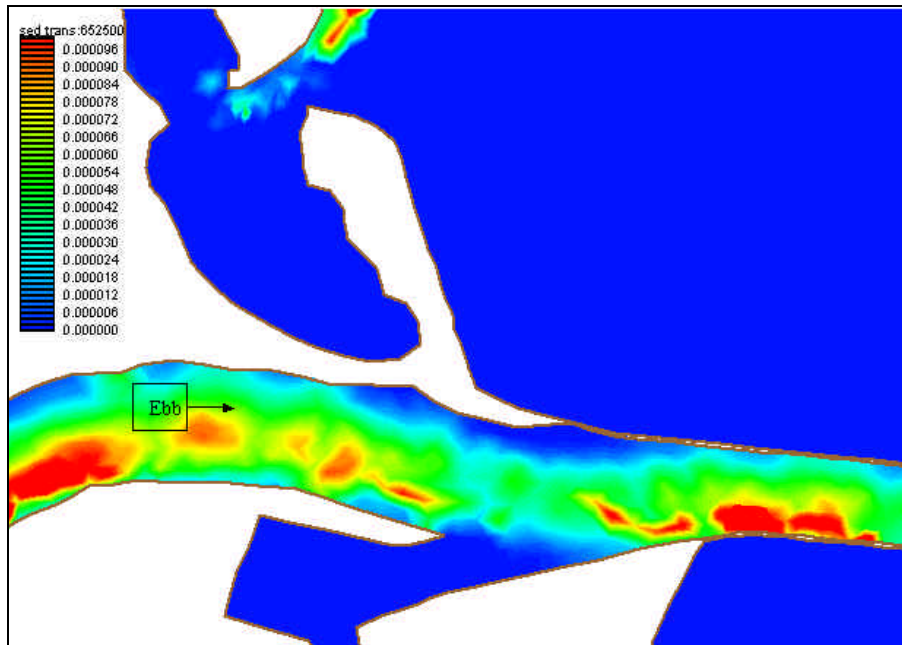


Figure 46. Contours of sediment transport rate ($\text{m}^3/\text{s}/\text{m}$) during peak ebb velocity for existing conditions in the St. Johns River

Alternative 1: Flood Shoal Mining

The next set of figures gives a description of sediment transport for the first alternative (flood shoal mining). Figures 47 and 48 illustrate the primary area of sediment transport occurs through the throat of the inlet during both flood and ebb conditions. Figure 47 suggests that during flood flow, sediment will erode from the inlet throat, where a high transport potential exists, and deposit in the bay area and bridge vicinity, where the transport potential decreases toward zero. The velocity vectors during this flow condition, Figure 29, indicate that while some of the flow turns south into the dead-end system of the bay, the majority of flow heads north through the bridge along the west bank. Thus, a flood shoal will likely redevelop with a possible slight westward change in its location. Figure 48, depicting sediment transport rates during ebb flow, indicates that the ebb shoal complex will likely reorient to the south given the new inlet orientation. Since both figures indicate high transport rates through the throat of the inlet, this alternative should not reduce the erosion rates experienced along the southern tip of Little Talbot Island.

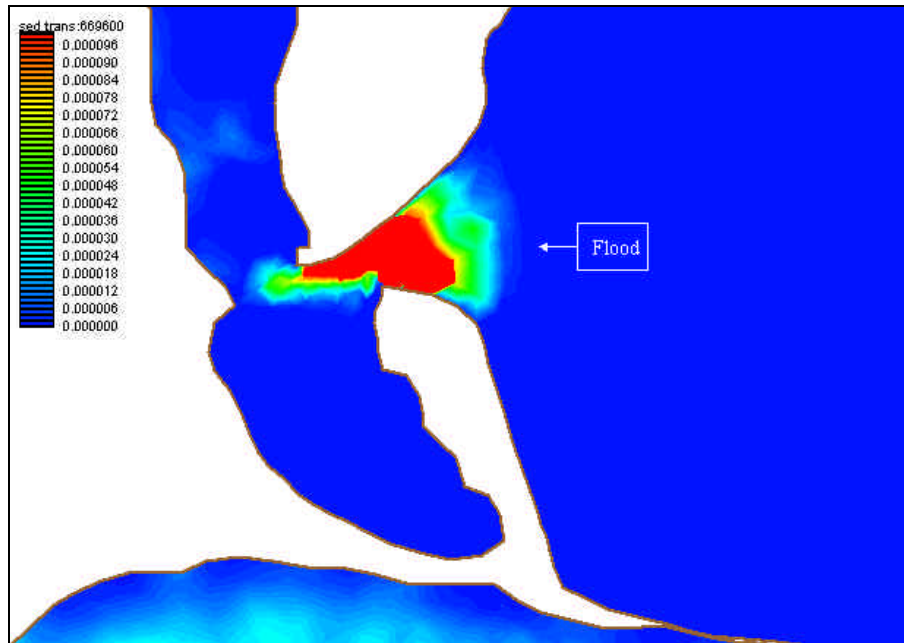


Figure 47. Contours of sediment transport rate ($\text{m}^3/\text{s}/\text{m}$) during peak flood velocity for Alternative 1

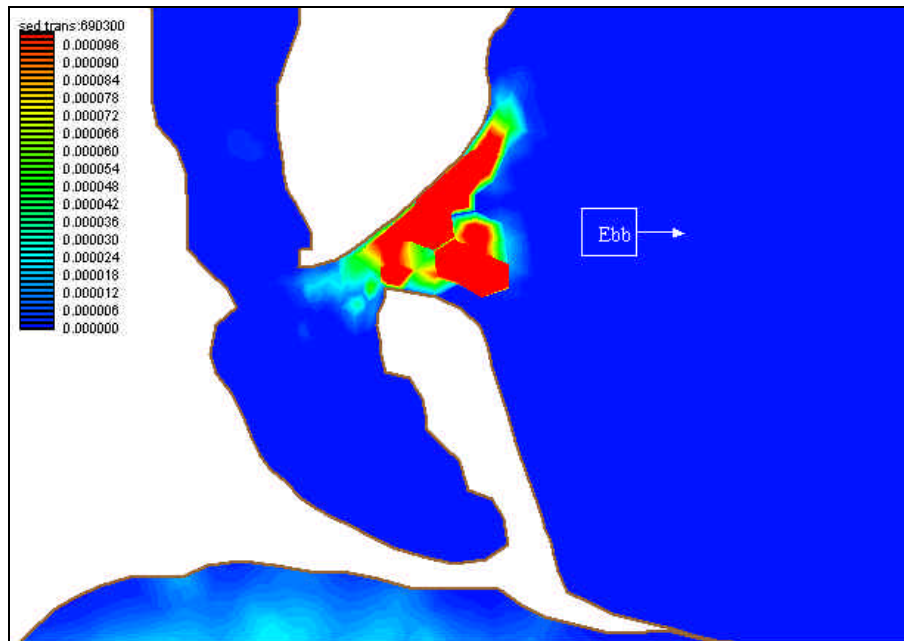


Figure 48. Contours of sediment transport rate ($\text{m}^3/\text{s}/\text{m}$) during peak ebb velocity for Alternative 1

Difference plots (Figures 49 and 50) that show the changes in sediment transport between existing conditions and this alternative provide a clearer picture of how the alternative modifies the sediment transport climate. The difference plot during flood flow indicates that removing the flood shoal and

backpassing the sediment to Little Talbot Island results in significant increases in sediment transport potential through the inlet throat and significant decreases in the sediment transport rate near the removed flood shoal. This may indicate increased erosion in the inlet throat including the extended Little Talbot Island and the reformation of a flood shoal north of the bridge. The difference plot during ebb flow, Figure 50, shows a decrease in sediment transport potential in the area of the removed shoal. Because the sediment transport plot (Figure 48) does not suggest a great deal of suspended sediment in the flow at this time and location, little deposition will result. The figure does indicate increased sediment transport potential through the inlet. This occurs, in part, due to a shift of the main channel through the inlet to a more southern location in response to the nourishment of Little Talbot Island. It may also suggest possible erosion occurring along the adjacent shorelines — Little Talbot Island and Ward’s Bank. Both difference plots suggest that dredging the flood shoal with backpassing to Little Talbot Island would not abate the processes that currently contribute to the erosion of the southern shoreline of the island. In fact, as the green contours show, this alternative may actually exacerbate the problem.

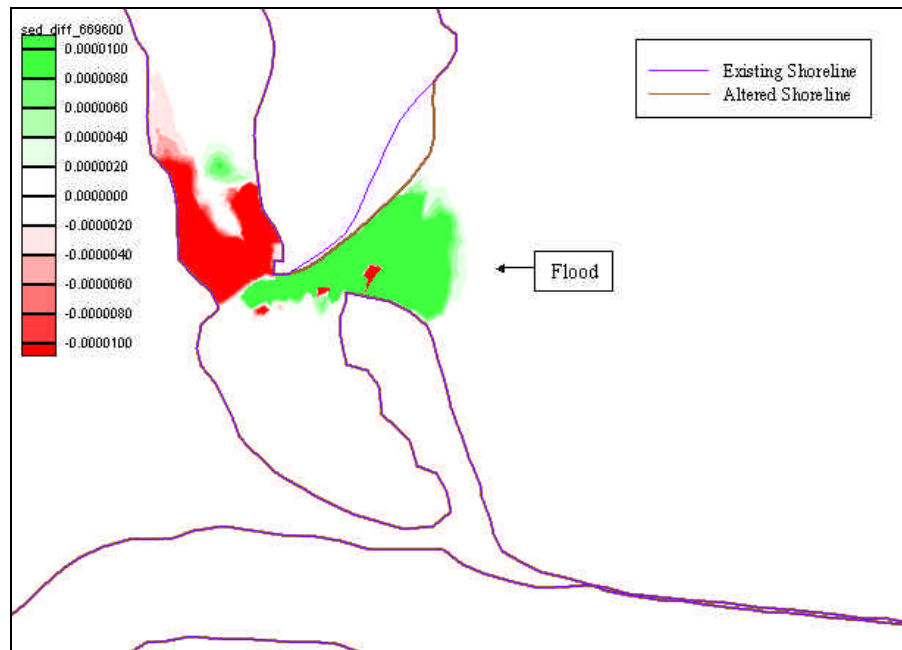


Figure 49. Contours of differences in sediment transport rate ($m^3/s/m$) between Alternative 1 and existing conditions during peak flood velocity

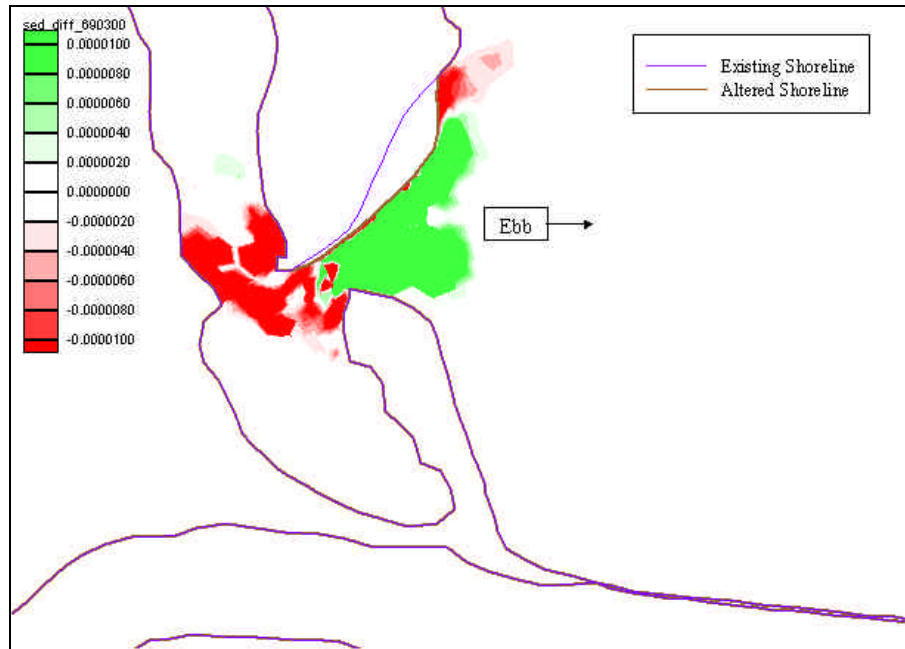


Figure 50. Contours of differences in sediment transport rate ($m^3/s/m$) between Alternative 1 and existing conditions during peak ebb velocity

Alternative 2: Ward's Bank Mining

The next set of figures (Figures 51 through 54) illustrates the sediment transport rates for Alternative 2 (Ward's Bank mining) during peak flood and ebb velocity. For this alternative, during flood flow, significant sediment transport occurs immediately north of the bridge. Rates are especially high along the west bank. This may suggest a slight northern migration and reshaping of the flood shoal, as well as possible erosion of the west bank. During ebb flow, as Figure 52 shows, areas of high sediment transport occur along the east and west banks near the bridge. This suggests possible erosion beneath the bridge.

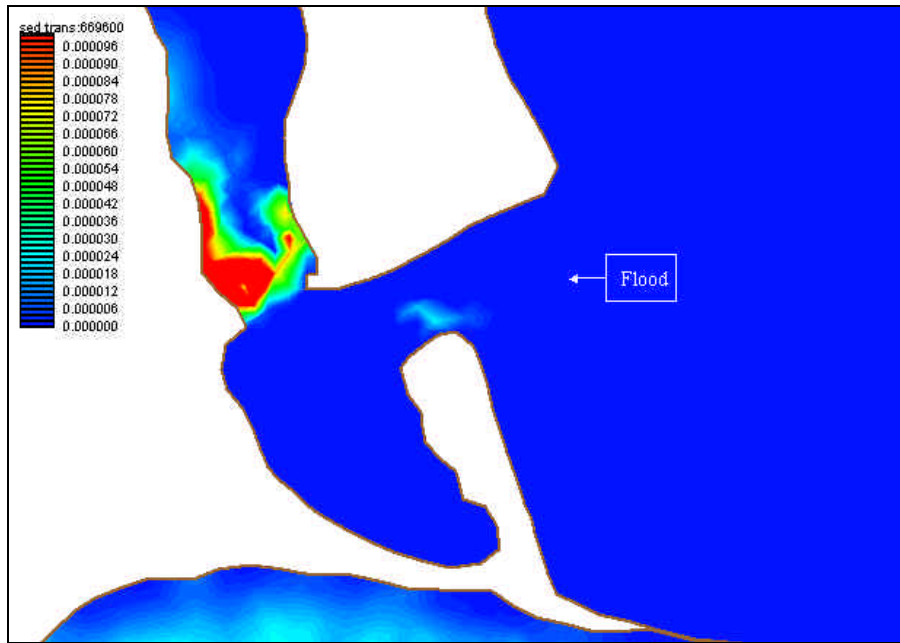


Figure 51. Contours of sediment transport rate ($m^3/s/m$) during peak flood velocity for Alternative 2

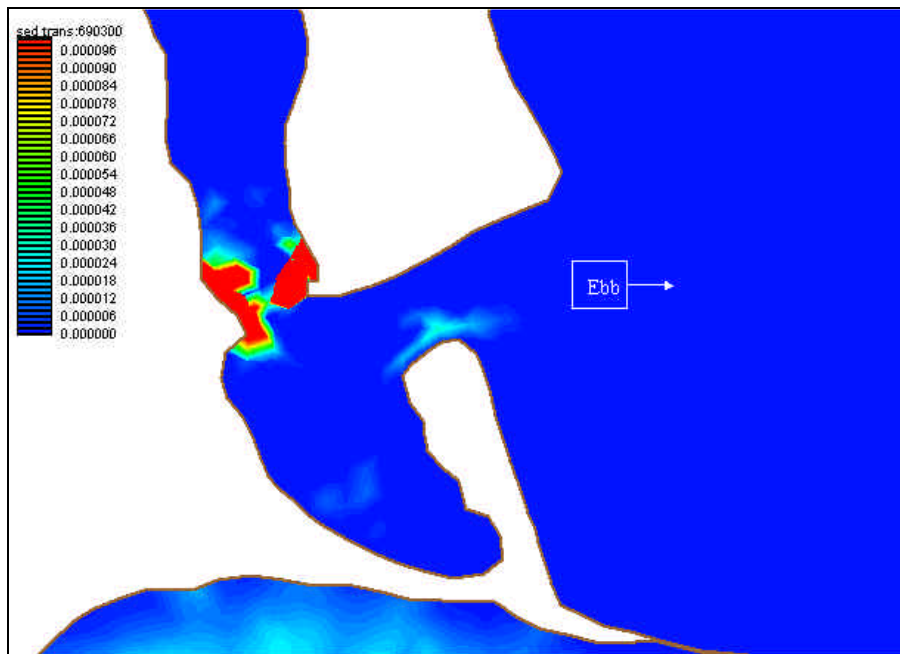


Figure 52. Contours of sediment transport rate ($m^3/s/m$) during peak ebb velocity for Alternative 2

Figures 53 and 54 show the difference in sediment transport potential between this alternative and the existing conditions during peak flood and ebb flows. During both flood and ebb, an increase in sediment transport occurs immediately north of the bridge, and a decrease in sediment transport

potential occurs throughout the inlet throat. These trends are direct responses to the increased prism through the inlet. This alternative did not involve any modification to the Ft. George River north of the bridge. As such, the river will tend to increase its depth in response to the increased flow rate. Conversely, the inlet throat, deepened significantly as part of this alternative, will tend to shoal. The decrease in sediment transport in the throat of the inlet may also result in part from the southern shift of the main channel through the inlet due to the Little Talbot Island extension.

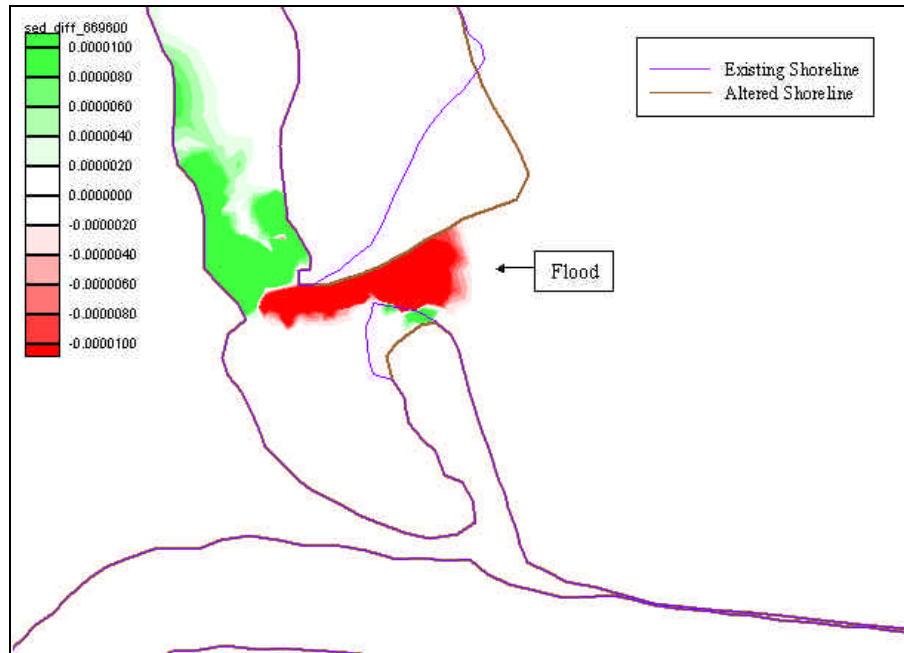


Figure 53. Contours of differences in sediment transport rate ($m^3/s/m$) between Alternative 2 and existing conditions during peak flood velocity

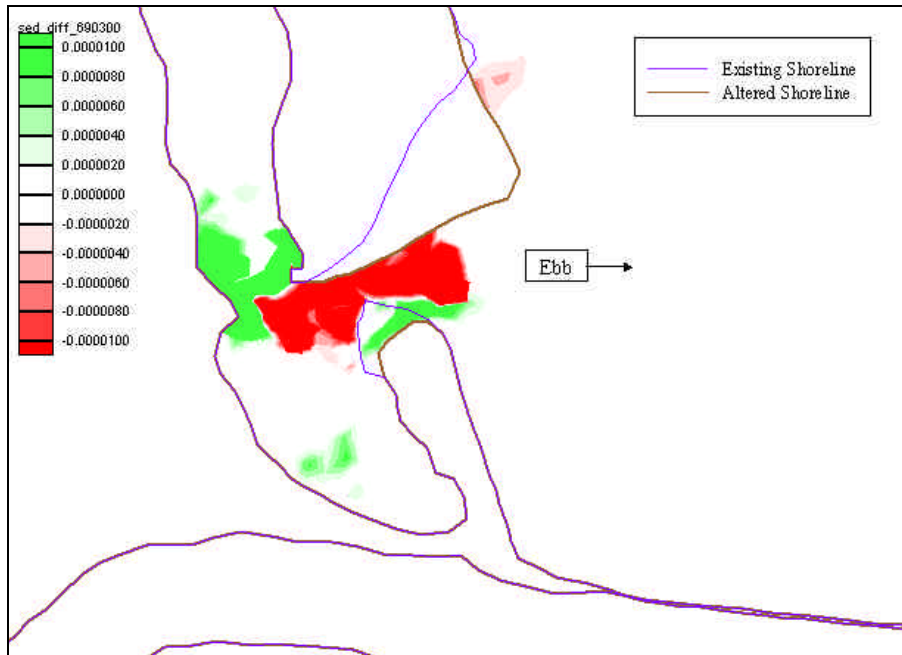


Figure 54. Contours of differences in sediment transport rate ($\text{m}^3/\text{s}/\text{m}$) between Alternative 2 and existing conditions during peak ebb velocity

Alternative 3: North Jetty Shoal Mining

Figures 55 and 56 display the sediment transport potentials for the third alternative, north jetty shoal mining, for flood and ebb flows. During both flood and ebb, the model predicts low sediment transport potential near the Mayport Basin Entrance and in the area of the dredging operations. The model predicts higher sediment transport rates both east and west of this location. The effective channel widening that results from shoal removal induces a decrease in velocity and, hence, a decrease in sediment transport potential. The abrupt change in bathymetry at the ends of the shoal removal area also affects sediment transport. As flow travels from a deep to shallow bathymetry, velocity increases and thus the sediment transport potential increases as well. This leads to increased sediment suspension. Conversely, as flow travels from a shallow to deep area, velocity decreases. Decreased velocity reduces sediment transport potential and leads to sediment deposition. Figures 55 and 56 also illustrate that the resulting sediment deposition will cause shoal redevelopment by tidal mechanisms and possible shoaling within the channel.

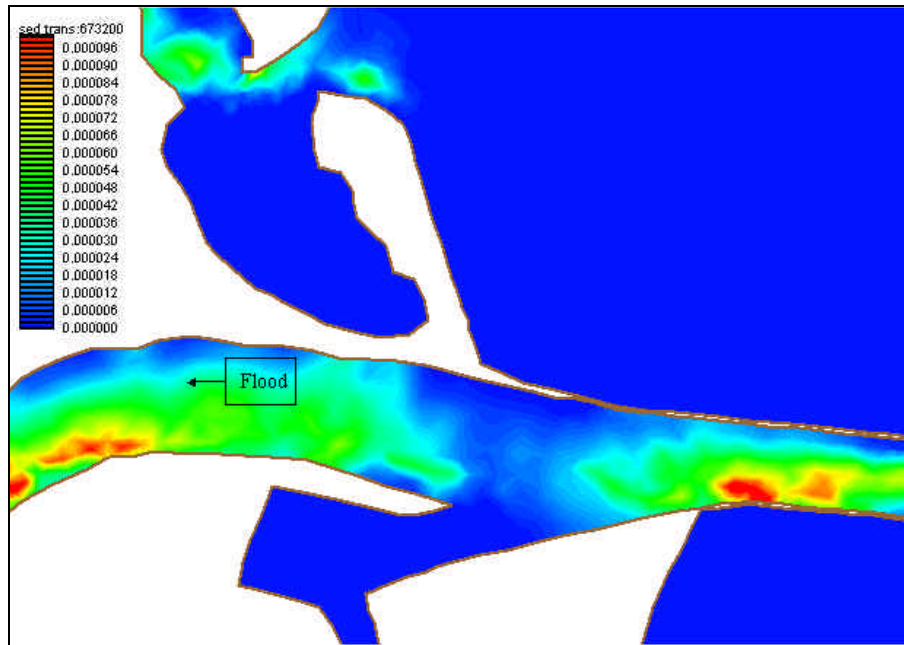


Figure 55. Contours of sediment transport rate ($m^3/s/m$) during peak flood velocity for Alternative 3

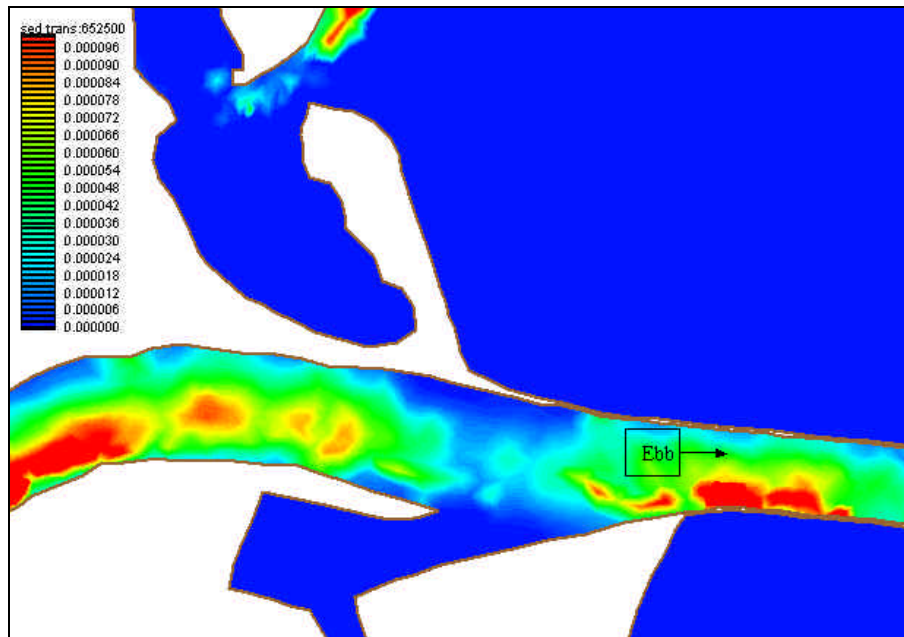


Figure 56. Contours of sediment transport rate ($m^3/s/m$) during peak ebb velocity for Alternative 3

Figures 57 and 58 show the difference in sediment transport potential between this alternative and the existing conditions. Both the flood and ebb figures indicate a decrease in sediment transport across the channel near the shoal location and Mayport Basin Entrance due to the north jetty shoal

removal. A larger, more extensive decrease in transport potential occurs on ebb flow. As a net result, tidally transported sediments would increase shoaling in the navigation channel. The figures also display increases in sediment transport east and west of the dredged area. These likely result from the changes in bathymetry and flow patterns at these locations. Before shoal mining, flow moved around the shoal such that these areas experienced low velocities. With the shoal mining, the flow velocities in these areas increase and thus increase sediment transport. The patterns in this area suggest increased shoaling near the north jetty following shoal removal. However, as stated in Chapter X, the formation of this shoal most likely resulted from littorally transported sediments. Re-establishment of this shoal will therefore likely be dominated by this mechanism (littoral transport) rather than the increased tidal shoaling contribution.

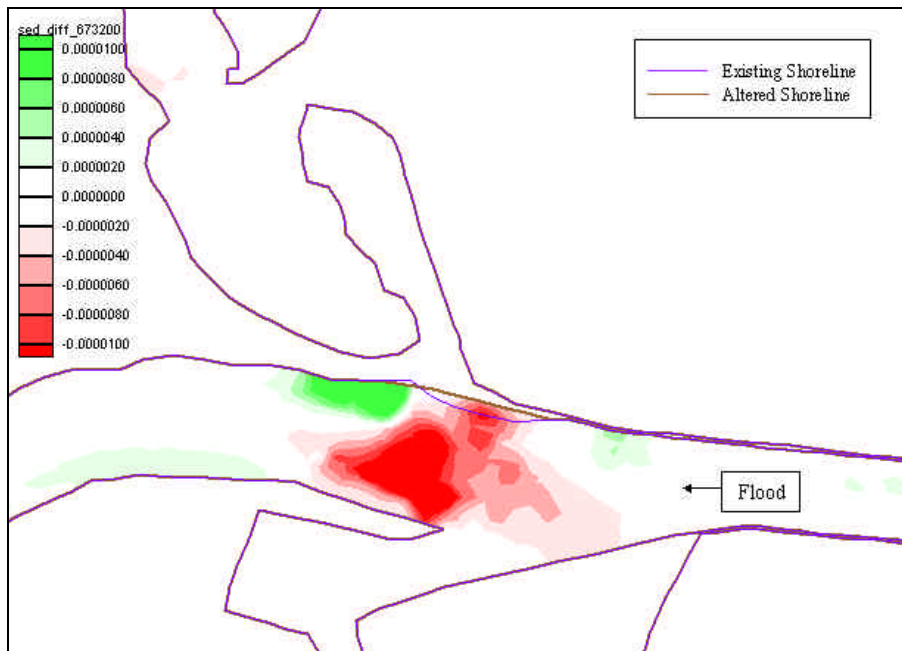


Figure 57. Contours of differences in sediment transport rate ($m^3/s/m$) between Alternative 3 and existing conditions during peak flood velocity

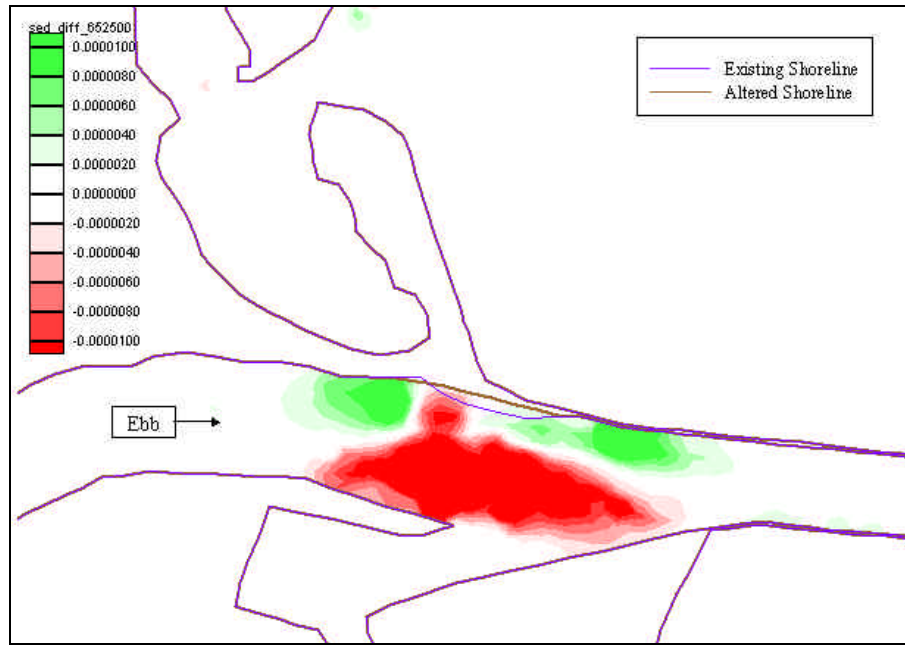


Figure 58. Contours of differences in sediment transport rate ($m^3/s/m$) between Alternative 3 and existing conditions during peak ebb velocity

4 Nearshore Wave Modeling and Littoral Transport Analyses

Other coastal processes that may change as a result of the proposed alternatives include wave climate and the associated littoral transport. The following sections describe work performed to support the wave transformation aspect of this study. This work includes the analysis of wave data, characterization of the wave climate, and computation of the alongshore sediment transport potential. The analysis addresses existing wave conditions, wave conditions associated with the alternatives that modify the offshore wave climate, as well as the transport node downdrift of the St. Johns River Entrance.

Wave Modeling

Wave Climate

The wave analysis intends to characterize representative wave conditions in the Ft. George River area. The modeling efforts first required a characterization of the offshore wave climate. This characterization makes use of the U.S. Army Corps of Engineers Wave Information Study (WIS) hindcast data. The WIS data provides hindcast wave parameters at stations along the coasts of the Pacific and Atlantic Oceans, Great Lakes, and the Gulf of Mexico. WIS Station 26, located at latitude 30.25°N and longitude 81.25°, provided hindcast wave data deemed representative of the waves reaching Ft. George Inlet. The wave data includes three-hourly spectrally based significant wave height, H_{mo} , wave peak period, T_p , and wave mean direction, θ , from 1976 to 1995.

The analysis began with the 20-yr WIS data sorted by angle of incidence into 16 bands each having 22.5° intervals. Because the representative wave conditions provide the inputs to estimate the long-term alongshore sediment transport potential, the analysis considered only the waves propagating into the inlet area. Table 12 shows the wave angle band limits relative to true north and to the approximate shore normal (1.7° west of true north). Waves in each band were further sorted into three period bands: $T=6$ sec, $6<T<10$

sec, and $T=10$ sec. Table 13 shows the sorted WIS data by number of events, percentage of occurrence, averaged wave height, period, and direction. Representative wave cases shown in Table 14 were selected from Table 13 based on their probability of occurrence ($> 1\%$) and from working knowledge of the seasonal and episodic wave directions at Ft. George Inlet.

Angle Band	Band Limits Relative to True North	Band Limits Relative to shore normal
2	9.5° to 32°	78.8° to 56.3°
3	32° to 54.5°	56.3° to 33.8°
4	54.5° to 77°	33.8° to 11.3°
5	77° to 99.5°	11.3° to -11.3°
6	99.5° to 122°	-11.3° to -33.8°
7	122° to 144.5°	-33.8° to -56.3°
8	144.5° to 167°	-56.3° to 78.8°

Angle Band	Period Band	No. of Events	Percent Occurrence	H_{mo} (m)	T_p (sec)	T (azimuth)
2	1	600	1.0%	1.4	5	21.9°
2	2	314	0.5%	1.5	8	23.5°
2	3	681	1.2%	1.1	13	22.3°
3	1	696	1.2%	1.2	5	44.3°
3	2	1,116	1.9%	1.5	8	46.0°
3	3	1,547	2.6%	1.3	12	45.4°
4	1	1,282	2.2%	1.1	5	67.4°
4	2	5,274	9.0%	1.3	8	68.8°
4	3	8,822	15.1%	1.3	13	69.4°
5	1	1,628	2.8%	0.9	6	88.0°
5	2	13,549	23.2%	0.9	8	89.6°
5	3	8,857	15.2%	1.1	12	86.0°
6	1	858	1.5%	0.9	5	108.8°
6	2	3,900	6.7%	0.8	8	106.6°
6	3	1,457	2.5%	1.0	12	108.6°
7	1	378	0.6%	1.1	5	132.9°
7	2	835	1.4%	0.9	8	132.2°
7	3	530	0.9%	1.0	12	132.2°
8	1	317	0.5%	1.0	4	154.9°
8	2	427	0.7%	0.9	8	154.4°
8	3	272	0.5%	1.0	12	154.4°

Case No.	No. of Events	Percent Occurrence	H_{mo} (m)	T_p (sec)	? (azimuth)	Peakedness Parameter ξ	Directional Spreading Coefficient nn
21	600	1.0%	1.4	5	21.9°	3.3	4
23	681	1.2%	1.1	13	22.3°	5.0	12
31	696	1.2%	1.2	5	44.3°	3.3	4
32	1,116	1.9%	1.5	8	46.0°	3.3	4
33	1,547	2.6%	1.3	12	45.4°	4.0	10
41	1,282	2.2%	1.1	5	67.4°	3.3	4
42	5,274	9.0%	1.3	8	68.8°	3.3	4
43	8,822	15.1%	1.3	13	69.4°	5.0	12
51	1,628	2.8%	0.9	6	88.0°	3.3	4
52	13,549	23.2%	0.9	8	89.6°	3.3	4
53	8,857	15.2%	1.1	12	86.0°	4.0	10
61	858	1.5%	0.9	5	108.8°	3.3	4
62	3,900	6.7%	0.8	8	106.6°	3.3	4
63	1,457	2.5%	1.0	12	108.6°	4.0	10
72	835	1.4%	0.9	8	132.2°	3.3	4
TOTAL	51,102	87.4%					

Wave Model Setup

The wave model requires two inputs to calculate wave transformations. These inputs include a description of the bathymetry in the form of a Cartesian grid and the input incident wave spectrum at the offshore boundary. The Morgan & Eklund, Inc. July 2001 survey provided the most recent bathymetry data around the Ft. George River. Bathymetry data for areas outside the survey coverage were identical to those described in Chapter 3 for the circulation modeling. These combined data sets provided the input to create a 419 x 405 bathymetric grid with 50 m spacing in both cross-shore and alongshore directions. This grid, therefore, measured 20.95 km cross-shore and 20.25 km alongshore. As shown in Figure 59, the alongshore axis of the grid orients 1.7° west of true north to align the offshore boundary close to the shore. Horizontal coordinates reference the UTM North American Datum 1983, Zone 17, in meters. All grid point elevations refer to the mean tide level (MTL) in meters.

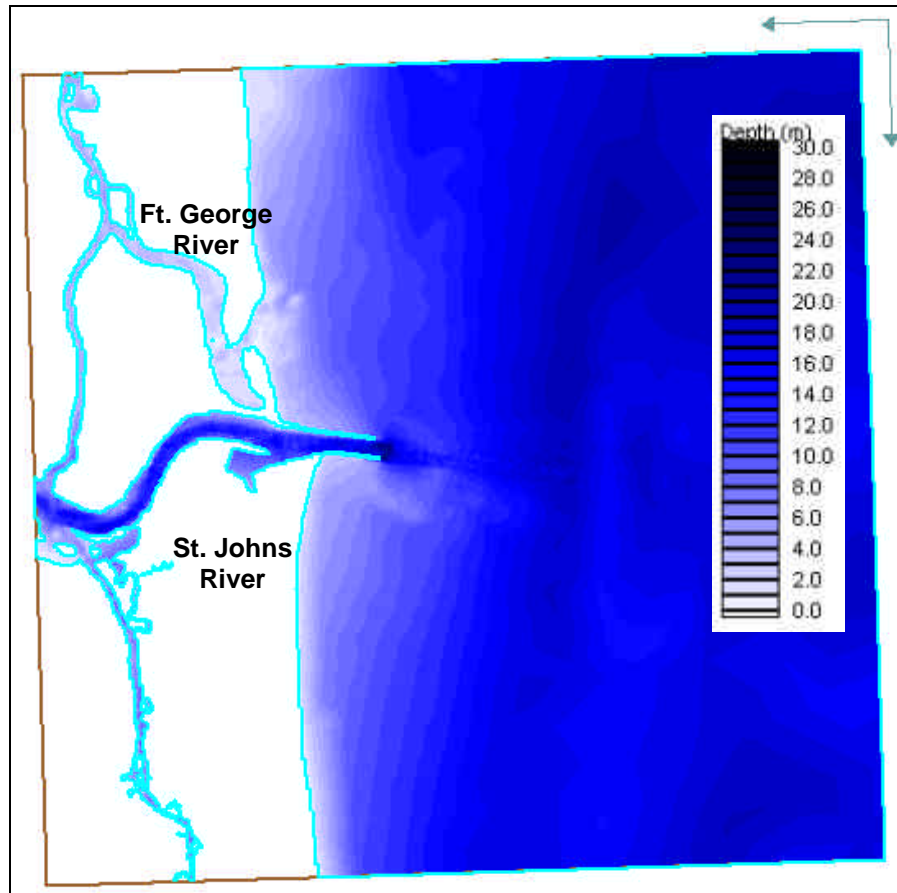


Figure 59. Model domain and existing depth contours

Refraction and Shoaling Computations

The finite-difference phase-averaged spectral wave model STWAVE (Resio 1987, 1988a, 1988b; Davis 1992; Smith et al. 2001) provided estimates of wave refraction and shoaling from offshore depths of approximately 17 m to the shoreline. Table 14 shows the representative incident wave conditions as wave cases. A one-dimensional shallow-water TMA parametric spectral shape (named for the data sets reduced to develop the spectrum: TEXEL storm, MARSEN, and ARSLOE [Bouws et al., 1985]), together with a directional spreading function, was applied at the offshore boundary as a two-dimensional incident wave spectrum. The TMA spectrum and directional spreading function were generated through the Surfacewater Modeling System (SMS) Version 7.1 for each wave case condition. Table 14 lists the inputs for calculating the spectrum, wave height, peak period, and mean direction at an offshore boundary depth of 17 m. Thompson et al. (1996) provided a guide for selecting spectral peakedness parameter, g and directional spreading coefficient, mn .

The generated spectrum describes the distribution of energy density of a wave group as a function of wave frequency and incident direction. Each

spectrum was generated with 60 wave frequency bands (from 0 to 0.6 Hz) and 35 directional bands. STWAVE then computed the wave transformation for each wave condition by specifying the spectrum corresponding to each wave case at the offshore boundary. The results of the computations are discussed later in this chapter.

Alongshore Transport Computation

STWAVE provided the wave height and angle at each grid point from the offshore boundary toward the shoreline for every wave condition listed in Table 14. STWAVE Version 3.0 provides the location of the breaker line (defined as the grid cell within which the wave broke). For grid rows where STWAVE did not indicate a breaking grid cell, the breaking depth was calculated by applying linear wave shoaling from the offshore side of the STWAVE-determined breaker line grid to the shoreline. Wave breaking was assumed to begin when the wave height reached the STWAVE Version 3.0 breaking wave height H_b : $H_b \geq 0.1 L \tanh \frac{2d}{L}$ where d is the water depth and L is the wavelength. This procedure allows the estimation of the breaking depth, wave breaking height, and breaking angle along the coastline.

The breaking wave height H_b provides the input to compute the breaking wave energy density E :

$$E = \frac{1}{8} \rho g H_b^2 \quad (14)$$

where ρ is the density of seawater and g is the acceleration due to gravity. The CERC formula (USACE 1984) provides the alongshore sediment transport potential as a function of wave height H_b and angle α_b :

$$Q = 1290 \left(0.0884 \rho g^{3/2} H_b^{5/2} \sin 2\alpha_b \right) \quad (15)$$

where Q is in m^3/yr .

The wave energy density and the alongshore sediment transport potential calculated from equations (14) and (15) for each wave condition was weighted by the annual percentage of occurrence of the wave conditions (Table 14). The annual average energy density and alongshore sediment transport potential equaled the sum of all the weighted cases.

Wave Model Results

This section describes the results of the STWAVE wave transformation from the offshore boundary to the shoreline and the alongshore transport computed with Equation 15. This chapter examined only two bathymetries:

existing conditions and Alternative 2 (Ward's Bank mining). Neither Alternative 1 (flood shoal mining) nor Alternative 3 (north jetty shoal mining) involved significant changes to the offshore bathymetry. As such, the wave climate following implementation of these alternatives remained essentially identical to the wave climate for the existing conditions simulations. In addition to examining the wave climate near Ft. George Inlet, this section identifies the location of the transport node downdrift of the St. Johns River Entrance.

Existing Conditions

Figures 60 and 61 show the contours of the computed wave height and the vectors of wave direction from the offshore boundary to the shoreline. The appendix contains all other cases simulated for this study. Figure 60 shows the nearshore wave climate for Case 33 where the incident wave height $H_{mo} = 1.3$ m, wave period $T_p = 12$ sec, and incident angle $q = 45.4^\circ$ clockwise from true north. The northeastern waves increase to approximately 1.4 m in height before breaking. The vectors show wave refraction as waves reach shallower depths. The sharp change in contour color from green to yellow indicates the breaker line. In some areas, waves break as close as 50 m from the shoreline. Waves penetrating into the inlet are slightly refracted before quickly dissipating a few hundred meters into the river. The waves within a 500-m distance south of the jetties measured approximately 0.5 m in height due to wave diffraction and the sheltering effect of the jetties (Figure 60b). Waves entering the jetties (0.6 m in height) quickly disperse to below 0.25 m.

Figure 61 shows the nearshore wave climate for Case 52 where the incident wave height $H_{mo} = 0.9$ m, wave period $T_p = 8$ sec, and incident angle $q = 89.6^\circ$ clockwise from true north. This case, waves originating from the east, has the highest frequency of occurrence. Waves near the shoreline reach approximately 1 m in height before breaking. Minimal wave refraction occurs because the waves propagate almost perpendicular to the depth contours. Some wave refraction occurs very near to the shoreline, particularly near the jetties where the wave directions tend to approach the structures at a right angle. Waves entering Ft. George Inlet refract southward. This refraction allows the waves to penetrate farther into Ward's Bay where they quickly disperse.

The STWAVE model outputs wave height and angle for all grid points in the model domain. The alongshore sediment transport potential was calculated from Equation 15 with inputs of calculated wave breaking height and angle along the breaker line. Figure 62 shows graphs of the computed southward, northward, gross, and net alongshore sediment transport potential along the north and south coastlines from the St. Johns River jetties. In each graph, the vertical axis is the sediment transport potential and the horizontal axis is the distance along the coastline from the centerline of the St. Johns River. Given the absence of calibration data for this area, the sediment transport potential was normalized with the maximum calculated net

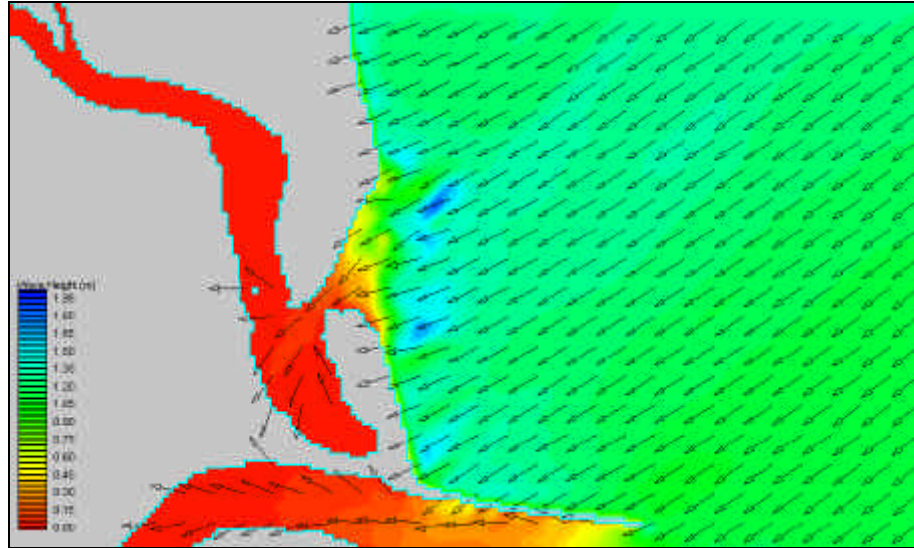
sediment transport potential on each graph. While this does not provide absolute estimates of littoral drift rates, it does provide information concerning relative magnitudes and direction of transport. Non-zero gradients of net sediment transport rate indicate areas along the coast where erosion or accretion can occur. Points coinciding with rapid changes in sediment transport rate slope show places that usually experience either strong erosion or accretion depending on whether the slope increases or decreases. A constant sediment transport rate slope between adjacent points along the coastline will result in sediment transport between these points. These points, however, will not experience erosion or accretion because of the dynamic equilibrium between the points.

Figure 62 indicates that immediately north of the St. Johns River, the net alongshore sediment transport potential occurs southward. A transport node lies approximately 1.4 km north of the St. Johns River. North of this node, the net transport occurs northward toward Ft. George Inlet. These trends are consistent with the overall behavior of Ward's Bank. Specifically, it explains the continued lengthening of the spit to the north and erosion at the center. The behavior north of the inlet is somewhat convoluted, however. The trends predict accretion immediately north of the inlet, which in fact occurs. However, north of this point, the calculations predict a net northward transport and an erosional trend, behavior the shoreline change analysis in Chapter 2 does not support. This analysis, however, does not take into account the effects of the tides that tend to pull sediments toward the inlet on both phases.

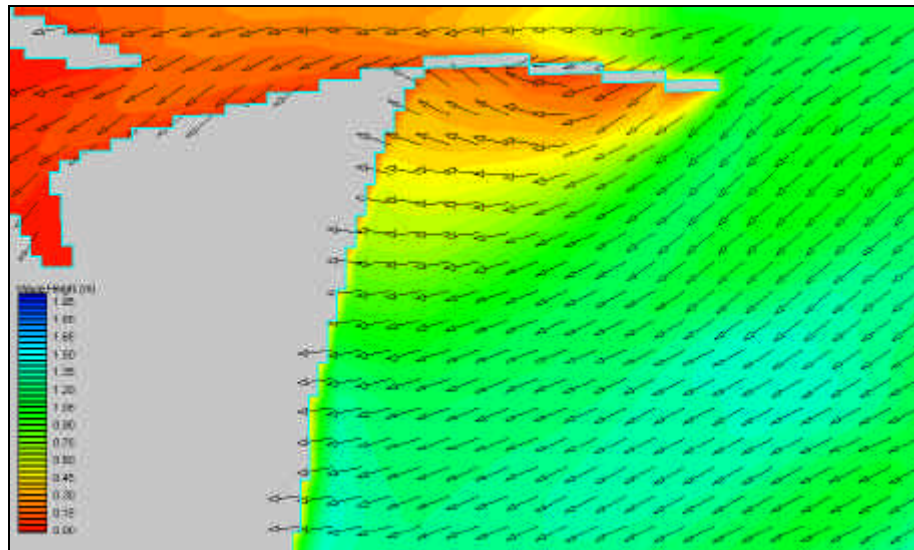
The following list summarizes the net sediment transport behavior around Ft. George Inlet.

- Sediments enter the area from the north, through either wave action or tidal flows.
- Sediments accumulate in the area of R-19 to R-20 updrift of the inlet.
- Tidal flows then transport sediments either offshore to form the ebb shoal or into the inlet for deposition in Ward's Bay or on the flood shoal north of the bridge.
- Wave action transports sediments from the ebb shoal around the inlet where they then settle onshore to Ward's Bank.
- From Ward's Bank, the wave climate transports sediments either north to elongate the spit or south through the jetties to form the shoal within the St. Johns River.
- The dynamic balance between the waves and tidal currents on the south side of the inlet leads to the elongation of Ward's Bank and migration of the inlet to the north.

South of the St. Johns River, the net sediment transport is typical of that found within the shadow zone of jetties (Figure 60b). Specifically, a net northward transport switches to a net southward transport approximately 0.75 km south of the St. Johns River centerline. South of this switch, transport decreases in magnitude but remains southward.

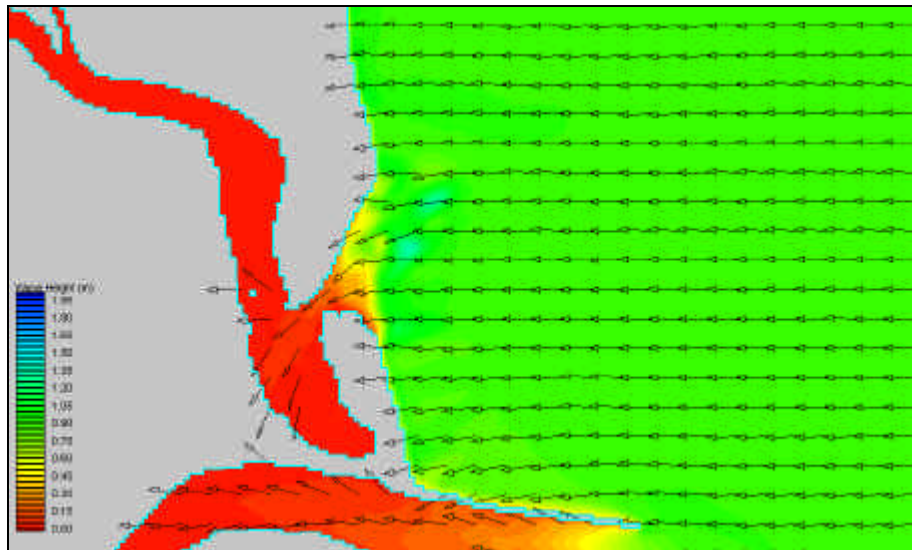


(a) North of Jetties

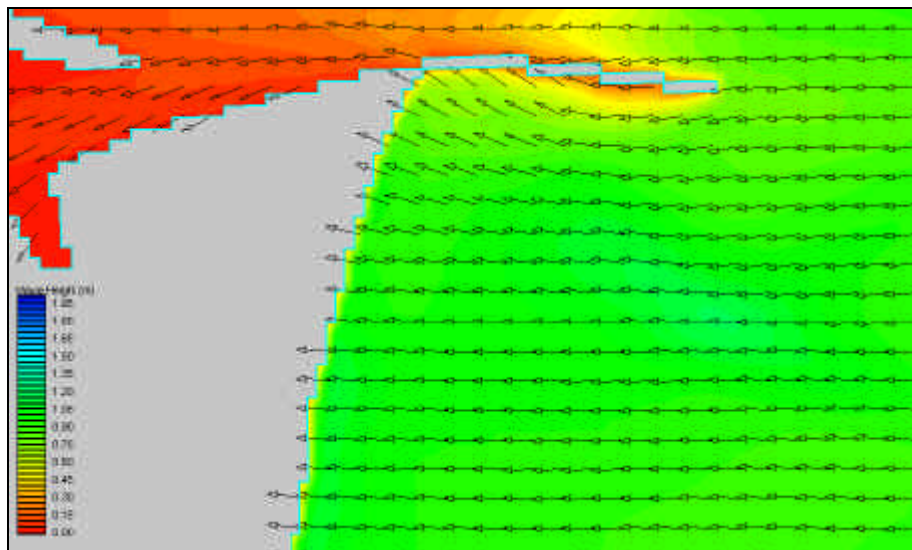


(b) South of Jetties

Figure 60. Computed wave heights and directions (Case 33: $H_{mo} = 1.3$ m, $T_p = 12$ sec)

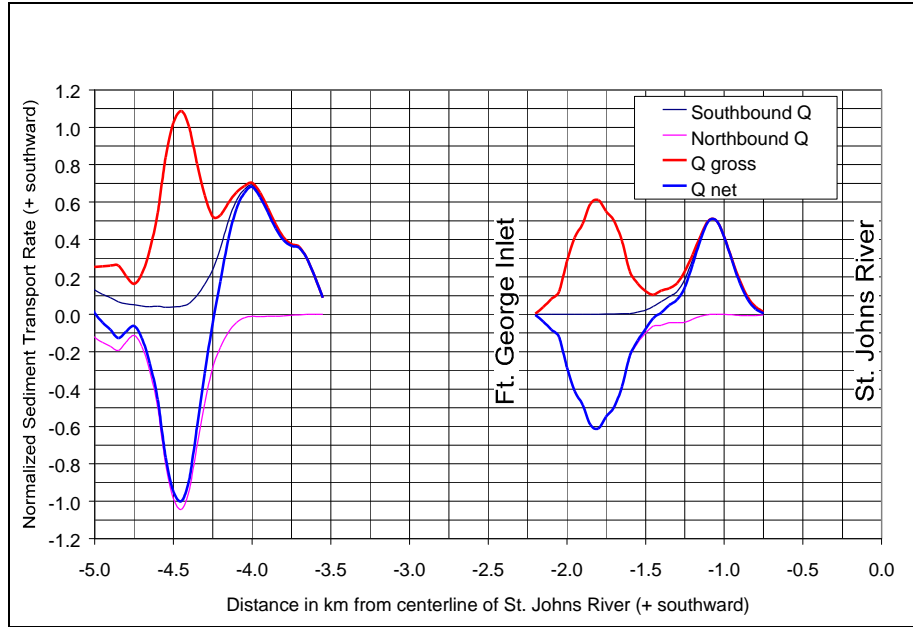


(a) North of Jetties

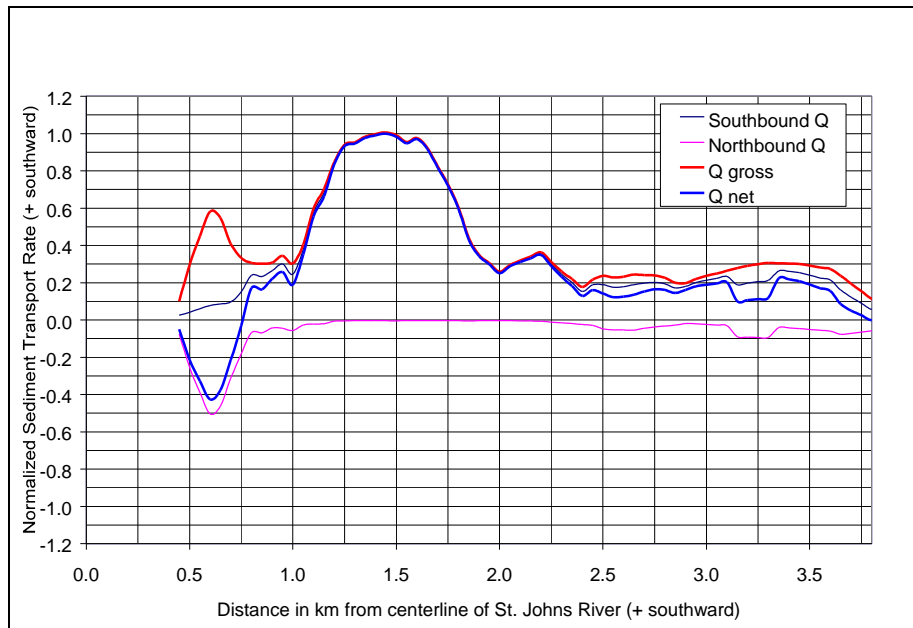


(b) South of Jetties

Figure 61. Computed wave heights and directions (Case 52: $H_{mo} = 0.9$ m, $T_p = 8$ sec)



(a) North of St. Johns River jetties



(b) South of St. Johns River jetties

Figure 62. Computed sediment transport potential (Existing Conditions)

Alternative 2: Ward's Bank Mining

Only Alternative 2 (Ward's Bank mining) involved significant modification to the offshore wave climate. As such, it is the only alternative presented and discussed in detail. For the other alternatives (1 and 3), the

wave climate and littoral drift mirror those presented in the previous section (Existing Conditions). This section discusses the effect on nearshore waves and on sediment transport potential of Alternative 2 (Ward's Bank mining). Figure 63 shows the Cartesian grid representing the bathymetry associated with this alternative. The model grid for this alternative starts with the existing conditions mesh and incorporates the changes associated with this alternative. The mouth of Ft. George Inlet and portions of Ward's Bank are dredged with the material backpassed to Little Talbot Island. Both Ward's Bank and Little Talbot Island are reshaped as shown in Figure 63 inset. The reshaped areas produce a shoreline reorientation and change in nearshore bathymetry. These, in turn, cause changes in the breaking wave heights and breaking angles when compared to existing conditions. Consequently, the alongshore sediment transport potential will also change.

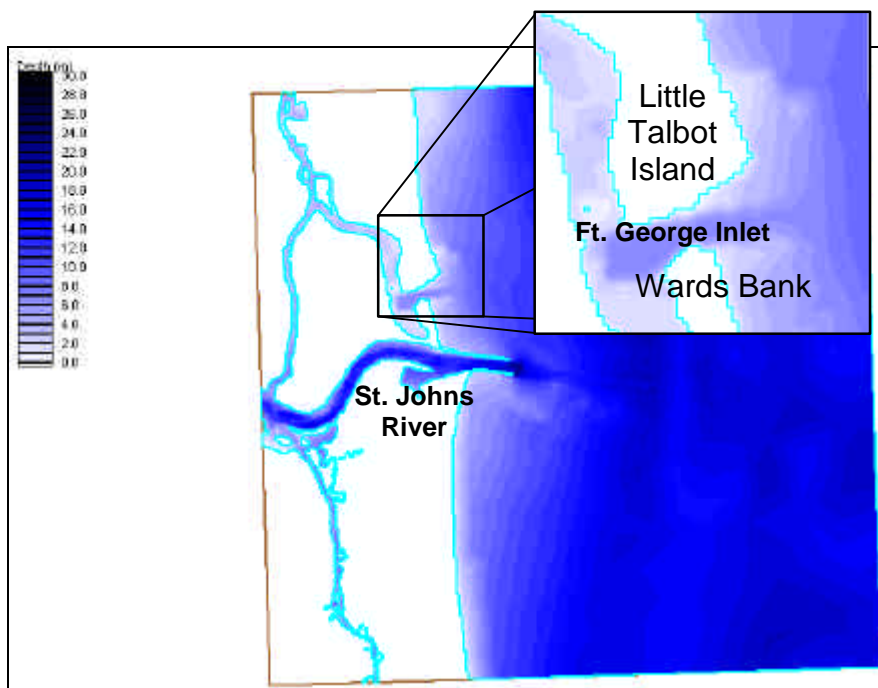


Figure 63. Alternative 2 (Ward's Bank mining) depth contours

Figures 64 through 66 show comparisons of nearshore waves near the mouth of the Ft. George River between existing conditions and the Ward Bank's alternative. Figures 64, 65, and 66 show three incident wave cases with waves entering from the northeast, east, and southeast quadrants. Each of these figures shows the computed nearshore wave climate under existing conditions, under this alternative, and the difference in wave heights (Ward's Bank wave heights minus existing conditions wave heights). Notably, the range in wave height change in the difference figures spans from -0.8 m (red) to +0.8 m (green). The vectors on the difference plots indicate the wave rays under the Ward's Bank mining alternative. The appendix contains figures showing wave heights, directions, and differences for all wave conditions studied.

The modification to the shoreline of Little Talbot Island and Ward's Bank widens the mouth of Ft. George Inlet, and dredging deepens the cross section. These modifications allow waves to penetrate farther into Ward's Bay and up the river before they break at shallower depths. The inlet mouth, therefore, should experience larger waves than usual (Point 2 in Figure 64). Under existing conditions, waves traveling toward Little Talbot Island's southeast shore refract south and enter the Ft. George River. With this alternative, the southeast shore of Little Talbot Island extends farther seaward (with the shallow depths associated with the shoreline moved eastward). This change in bathymetry induces waves to break further east than the existing conditions simulation predicts. Thus, at the alternative southeast shoreline of Little Talbot Island, wave heights decrease (on the order of 0.4 m to 0.7 m). This decrease occurs because under existing conditions, this area was deeper, and thus the waves had not shoaled as much. Waves traveling westward into the Ft. George River tend to break farther landward (red contours around Point 1 in Figure 64) with this alternative. Due to the deeper river mouth, waves decay at a slower rate and thus continue over longer distances into the river (green contours around Point 2). This alternative also changes the shape of the southern tip of Little Talbot Island. Compared with existing conditions, the orientation of the coastline north of Point 3 (Figure 64) shifts to a NNW alignment. From the vectors associated with the alternative, this change in orientation may reverse the direction of the longshore sediment transport northward. This would induce sediment movement away from the inlet mouth. Similar trends in wave height distributions occur in all the wave cases.

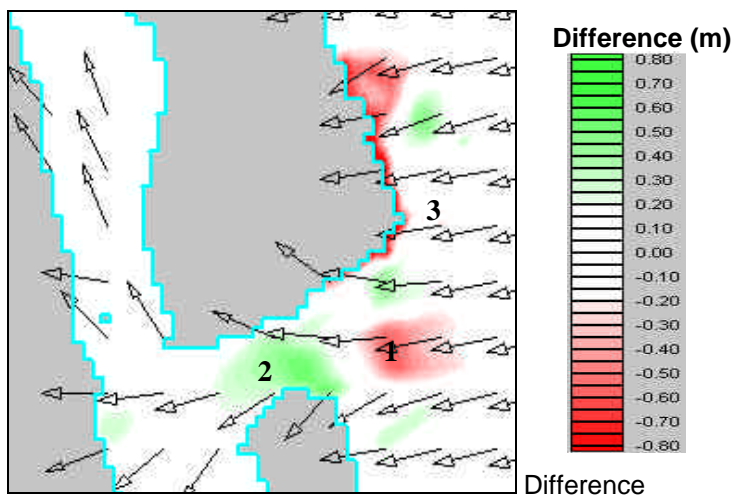
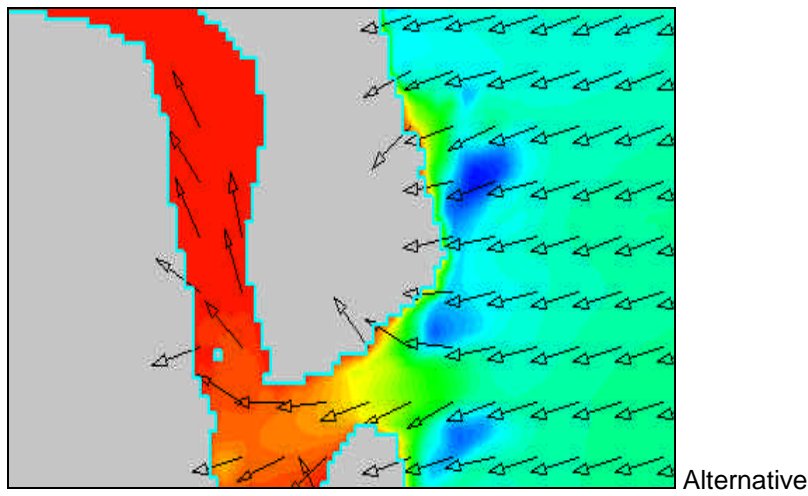
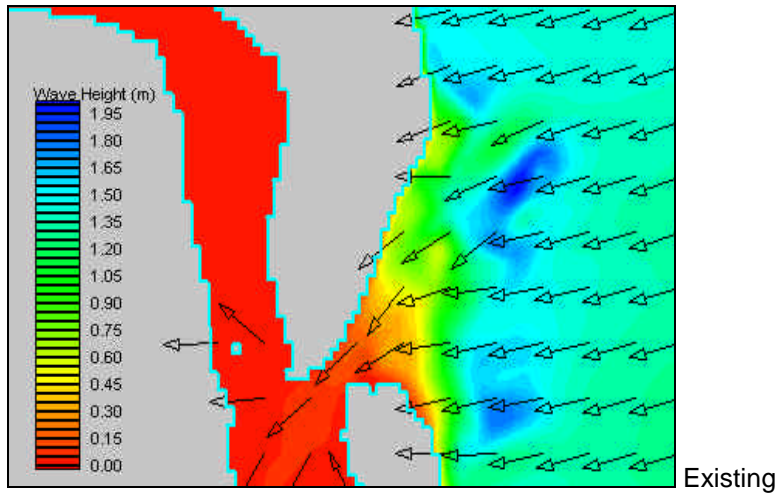


Figure 64. Wave results for case 43 ($H_{mo} = 1.3$ m, $T_p = 13$ s, $q = 69.4^\circ$)

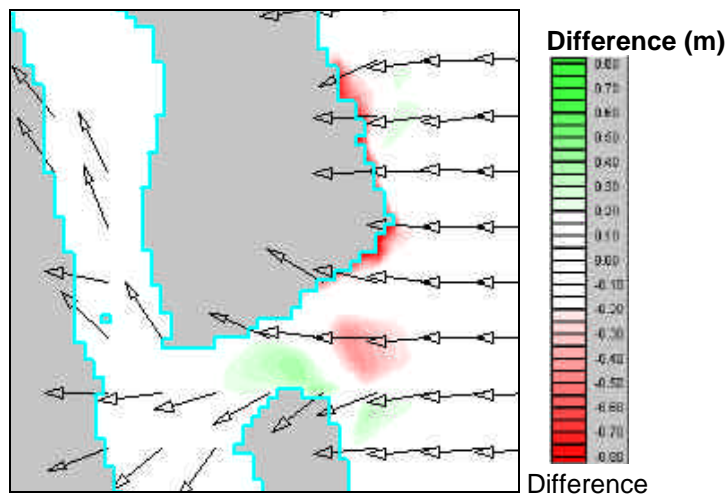
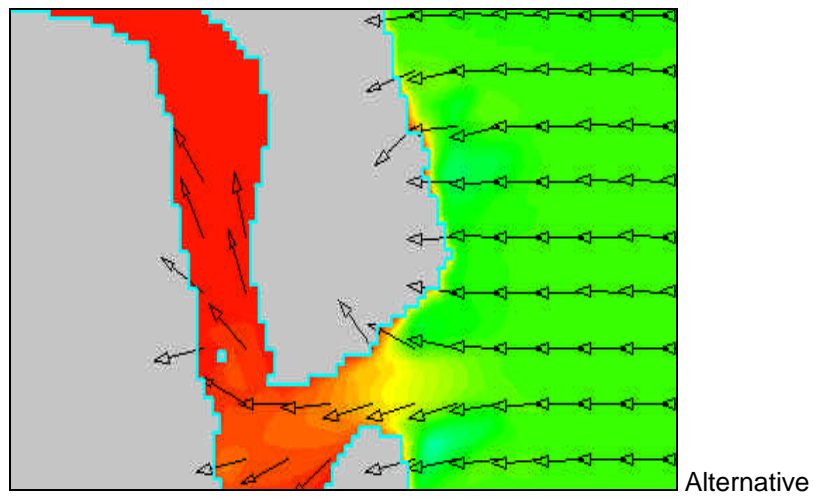
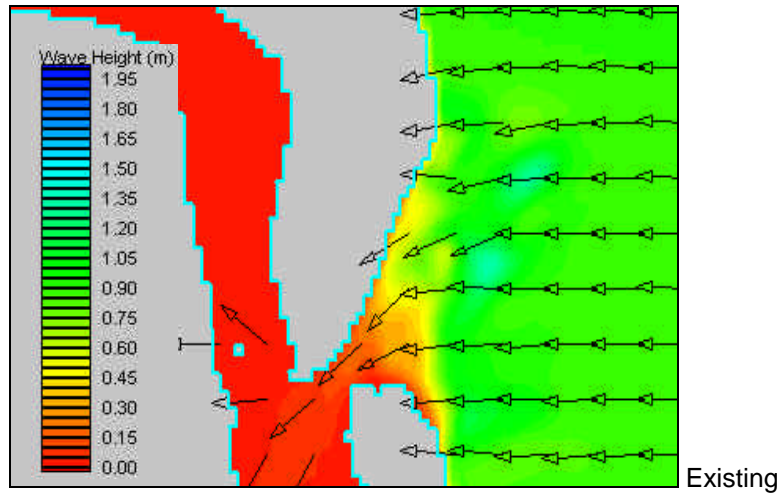


Figure 65. Wave results for case 52 ($H_{mo} = 0.9$ m, $T_p = 8$ s, $q = 89.6^\circ$)

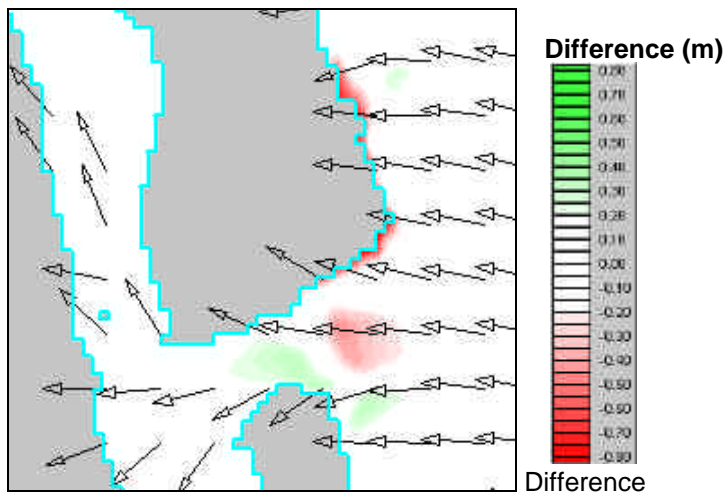
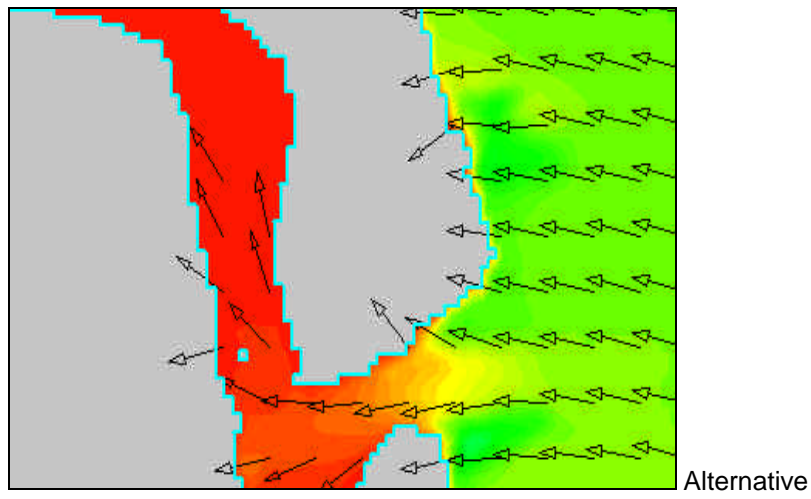
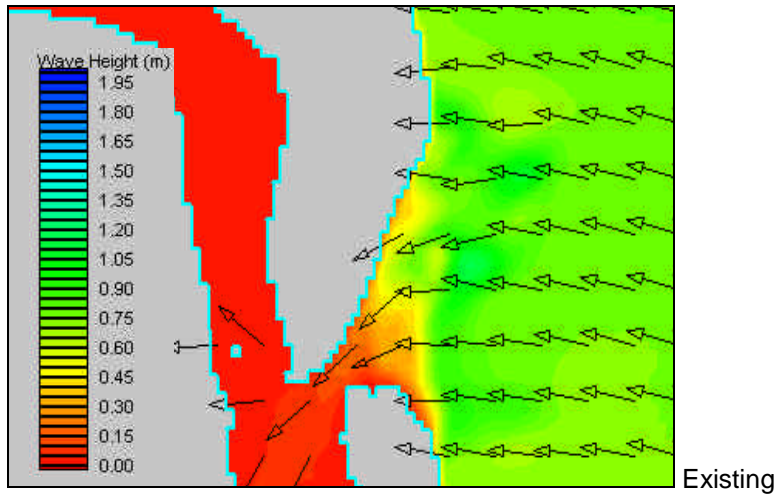


Figure 66. Wave results for case 62 ($H_{mo} = 0.8$ m, $T_p = 8$ s, $q = 106.6^\circ$)

Figure 67 shows a graph of the computed southward, northward, gross, and net longshore sediment transport potential associated with this alternative along the coastline north of the St. Johns River. The sediment transport rates shown in this figure were normalized by the same value as the calculations presented in the previous section (the maximum net sediment transport rate for the existing conditions simulations, Figure 62).

In Figure 67, this alternative produces a northward net sediment transport along the coastline 0.50 to 1.25 km north of Ft. George Inlet. The calculations predict a transport node approximately 1.25 km north of the inlet. Not surprisingly, the predicted node corresponds exactly to the area that currently exhibits shoreline accretion (R-19 to R-20). North of the node, the model predicts a net southward sediment transport. First identified in Figure 62, the transport node, located 1.75 km north of the inlet, appears in the same location for this alternative. South of the inlet, the net sediment transport exhibits similar trends as existing conditions. A transport node appears 1.25 km south of the inlet and the directions of the longshore sediment transport acts to elongate the existing spit.

Figure 68 shows the net longshore sediment transport for both the existing and alternative conditions. As this figure shows, the net longshore sediment transport remains unaffected 1.5 km north of the inlet. Between this point and the inlet, significant changes become apparent. The change in the shoreline of Little Talbot Island induces a net longshore sediment transport away (north) from the inlet. Also, the longshore sediment transport patterns would act to return the tip of the island to its existing configuration. South of the inlet, this alternative reduces the magnitude of longshore sediment transport. As a result, this alternative should induce a reduction in the elongation rate of Ward's Bank, at least temporarily.

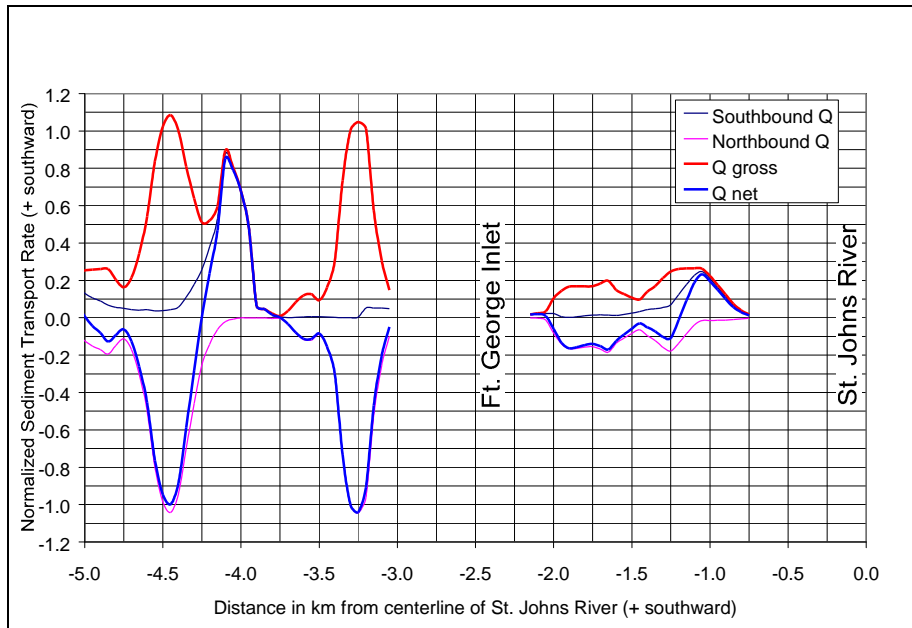


Figure 67. Computed sediment transport potential: Alternative 2

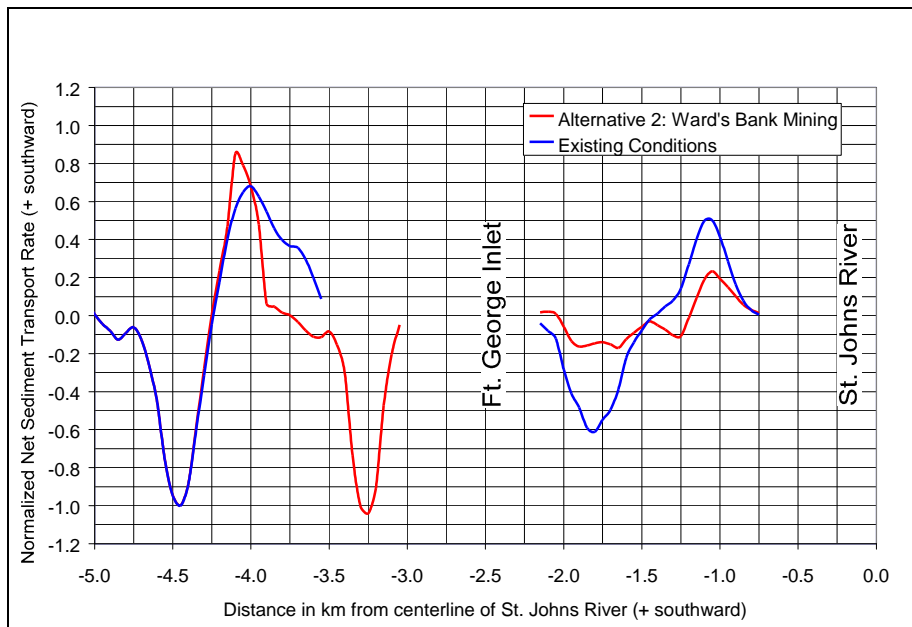


Figure 68. Net Sediment Transport Rate Potential (Alternative 2 and Existing Conditions)

5 Conclusions

This study evaluated the Regional Sediment Management Potential Demonstration Project concerning sediment handling in and around Ft. George Inlet. Specifically, this study evaluated the impacts of three proposed alternatives on the coastal processes (wave climate, tidal circulation, and their associated potential sediment transport) of the region. Alternative 1 involved dredging the flood shoal located in Ft. George River just north of the A1A Bridge and backpassing the dredged sediment to the southern tip of Little Talbot Island. This alternative would restore the island to its 1980 shoreline configuration. Alternative 2 involved dredging from Ward's Bay, across Ward's Bank, and into the ocean and backpassing the dredged sediment to the southern tip of Little Talbot Island. This alternative would restore the island to its 1970 shoreline configuration. Finally, Alternative 3 involved dredging the shoal located just south of the western tip of the St. Johns River Entrance north jetty and bypassing the dredged sediment to the beaches south of the St. Johns River Entrance. In addition to evaluating the coastal processes associated with these alternatives, this study also located the transport node south of the St. Johns River Entrance.

Alternative 1: Flood Shoal Mining

Modifications to the bathymetry associated with Alternative 1 (flood shoal mining with backpassing to Little Talbot Island) induce significant changes to tidal circulation through the inlet. On flood tides, high velocities occur through the inlet throat and along the west bank of Ft. George Inlet near the A1A Bridge. The removal of the flood shoal creates a more efficient flow path through the inlet on flood tides as the 18% increase in flood tidal prism indicates. North of the bridge, velocities in the vicinity of the former flood shoal decrease significantly with the increased local depths. On ebb tides, flow patterns exhibit similar behaviors to flood patterns. High velocities occur both in the inlet throat as well as along the west bank of Ft. George River. However, velocities decrease somewhat along the banks of the river (as compared with existing conditions) as the flow follows the deeper water associated with the dredging activities. Velocities also decrease slightly in Ward's Bay. Model simulations indicate that on spring ebb flow the tidal prism increases 4.3%. For this alternative, the spring flood to ebb tidal prism ratio equals 1.32 as compared with a value of 1.17 for existing conditions.

This indicates that the well-documented tidal pumping associated with this inlet will accentuate.

Tidal circulation modeling indicated that this alternative should have no detrimental impacts to structure-induced scour at the bridge. In fact, the reduction of velocities and flow reorientation actually reduce the scour potential. The sediment transport patterns the simulations predict indicate that the flow patterns will reestablish the flood shoal and possibly reorient the ebb shoal. Increases in sediment transport through the inlet on both flood and ebb tides indicate that this alternative has not addressed the instability associated with the inlet itself. Given that the wave climate remains identical to that associated with existing conditions and the high flows through the inlet throat, the life of the nourishment of the southern tip of Little Talbot Island should not exceed 20 years (the time between 1980 and the present). In fact, the nourishment would probably erode quicker than the 20-year estimate because the nourishment will not have the established vegetation and infrastructure that characterized Little Talbot Island in 1980.

Alternative 2: Ward's Bank Mining

The extensive bathymetric modifications associated with Alternative 2 (Ward's Bank mining and backpassing to Little Talbot Island) produce significant modifications to the flow patterns in and around Ft. George Inlet. On flood tides, the velocities through the throat of the inlet fall significantly below the velocities associated with existing conditions. The considerably larger cross section through the inlet becomes a much better flow conveyor. As such, the spring flood tidal prism increases by 26% as compared with existing conditions. North of the A1A Bridge, flood flow behaves similar to existing conditions. On ebb flow, the inlet experiences a dramatic increase (60%) in spring ebb tidal prism. The flood to ebb tidal prism ratio becomes 1.05 with this alternative, which also essentially eliminates the tidal pumping mentioned previously. This indicates that the tidal pumping associated with the inlet is largely a function of the inlet entrance configuration. The larger volume of water conveyed through the inlet on ebb produces much higher velocities in the Ft. George River north of the A1A Bridge. This alternative also increases the hydraulic pressure on the banks of the river as flow diverts around the flood shoal.

The increased flow and velocities through the bridge cross section may produce increased scour around the bridge foundations. Sediment transport patterns associated with the spring tides indicate that this alternative produces increased sediment transport rates in the river north of the bridge and decreased rates through the inlet. Following implementation of this alternative, these patterns indicate that the channel through the inlet should rapidly shoal in and the region north of the bridge should scour out. Sediment scoured from north of the bridge will transport either north farther up the river (relocation of the flood shoal) or south into the dredged area (channel shoaling).

Given the extensive changes to the offshore region, this alternative produced significant changes to the wave climate. The larger, deeper channel allows waves to pass more freely into Ward's Bay. This behavior should only last until the ebb shoal relocates south as it follows the channel. The change in shoreline orientation associated with the nourishment changes the predominant breaking wave angle. Predictions of littoral drift along the shoreline indicate that this alternative produces no change in littoral transport 1.5 km north of the inlet. South of this point, littoral drift transports sediment northward away from the inlet. This behavior will tend to erode the nourishment quickly. Similar to the previous alternative, the life of this nourishment should not last more than 30 years (the time between 1970 and the present). In fact, the nourishment would probably erode quicker than the 30-year estimate because the nourishment will not have the established vegetation and infrastructure that characterized Little Talbot Island in 1970. South of the inlet, littoral drift patterns indicate that the current trends reduce in magnitude. As a result, the rate of elongation of Ward's Bay should decrease.

Alternative 3: North Jetty Shoal Mining

The modifications to the bathymetry associated with this alternative (mining the shoal just south of the St. Johns River north jetty and bypassing to the beaches south of the river entrance) produce only localized impacts to the tidal circulation through the river entrance. Tidal circulation modeling indicated that this alternative produces only a small reduction in the velocities in the center of the river near the shoal on both ebb and flood flow. The simulations also predict a slight increase in velocity near the shoreline on either side of the dredged area. This alternative produces only negligible changes to the spring tidal prisms. The sediment transport patterns associated with these flows indicate a decrease in sediment transport potential near the center of the channel and a slight increase along the river's north bank. This implies that this alternative may increase shoaling in the navigation channel. The increase in transport rates near the bank indicates that flows should quickly fill in the dredged area. Also, sediment transported over the jetty and into this area should help reestablish the shoal. This alternative will not produce any change in the wave climate. Additionally, this alternative produces no adverse impacts to foundation scour at the A1A Bridge.

Littoral Drift Transport Node

Wave modeling of existing conditions south of the St. Johns River Entrance indicated the location of a transport node south of the river's south jetty. Here, crossing the node north to south, transport switches from northward directed to southward directed. The node lies approximately 1,500 ft south of the south jetty. This location corresponds approximately to temporary monument V-502 on the Mayport Naval Base property. Placement of sediments south of this location should reduce the likelihood of sediments returning to the river through wave transporting mechanisms.

Summary

This study examined three alternatives for sediment management in the Ft. George Inlet vicinity. Based on the findings, Alternative 3 causes the least impact to coastal processes. Alternative 1 provides additional shoreline protection to Little Talbot Island and reduces scour potential at the A1A Bridge. However, the life of the nourishment associated with this alternative will not last very long (relatively). Alternative 2 provides significant protection to Little Talbot Island. However, again, the nourishment will not last long, and this alternative may increase the foundation scour at the bridge. All alternatives provide viable sources of sediment for bypass or backpass operations. Selection of a course of action must weigh not only impacts to coastal processes and infrastructure, but also cost and volume of available sediment. Finally, should sand bypassing operations call for placement on the beaches south of the St. Johns River Entrance, placement of sediments south of monument V-502 should reduce the likelihood that sediments will return to the river via wave action.

References

- Bouws, E., Gunther, H., Rosenthal, W., and Vincent, C.L. (1985). "Similarity of the wind wave spectrum in finite depth waves; 1. Spectral form," *J. Geophys. Res.* 90(C1), 975-986.
- Davis, J.E. (1992). *STWAVE theory and program documentation, Coastal Modeling System User's Manual*, Instruction Report CERC-91-1, Supplement 1, M.A. Cialone, ed., U.S. Army Engineer Waterways Experiment Station, Vicksburg, MS.
- Gosselin, M.S., Cranston, E.A. and Carvalho, A. (2001) *DMS: Diagnostic Modeling System, Report 5, Jacksonville Harbor Navigation Project, Jacksonville, Florida, Evaluation of Problem Shoaling Areas, Channel Deepening, and Training Wall Structures*. Submitted for publication as an ERDC/CHL Technical Report, U.S. Army Corps of Engineers, Engineering Research and Development Center, Vicksburg, MS.
- Kojima, H. and Mehta, A. J. (1979) *Investigation of the Erosion Problem at Fort George Inlet*. University of Florida, Department of Coastal and Oceanographic Engineering, Gainesville.
- Le Provost, C., Genco, M.L., Lyard, F., Vincent, P., and Canceill, P. (1994). "Spectroscopy of the world ocean tides from a hydrodynamic finite element model," *Journal of Geophysical Research*, 99(C12), 24,777-24,797.
- Luetlich, R. A., Westerink, J. J., and Scheffner, N. W. (1992). *ADCIRC: An advanced three-dimensional circulation model for shelves, coasts, and estuaries; Report 1, theory and methodology of ADCIRC-2DDI and ADCIRC-3DL*, Technical Report DRP-92-6, U.S. Army Engineer Waterways Experiment Station, Vicksburg, MS.
- Marino, J. N., Kojima, H., and Mehta, A. J. (1990). "Case of an Updrift Migrating Inlet: Fort George Inlet, Florida." *Proceedings of the 1990 National Conference on Beach Preservation Technology*, FSBPA, Tallahassee.

- Mehta, A. J. and Marino, J. N. (1987). *Coastal Engineering Investigation of Erosion in the Vicinity of Fort George Inlet*. University of Florida, Department of Coastal and Oceanographic Engineering, Gainesville.
- Olsen Associates Inc. (1999). *Fort George Inlet Shoreline Erosion Study*. Olsen Associates Inc., Jacksonville, FL.
- Resio, D. T. (1987). "Shallow-water waves I: Theory," *J. Waterway, Port, Coastal, and Ocean Engineering*, ASCE, 113(3), 264-281.
- Resio, D. T. (1988a). "Shallow-water waves II: Data comparisons," *J. Waterway, Port, Coastal, and Ocean Engineering*, ASCE, 114(1), 50-65.
- Resio, D. T. (1988b). "A steady-state wave model for coastal applications," *In. Proc. 21st Coastal Engineering Conference*, ASCE, 929-940.
- Smith, J. M., Sherlock, A. R., and Resio, D. T. (2001). *STWAVE: Steady-State Spectral Wave Model User's Manual for STWAVE, Version 3.0*, ERDC/CHL SR-01-1, U.S. Army Engineer Research and Development Center, Coastal and Hydraulics Laboratory.
- Spechler, R. M., (1996). *Detection and Quality of Previously Undetermined Floridian Aquifer System Discharge to the St. Johns River, Jacksonville, to Green Cove Springs, Northeast Florida*. Water-Resources Investigations Report 95-4257. U.S. Geological Survey, Tallahassee.
- Taylor Engineering, Inc. (2000) *Hydraulic and Scour Analyses for the SR 105 (A1A) Fort George Bridge Replacement*. Technical Report, Jacksonville, FL.
- Thompson, E. R., Hadley, L. L., Brandon, W. A., McGehee, D. D., and Hubertz, J. M. (1996). *Wave response of Kahului Harbor, Maui, Hawaii*, Technical Report CERC-96-11, U.S. Army Engineer Research and Development Center, Vicksburg, MS.
- U.S. Army Corps of Engineers. (1997). *Duval County, Florida, Little Talbot Island, State Road-A1A/SR-105, Section 103 Shore Protection Feasibility Study, Detailed Project Report with Environmental Assessment*. U.S. Army Corps of Engineers, Jacksonville District. South Atlantic Division. Jacksonville, FL.
- U.S. Army Corps of Engineers. (1984). *Shore Protection Manual, Vol. I and II*. Waterways Experiment Station, Corps of Engineers, Vicksburg, Mississippi.
- U.S. Geological Survey. (1992). *Water Resources Data Florida Water Year 1992 — Volume 1A. Northeast Florida Surface Water*. Water Data Report FL-92-1A. Department of the Interior and the State of Florida.

- van Rijn, L. C. (1984a). "Sediment Transport, Part I: Bed Load Transport," *Journal of Hydraulic Engineering*, Vol. 110, No. 10, 1431-1456.
- van Rijn, L. C. (1984b). "Sediment Transport, Part II: Suspended Load Transport," *Journal of Hydraulic Engineering*, Vol. 110, No. 11, 1613-1641.
- van Rijn, L. C. (1984c). "Sediment Transport, Part III: Bed Forms and Alluvial Roughness," *Journal of Hydraulic Engineering*, Vol. 110, No. 12, 1733-1754.

Appendix

Wave Simulation Results

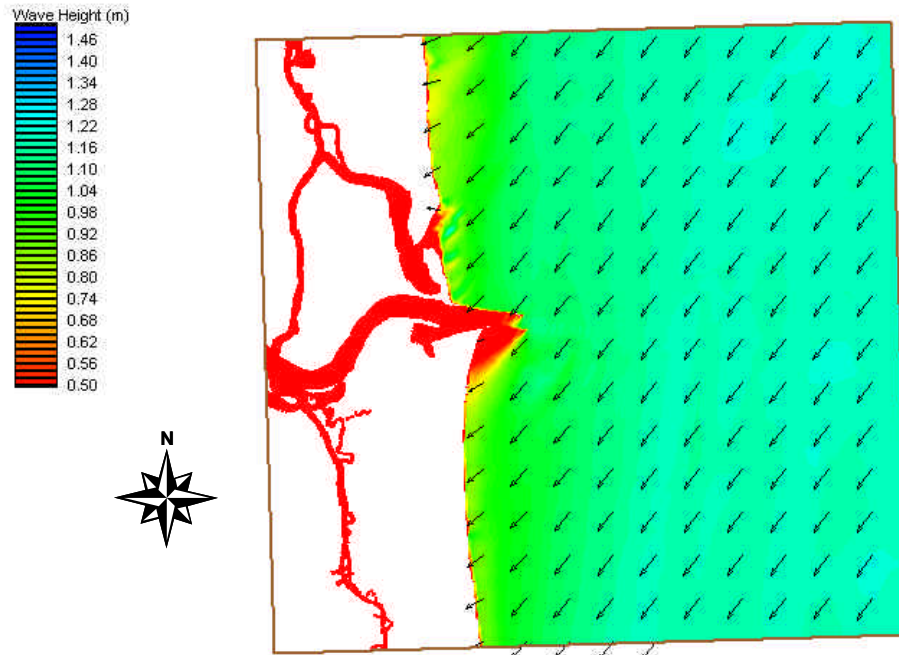


Figure A-1. Wave heights and directions (Case 21: $H_{m0} = 1.4$ m, $T_p = 5$ s, $\theta = 21.9^\circ$)

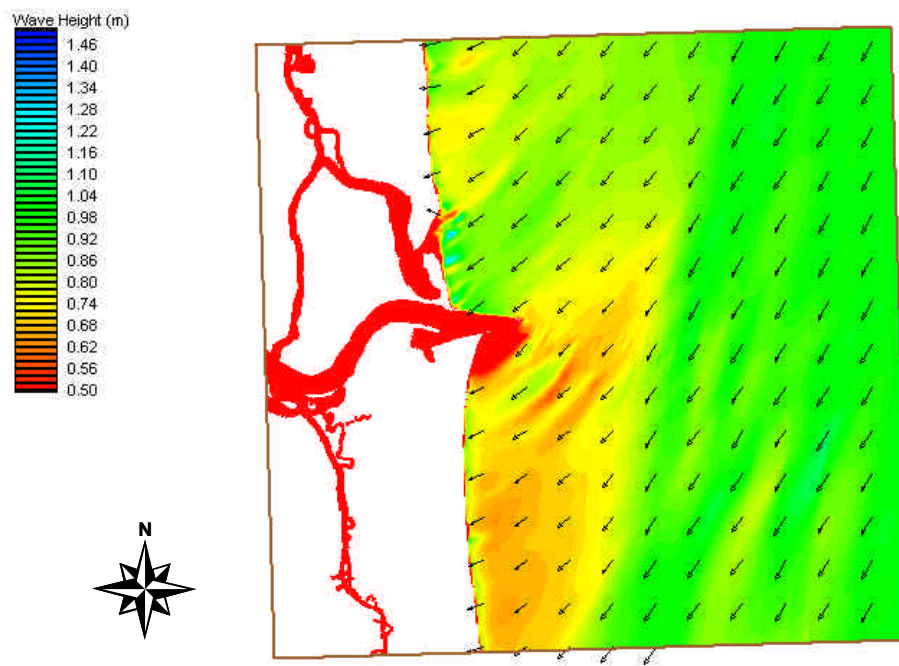


Figure A-2. Wave heights and directions (Case 23: $H_{m0} = 1.1$ m, $T_p = 13$ s, $\theta = 22.3^\circ$)

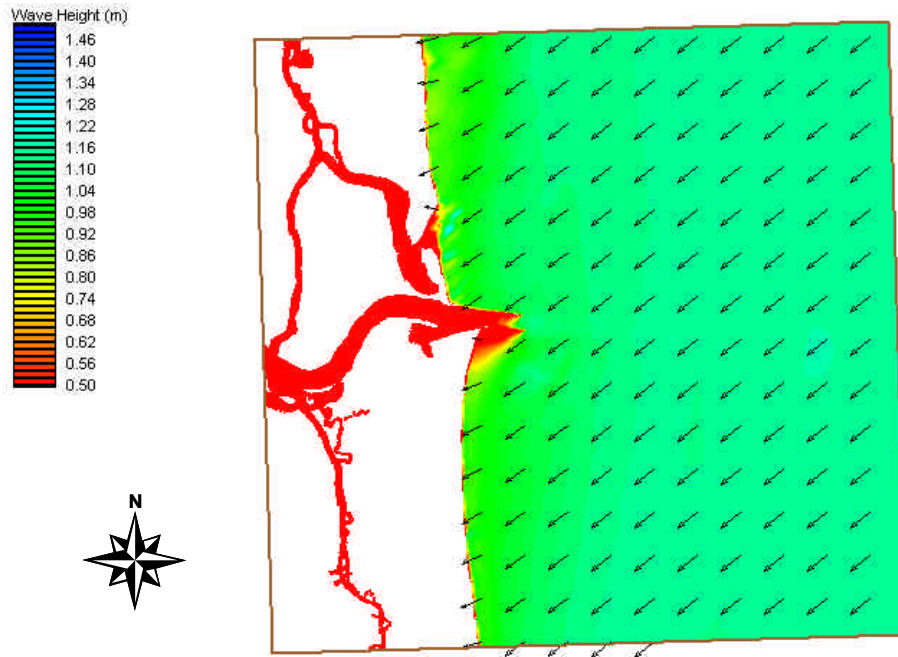


Figure A-3. Wave heights and directions (Case 31: $H_{m0} = 1.2$ m, $T_p = 5$ s, $\theta = 44.3^\circ$)

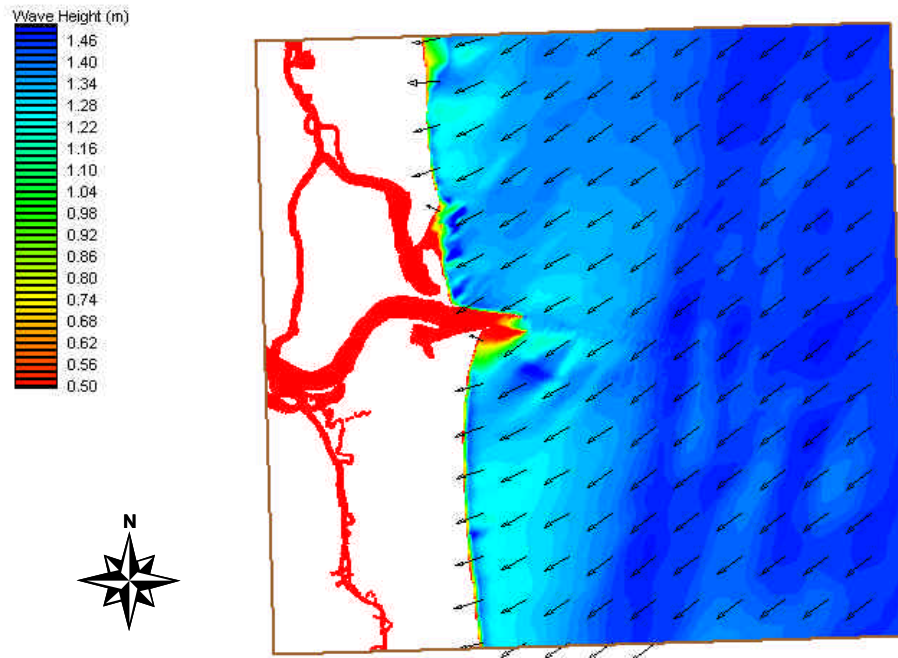


Figure A-4. Wave heights and directions (Case 32: $H_{m0} = 1.5$ m, $T_p = 8$ s, $\theta = 46.0^\circ$)

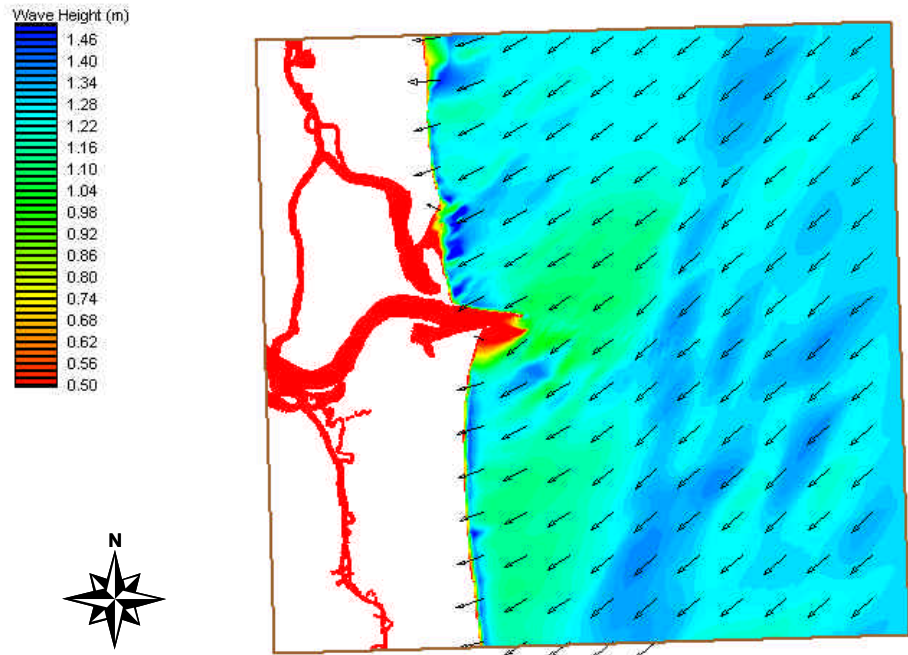


Figure A-5. Wave heights and directions (Case 33: $H_{m0} = 1.1$ m, $T_p = 5$ s, $\alpha = 67.4^\circ$)

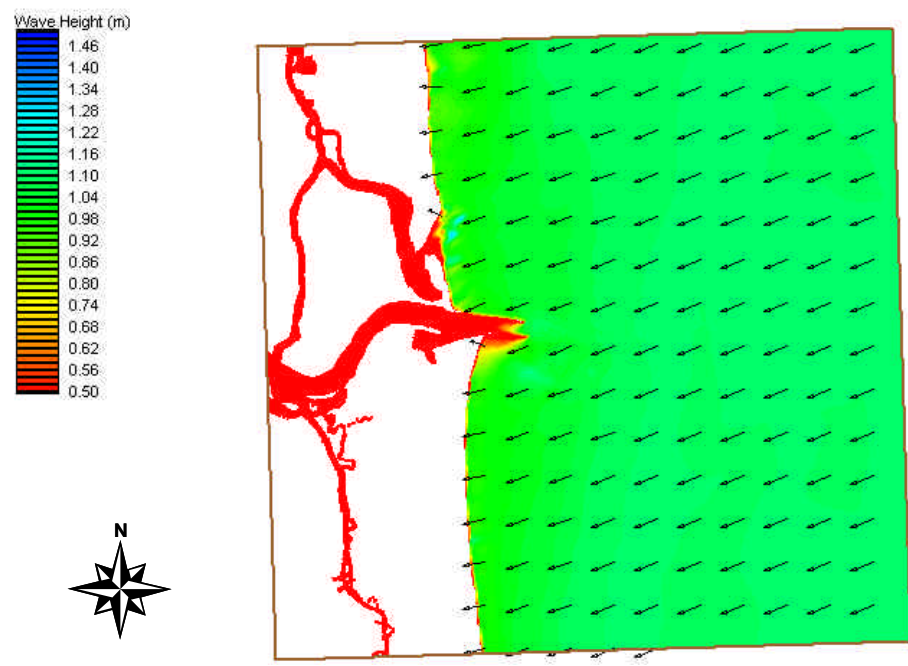


Figure A-6. Wave heights and directions (Case 41: $H_{m0} = 1.1$ m, $T_p = 5$ s, $\alpha = 67.4^\circ$)

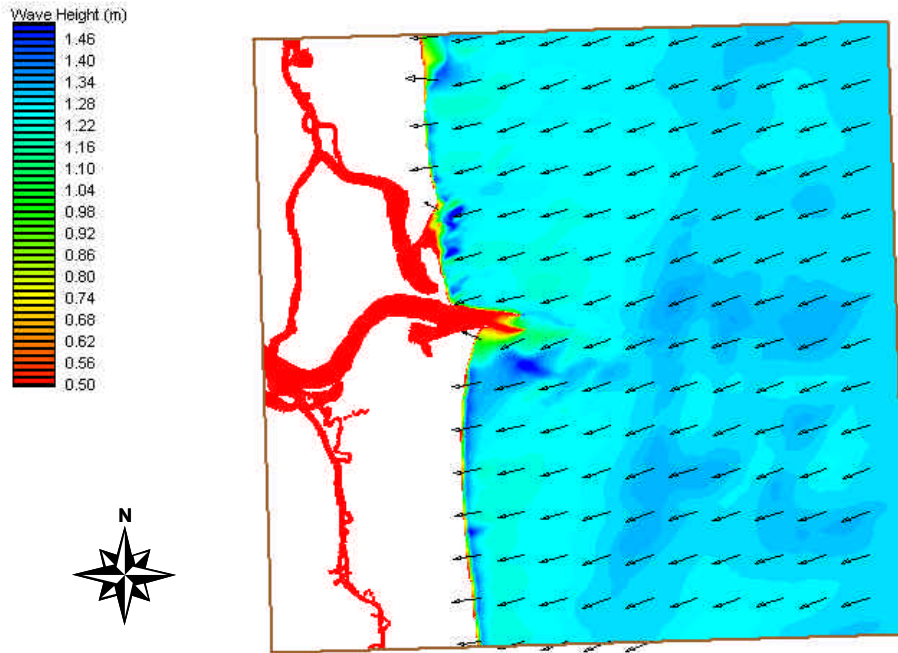


Figure A-7. Wave heights and directions (Case 42: $H_{m0} = 1.3$ m, $T_p = 8$ s, $\alpha = 68.8^\circ$)

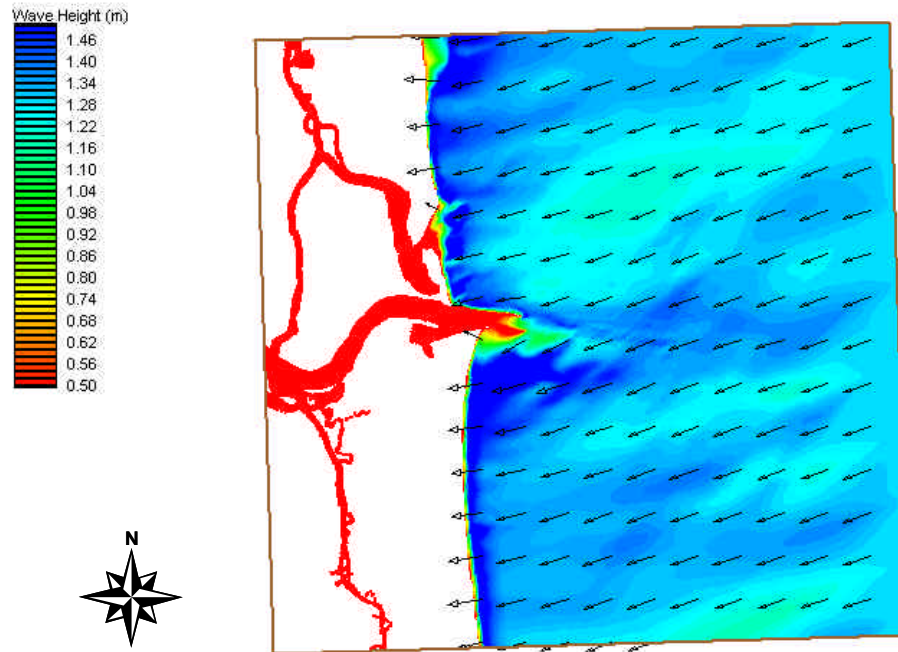


Figure A-8. Wave heights and directions (Case 43: $H_{m0} = 1.3$ m, $T_p = 13$ s, $\alpha = 69.9^\circ$)

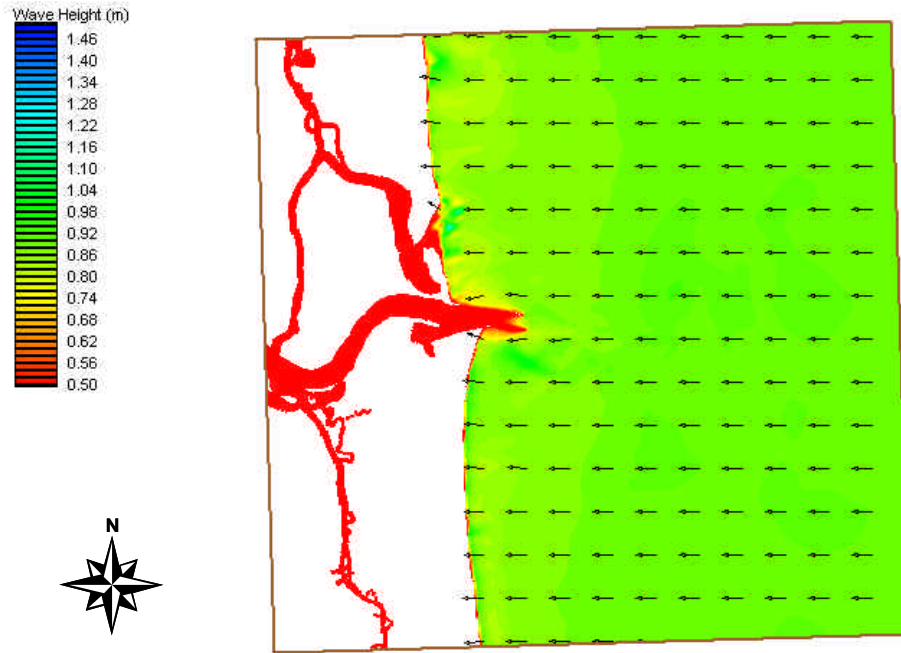


Figure A-9. Wave heights and directions (Case 51: $H_{m0} = 0.9$ m, $T_p = 6$ s, $\alpha = 88.0^\circ$)

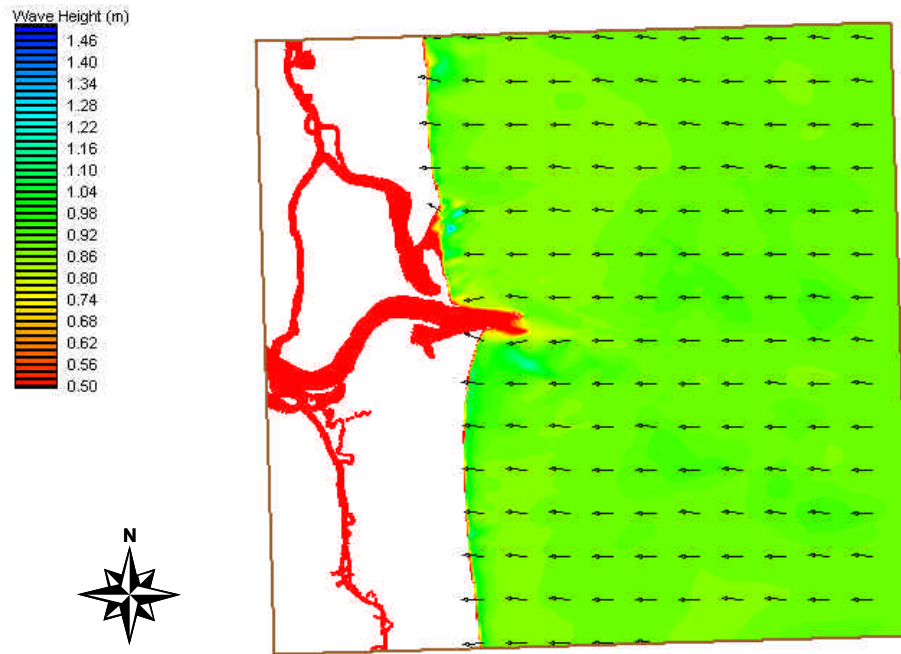


Figure A-10. Wave heights and directions (Case 52: $H_{m0} = 0.9$ m, $T_p = 8$ s, $\alpha = 89.6^\circ$)

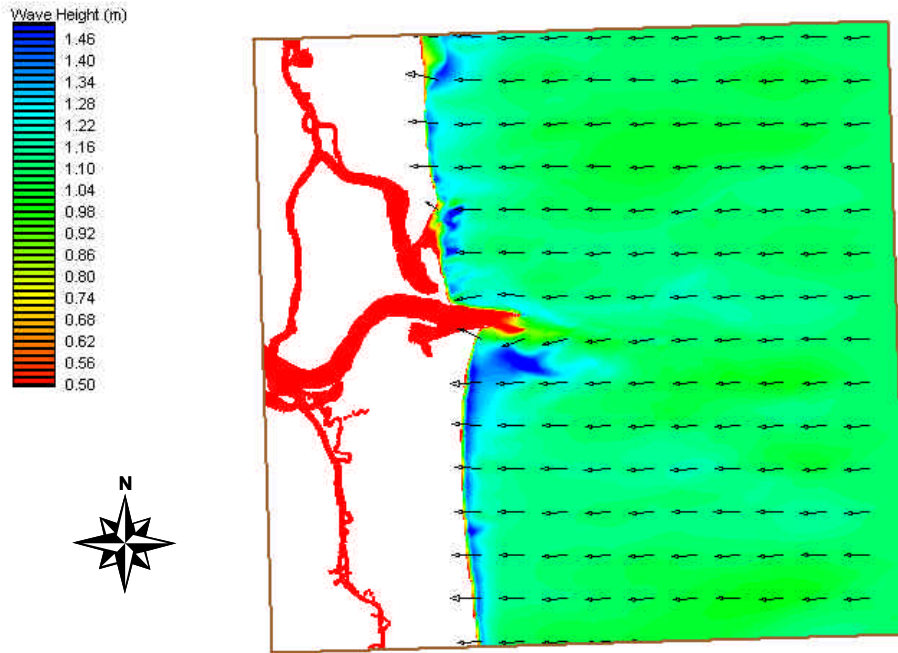


Figure A-11. Wave heights and directions (Case 53: $H_{m0} = 1.1$ m, $T_p = 12$ s, $\theta = 86.0^\circ$)

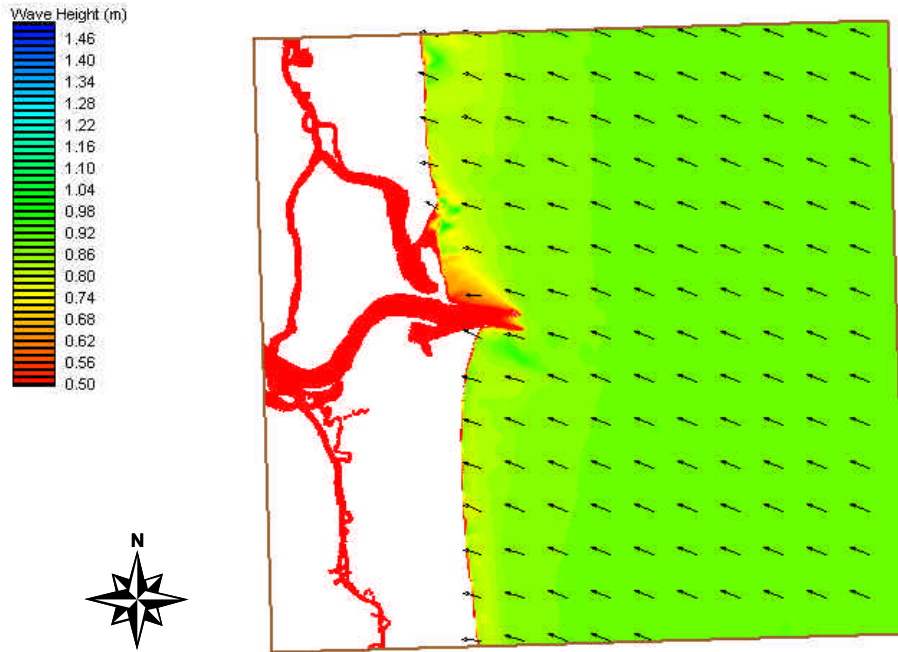


Figure A-12. Wave heights and directions (Case 61: $H_{m0} = 1.0.9$ m, $T_p = 5$ s, $\theta = 108.8^\circ$)

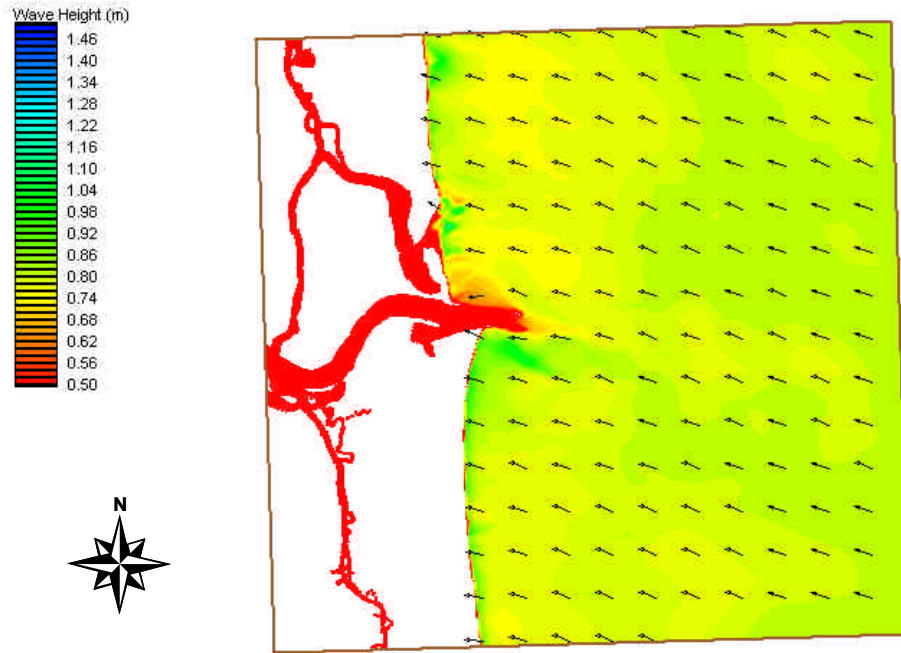


Figure A-13. Wave heights and directions (Case 62: $H_{m0} = 0.8$ m, $T_p = 8$ s, $\theta = 106.6^\circ$)

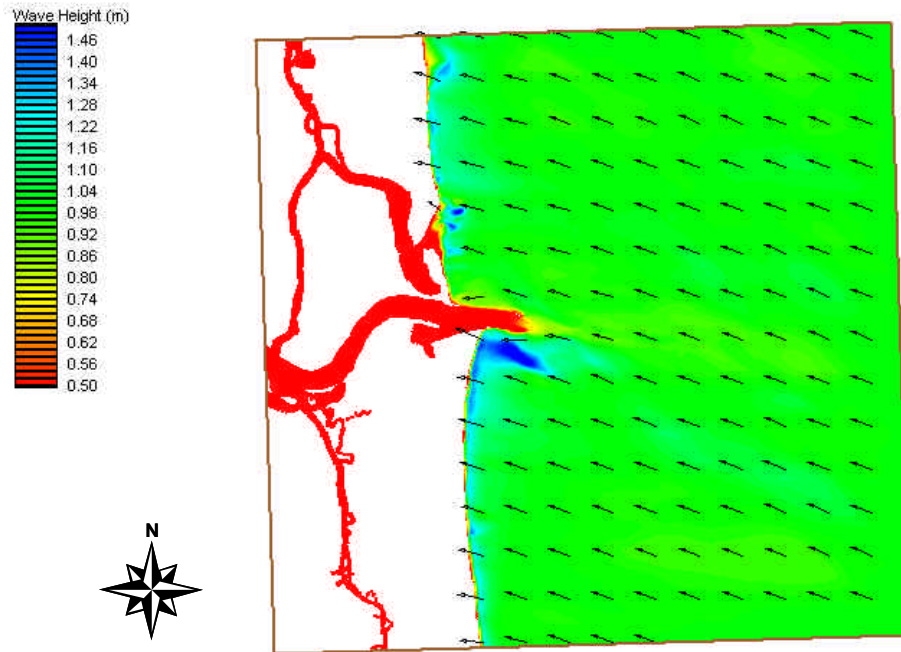


Figure A-14. Wave heights and directions (Case 63: $H_{m0} = 1.0$ m, $T_p = 12$ s, $\theta = 108.6^\circ$)

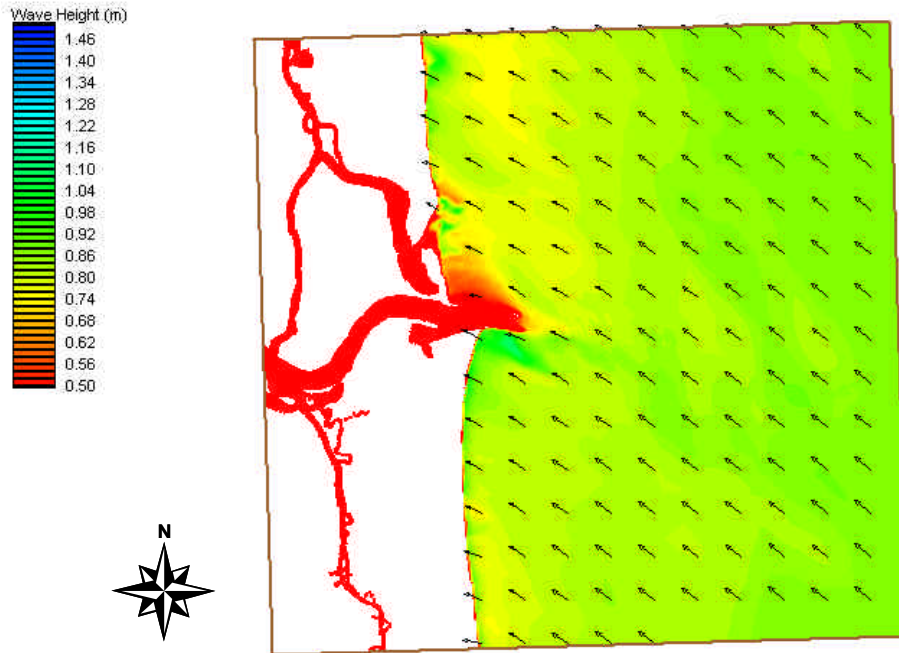


Figure A-15. Wave heights and directions (Case 72: $H_{m0} = 0.9$ m, $T_p = 8$ s, $\theta = 132.2^\circ$)

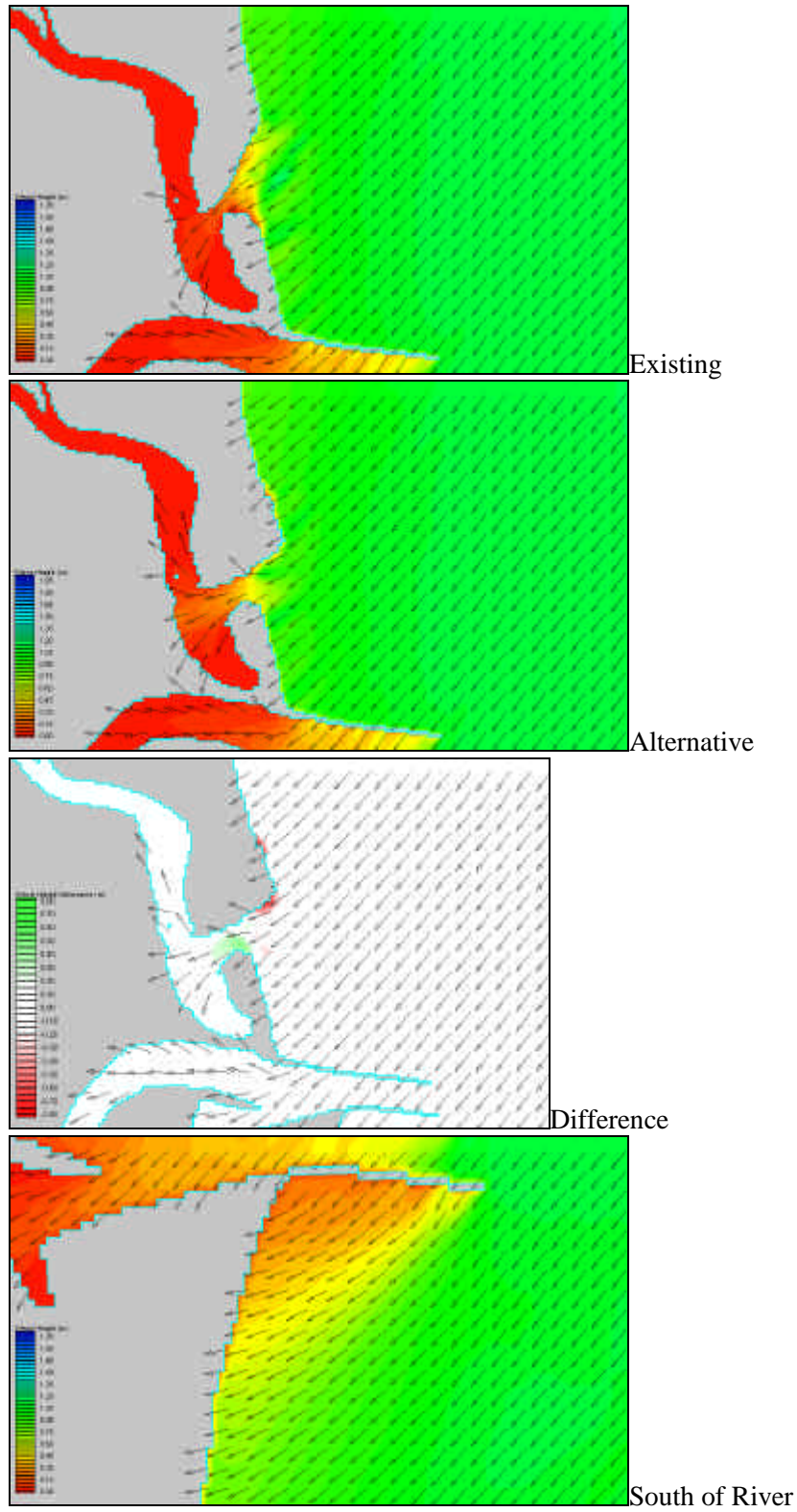


Figure A-16. Wave Simulation Results for Case 21

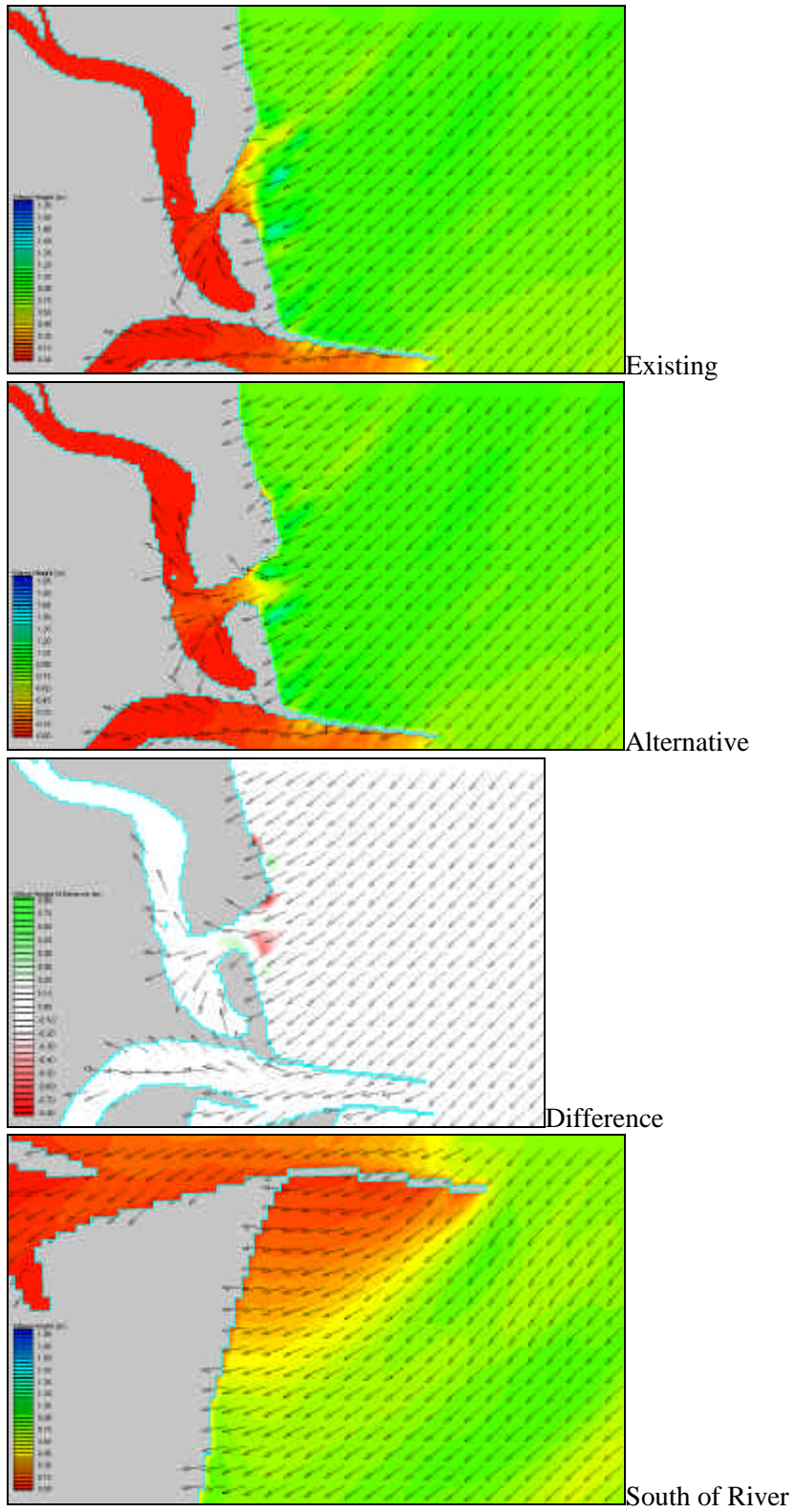


Figure A-17. Wave Simulation Results for Case 23

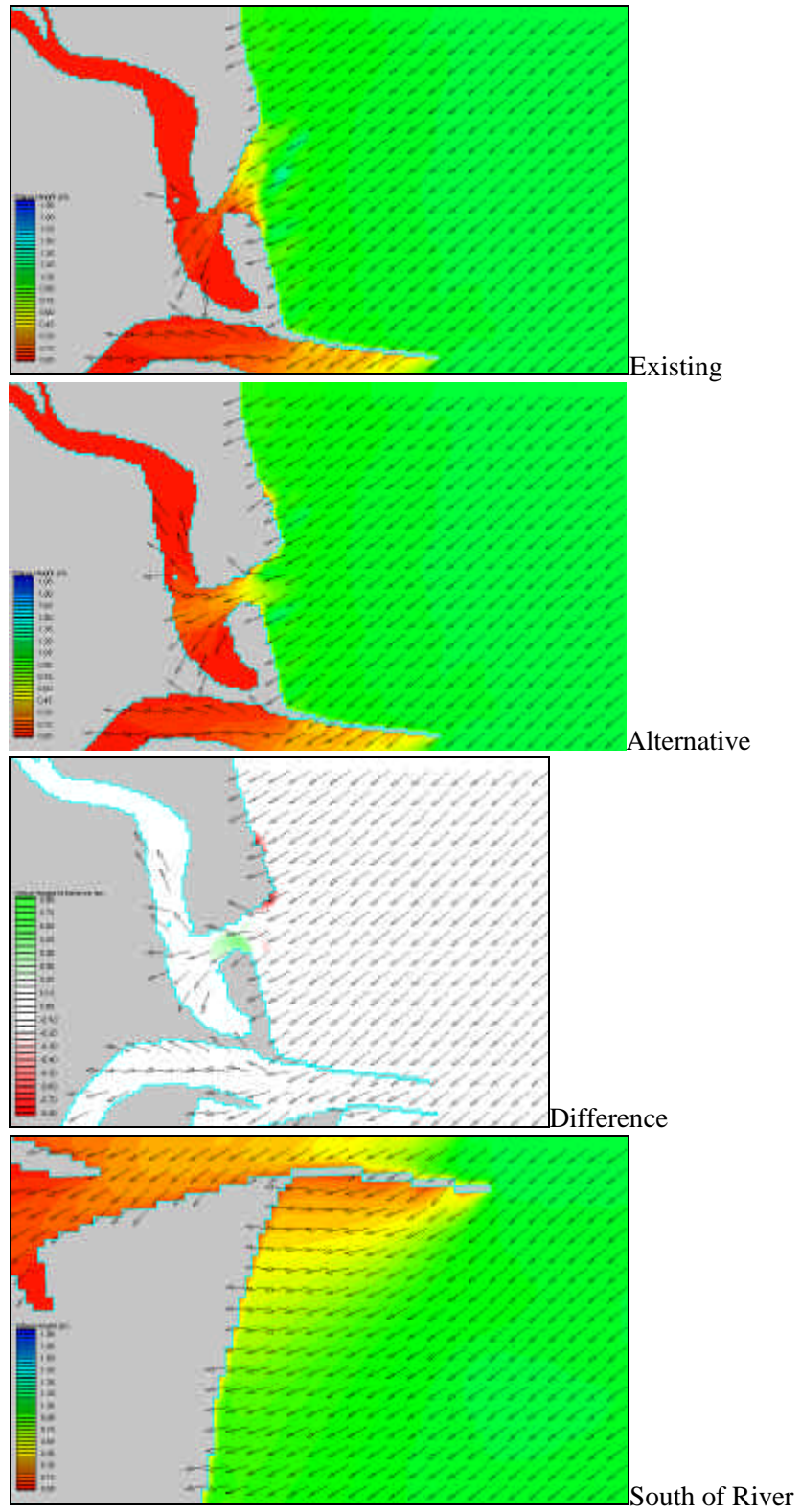


Figure A-18. Wave Simulation Results for Case 31

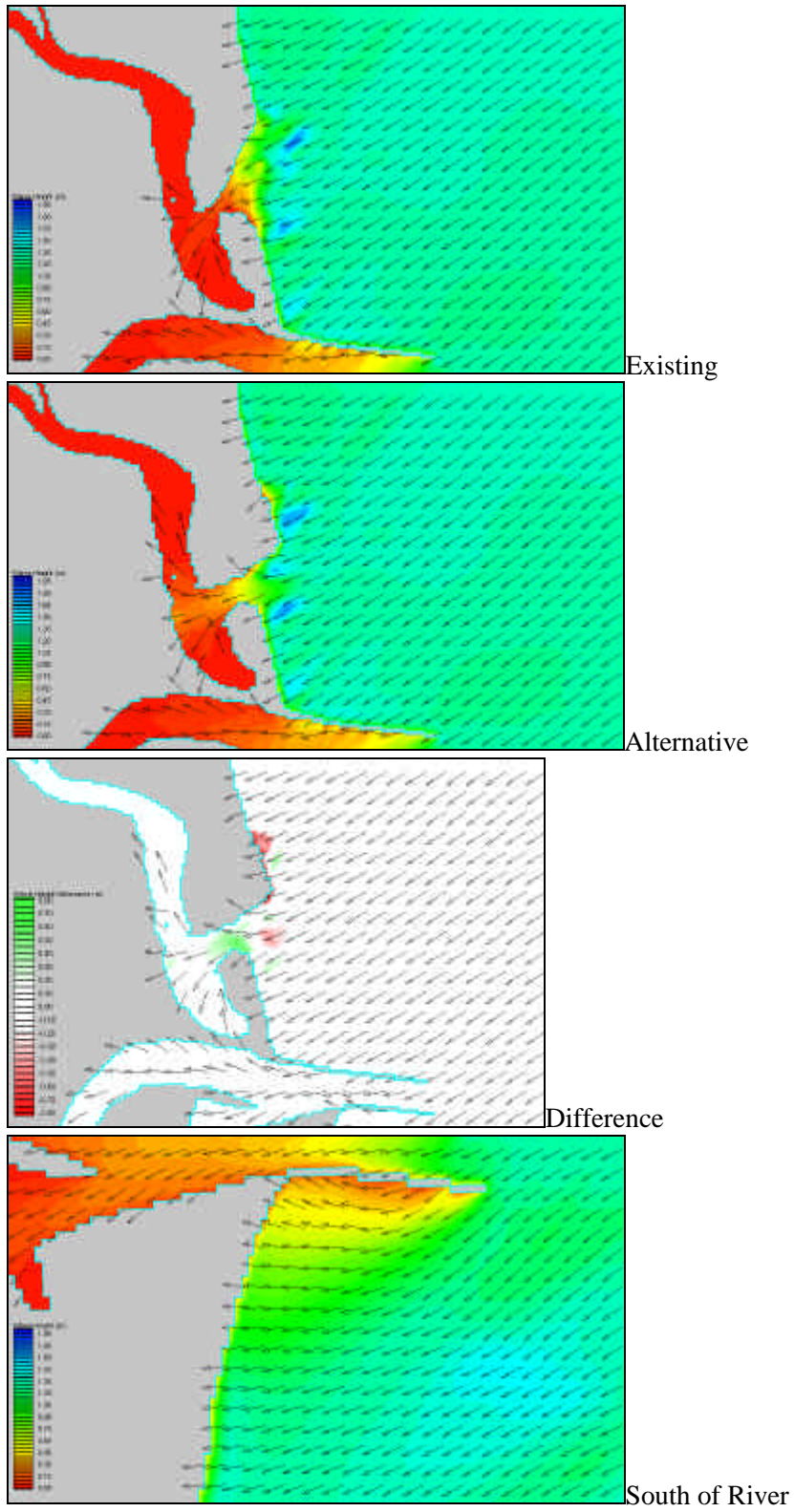


Figure A-19. Wave Simulation Results for Case 32

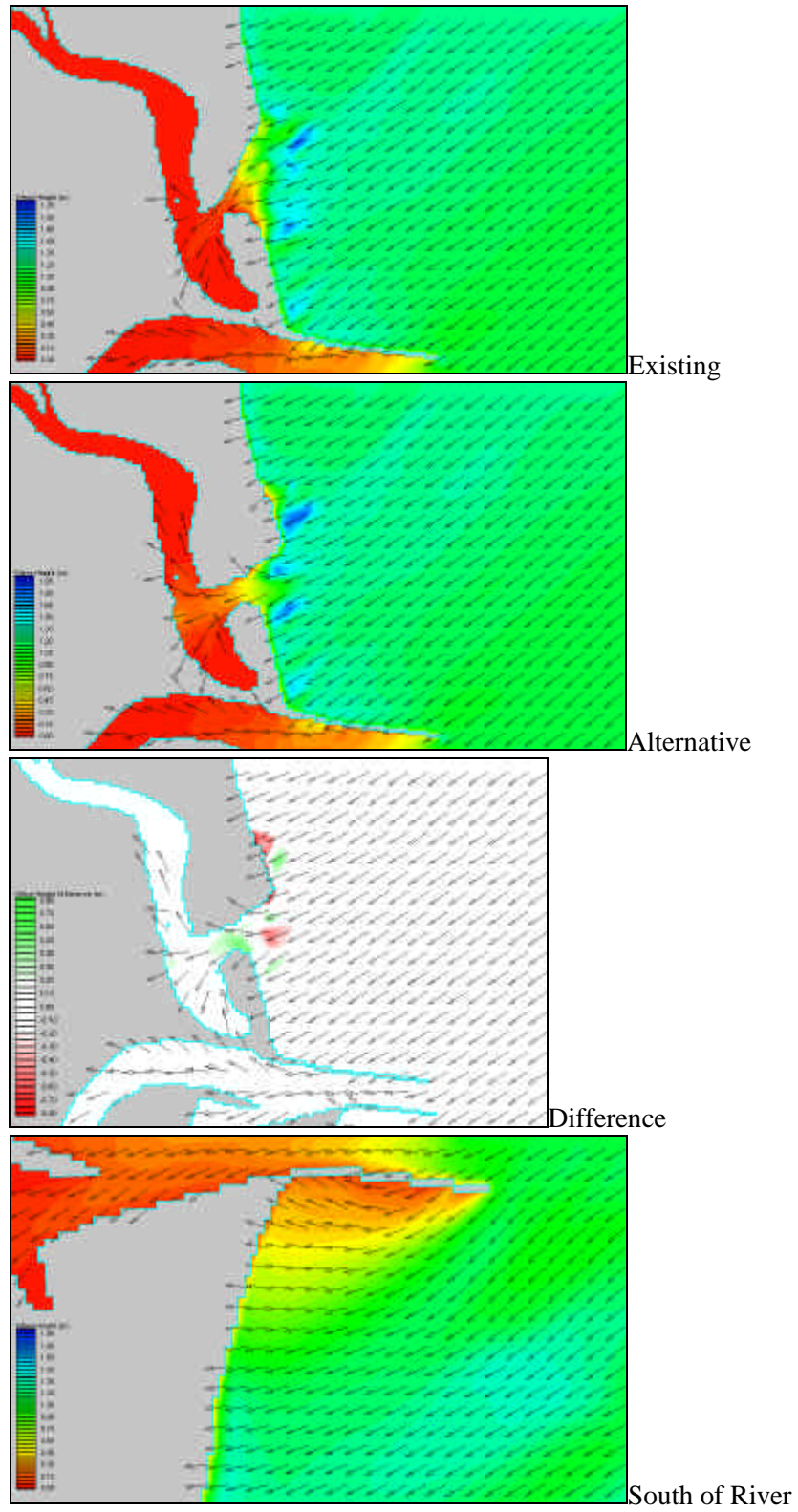


Figure A-20. Wave Simulation Results for Case 33

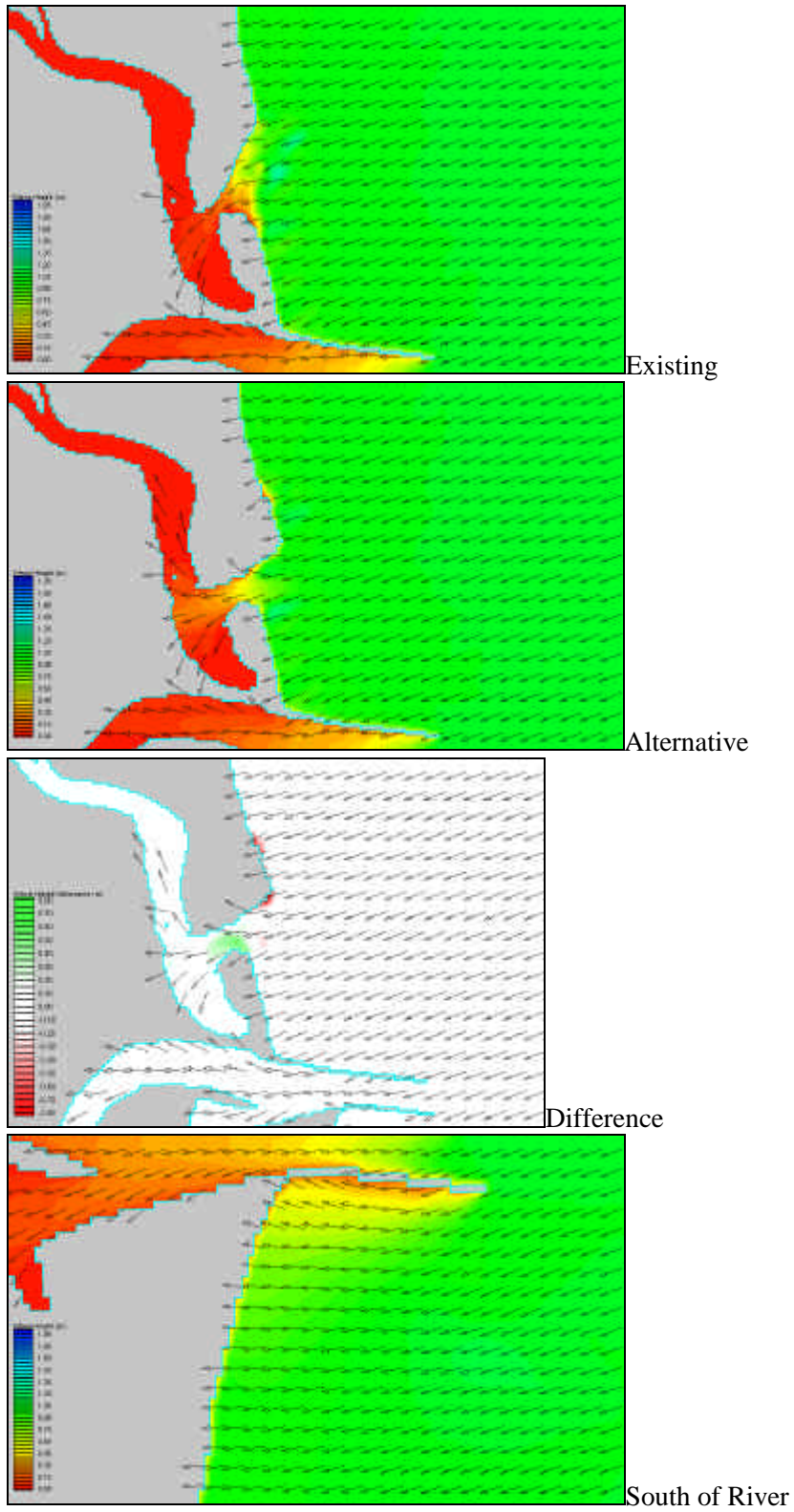


Figure A-21. Wave Simulation Results for Case 41

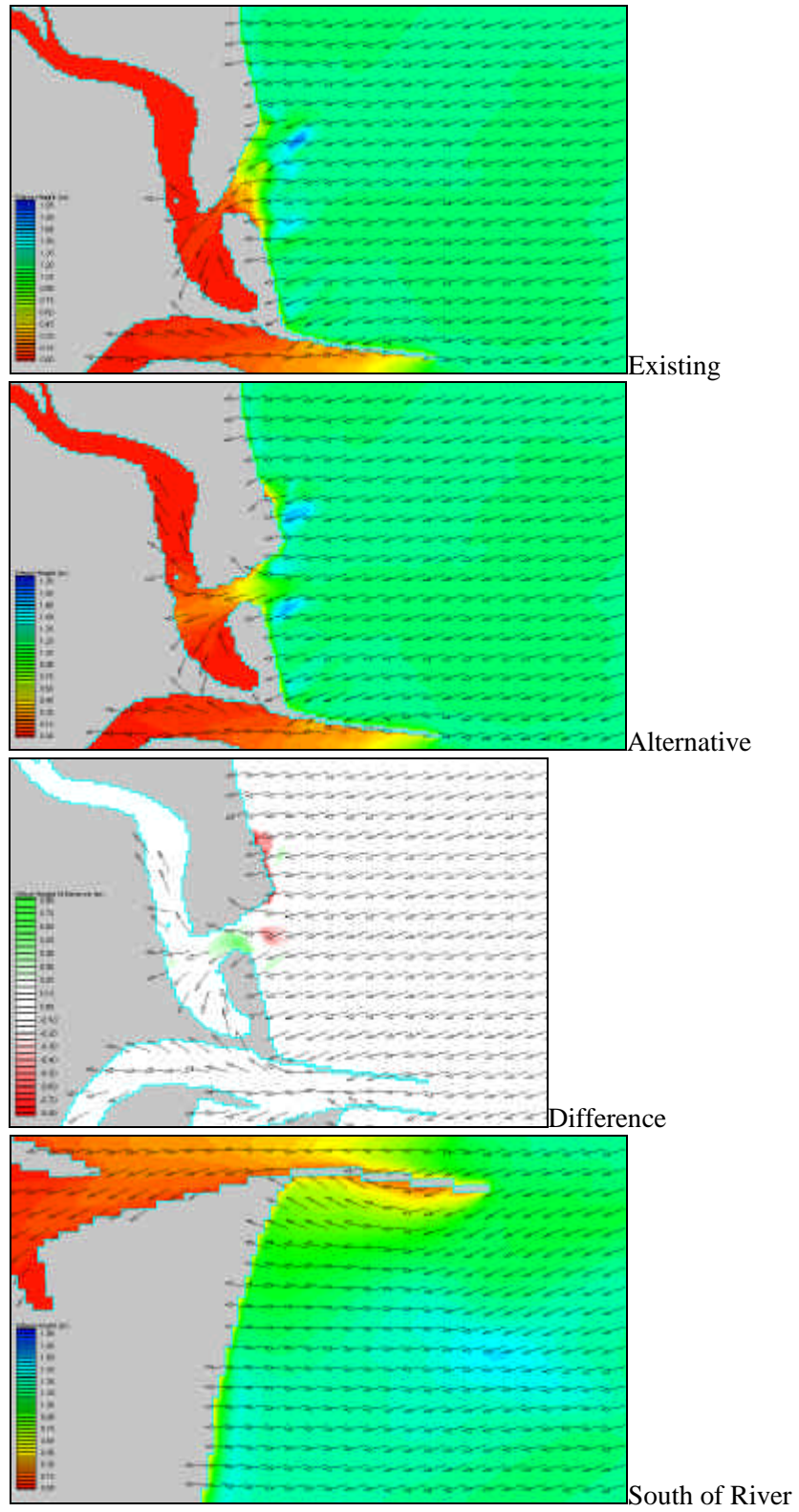


Figure A-22. Wave Simulation Results for Case 42

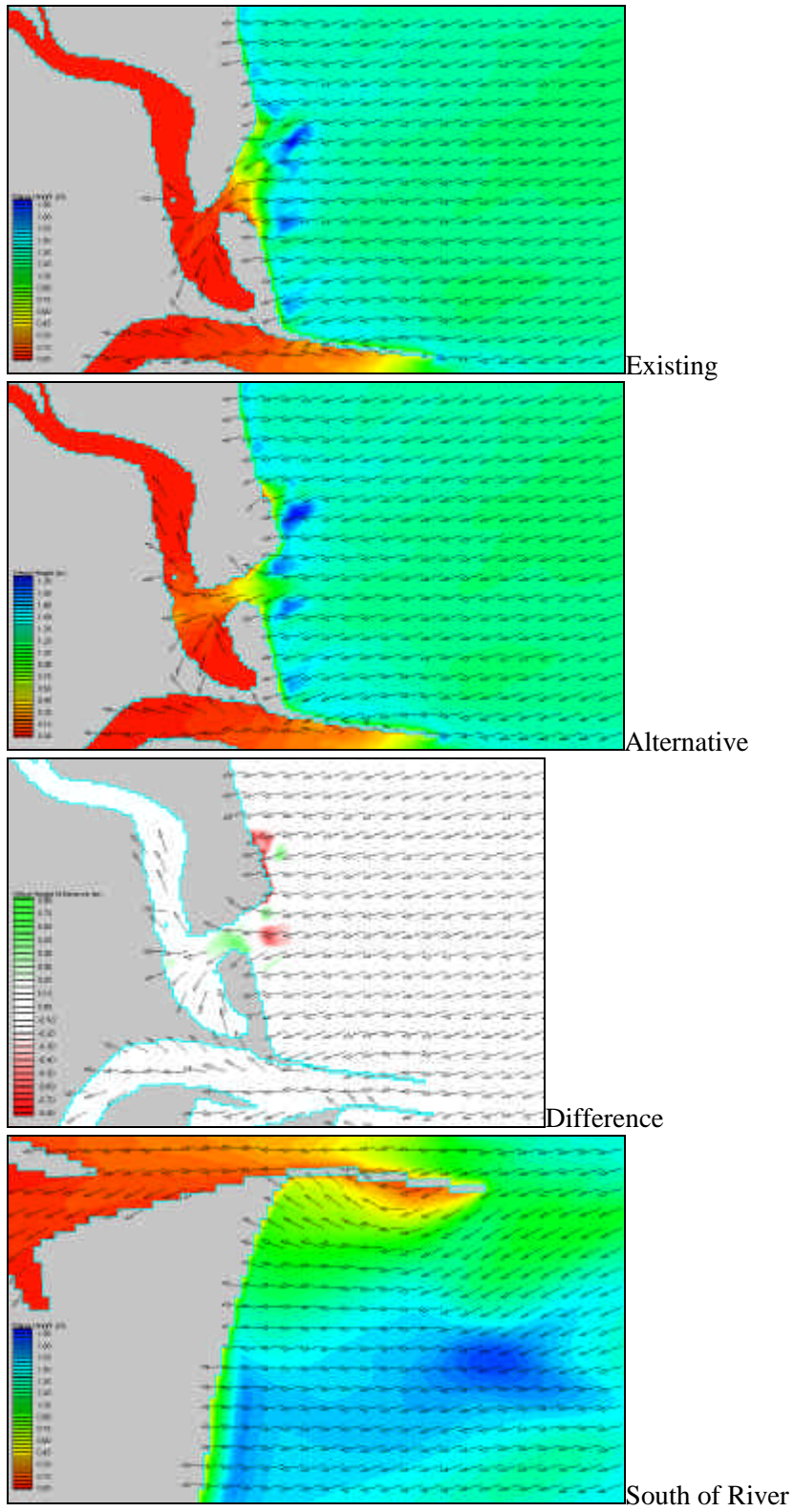


Figure A-23. Wave Simulation Results for Case 43

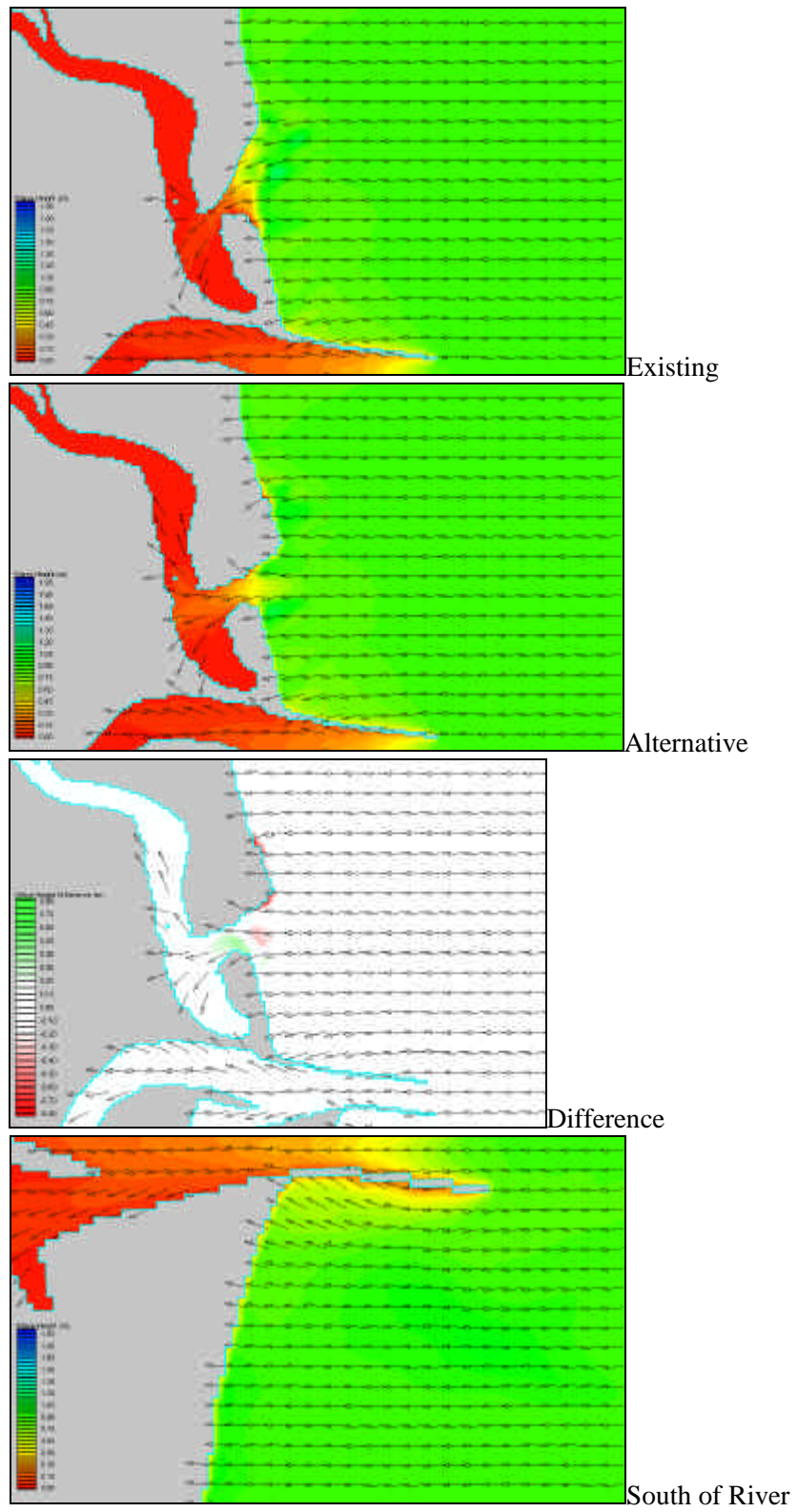


Figure A-24. Wave Simulation Results for Case 51

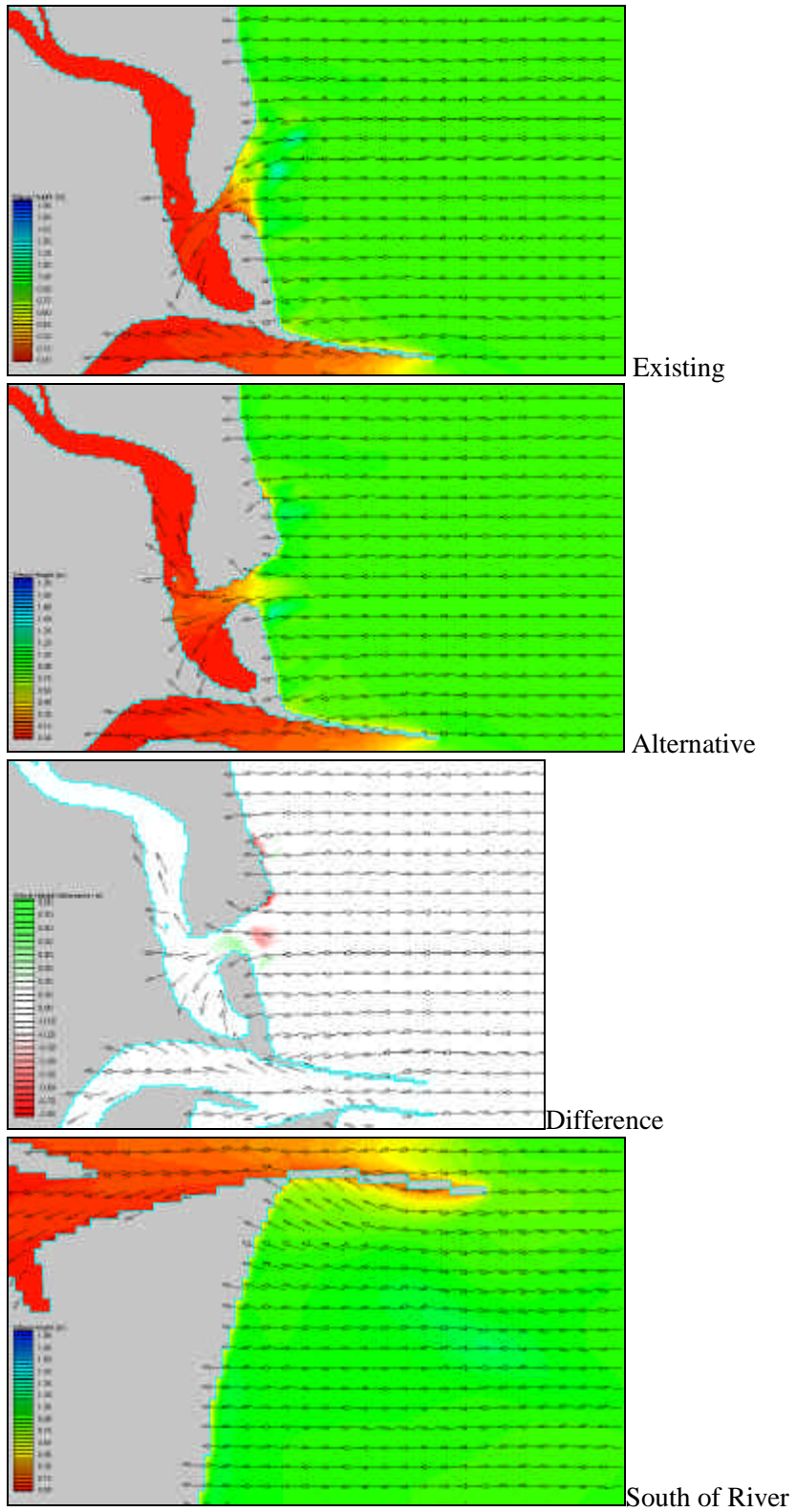


Figure A-25. Wave Simulation Results for Case 52

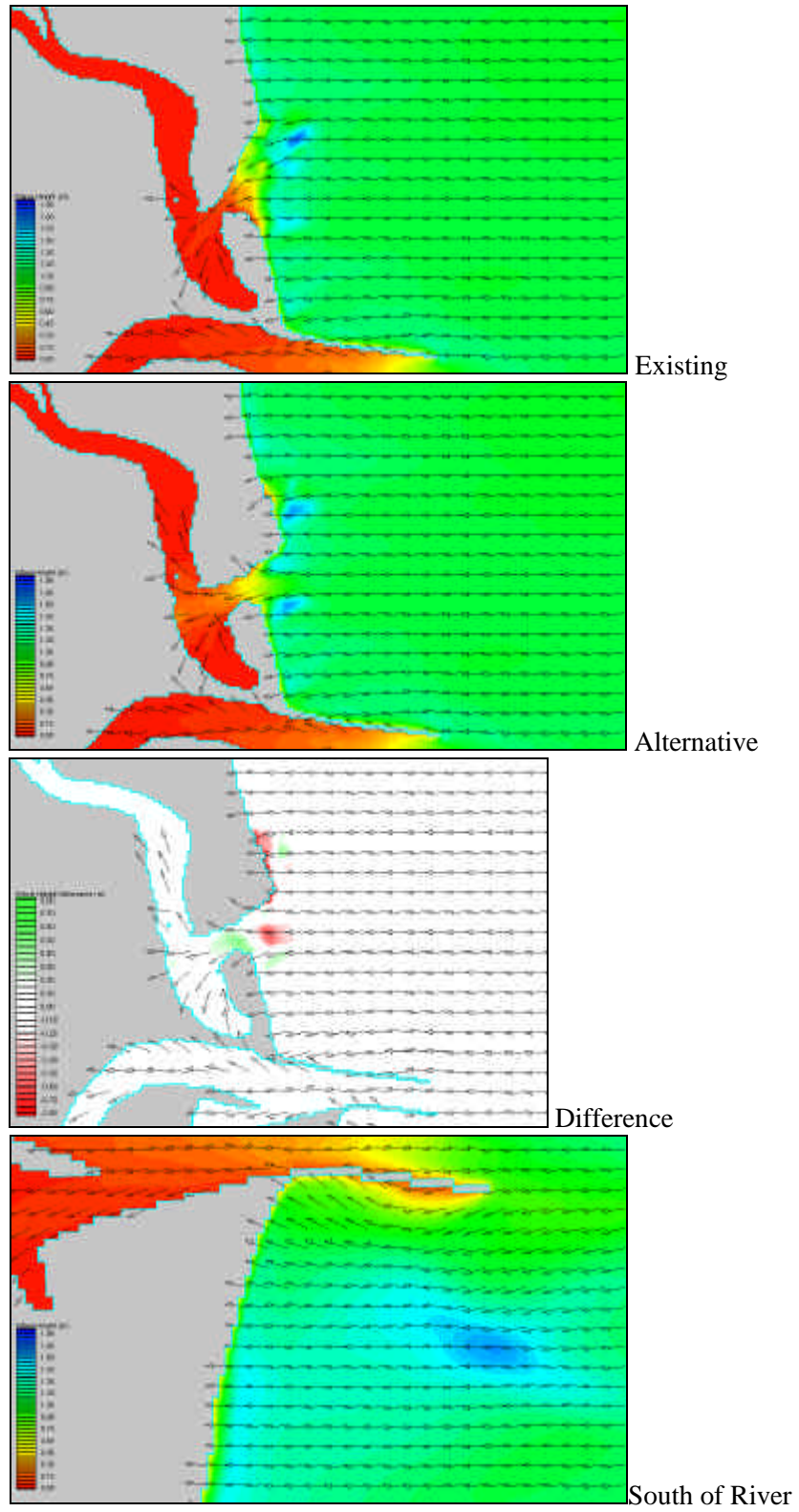


Figure A-26. Wave Simulation Results for Case 53

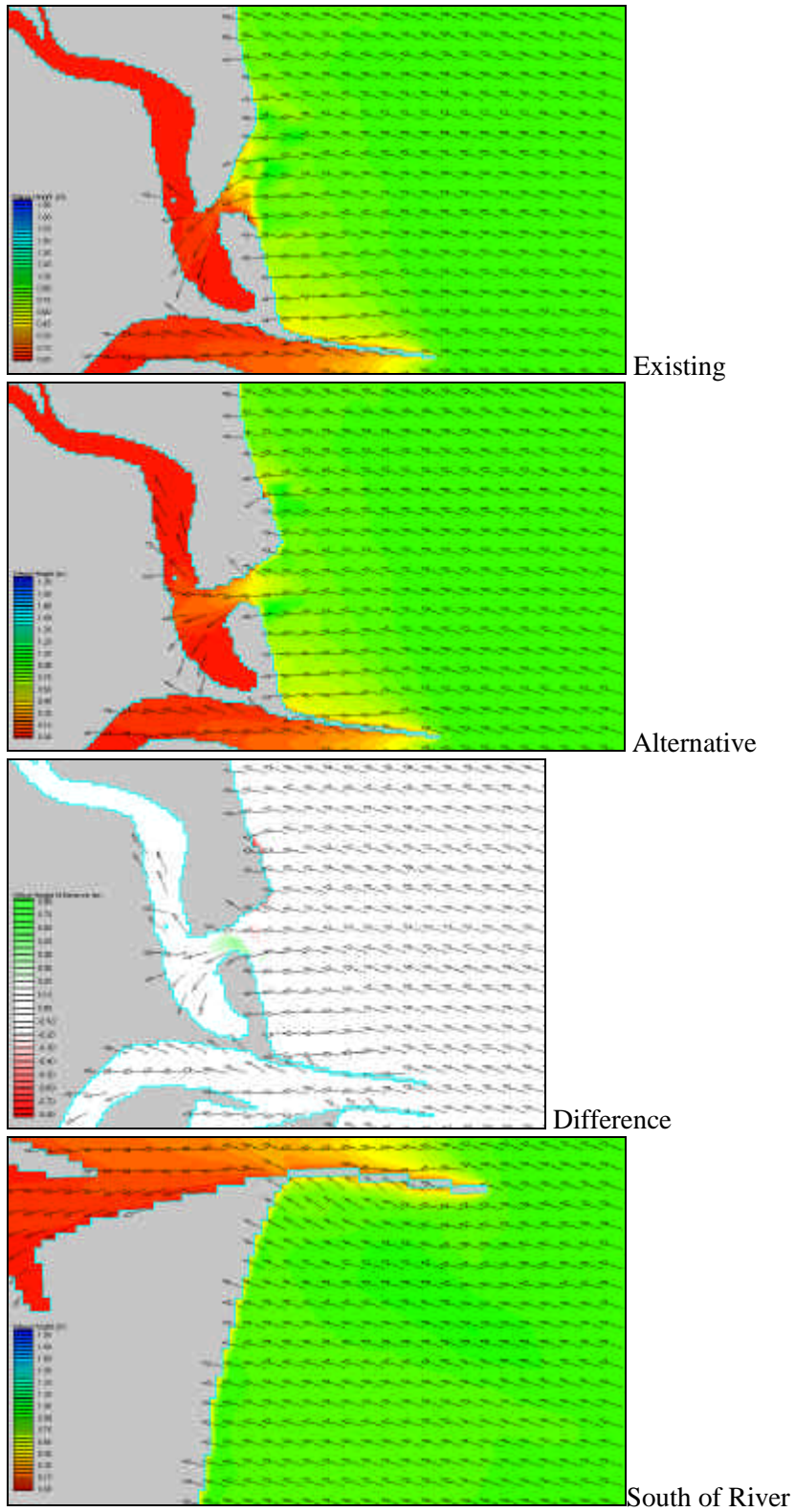


Figure A-27. Wave Simulation Results for Case 61

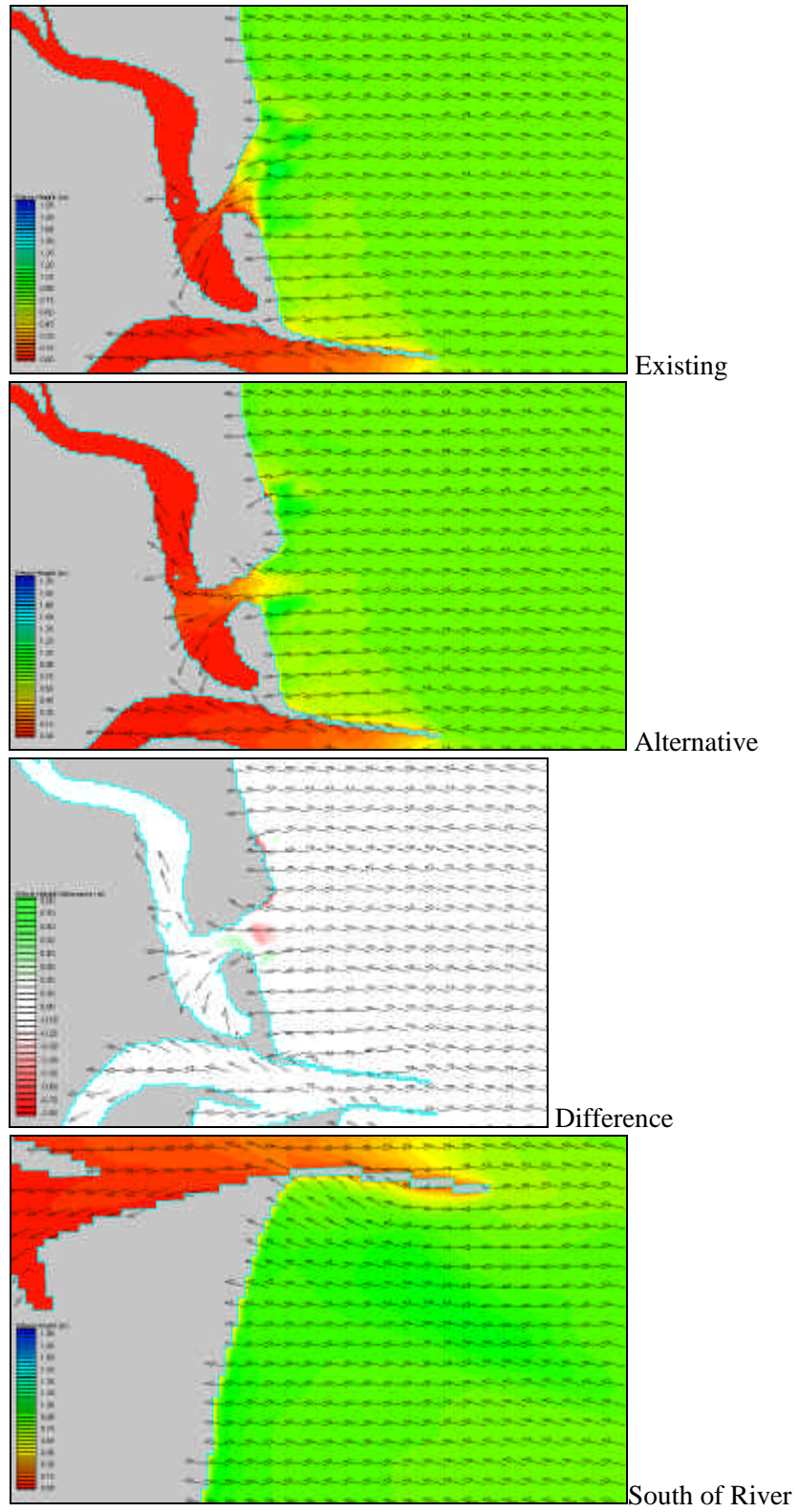


Figure A-28. Wave Simulation Results for Case 62

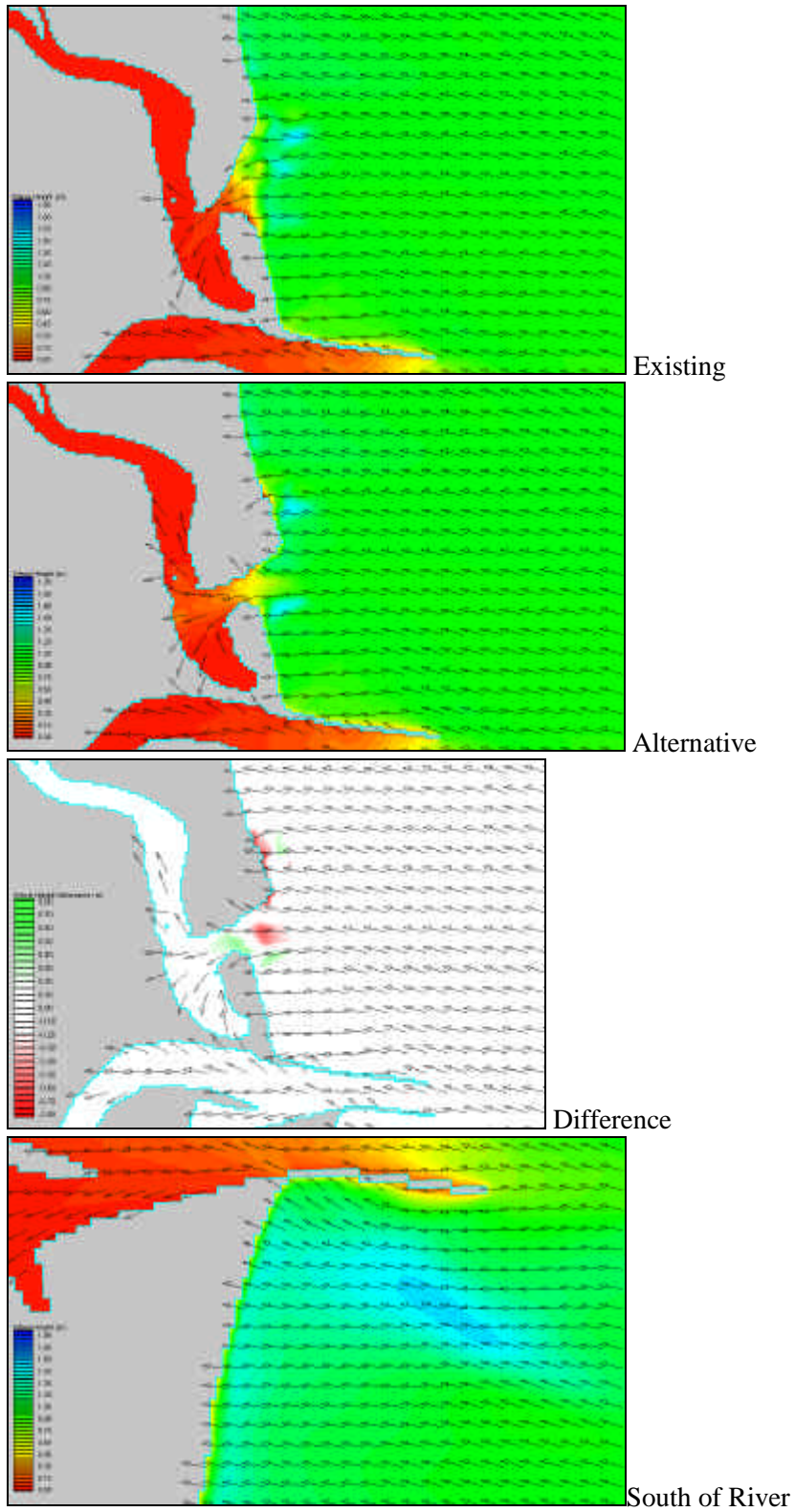


Figure A-29. Wave Simulation Results for Case 63

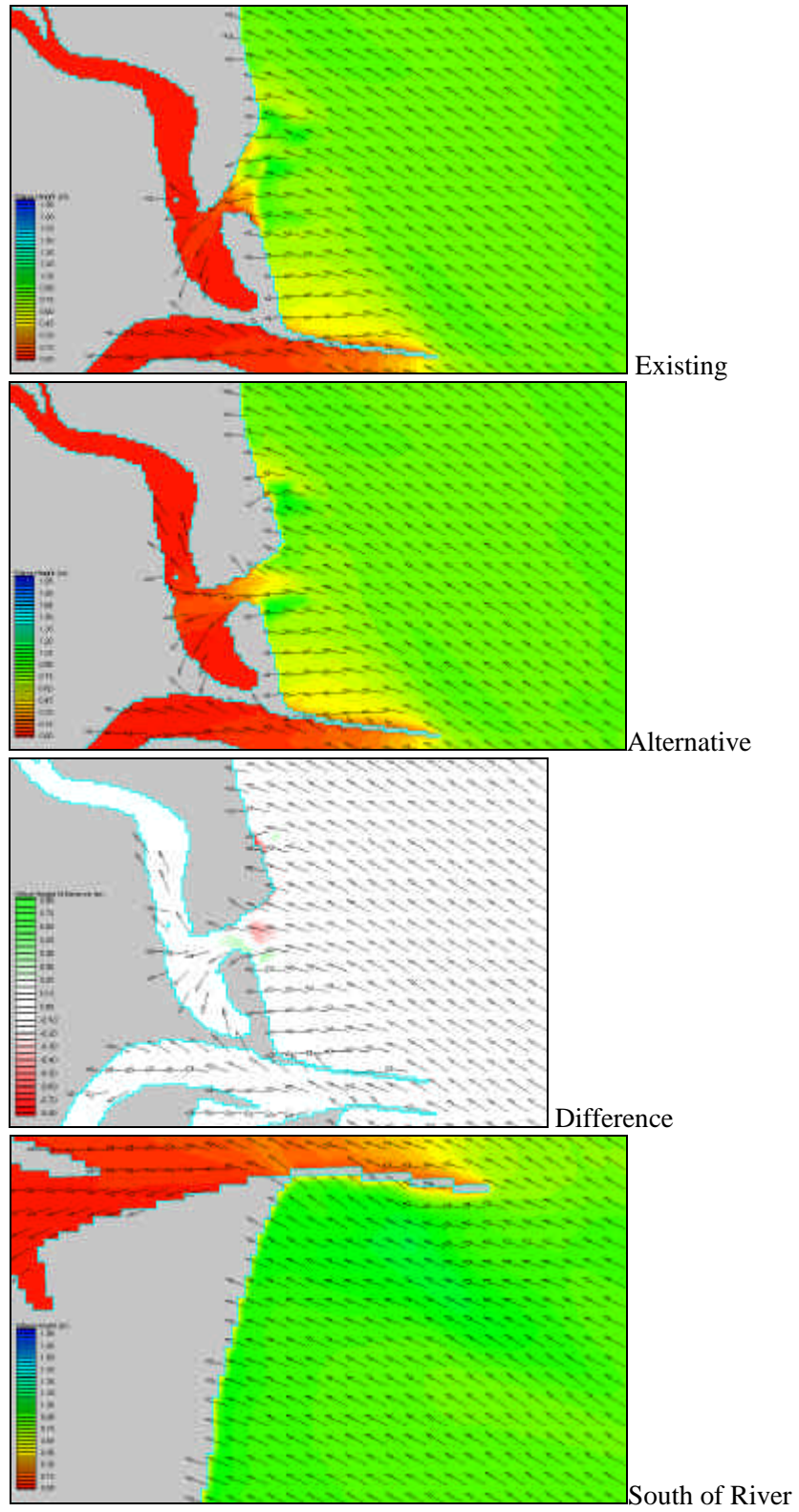


Figure A-30. Wave Simulation Results for Case 72